



January 2014

# Using Reanalysis Data For The Prediction Of Seasonal Wind Turbine Power Losses Due To Icing

Daniel Burtch

Follow this and additional works at: <https://commons.und.edu/theses>

## Recommended Citation

Burtch, Daniel, "Using Reanalysis Data For The Prediction Of Seasonal Wind Turbine Power Losses Due To Icing" (2014). *Theses and Dissertations*. 1509.

<https://commons.und.edu/theses/1509>

This Thesis is brought to you for free and open access by the Theses, Dissertations, and Senior Projects at UND Scholarly Commons. It has been accepted for inclusion in Theses and Dissertations by an authorized administrator of UND Scholarly Commons. For more information, please contact [zeinebyousif@library.und.edu](mailto:zeinebyousif@library.und.edu).

USING REANALYSIS DATA FOR THE PREDICTION OF  
SEASONAL WIND TURBINE POWER LOSSES DUE TO ICING

by

Daniel G. Burtch  
Bachelor of Engineering, Carleton University, 2009

A Thesis

Submitted to the Graduate Faculty

of the

University of North Dakota

in partial fulfillment of the requirements

for the degree of

Master of Science

Grand Forks, North Dakota

May

2014

Copyright Daniel Burtch 2014

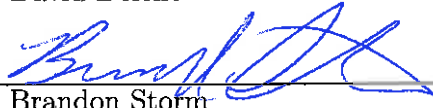
This thesis, submitted by Daniel G. Burtch in partial fulfillment of the requirements for the Degree of Master of Science from the University of North Dakota, has been read by the Faculty Advisory Committee under whom the work has been done and is hereby approved.



Gretchen Mullendore

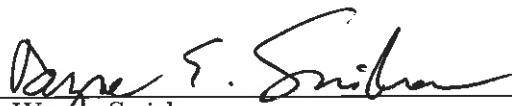


David Delene



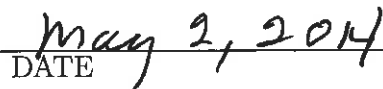
Brandon Storm

This thesis is being submitted by the appointed advisory committee as having met all of the requirements of the School of Graduate Studies at the University of North Dakota and is hereby approved.



Wayne Swisher

Dean of the School of Graduate Studies



DATE

## PERMISSION

Title	Using Reanalysis Data for the Prediction of Seasonal Wind Turbine Power Losses Due to Icing
Department	Atmospheric Sciences
Degree	Master of Science

In presenting this thesis in partial fulfillment of the requirements for a graduate degree from the University of North Dakota, I agree that the library of this University shall make it freely available for inspection. I further agree that permission for extensive copying for scholarly purposes may be granted by the professor who supervised my thesis work or, in her absence, by the Chairperson of the department or the dean of the School of Graduate Studies. It is understood that any copying or publication or other use of this thesis or part thereof for financial gain shall not be allowed without my written permission. It is also understood that due recognition shall be given to me and to the University of North Dakota in any scholarly use which may be made of any material in my thesis.

Daniel Burtch  
May 8, 2014

## TABLE OF CONTENTS

LIST OF FIGURES . . . . .	vii
LIST OF TABLES . . . . .	xiii
ACKNOWLEDGMENTS . . . . .	xv
ABSTRACT . . . . .	xvi
CHAPTER	
1 INTRODUCTION . . . . .	1
2 BACKGROUND . . . . .	3
2.1 Physics of Wind Energy Extraction . . . . .	4
2.2 Wind Turbine Overview . . . . .	5
2.3 Power Losses Due to Icing . . . . .	7
2.3.1 Methods of Determining Icing Conditions . . . . .	11
2.3.2 Modeling of Icing . . . . .	12
3 DATA AND METHODOLOGY . . . . .	15
3.1 Experimental Data . . . . .	15
3.1.1 Modern-Era Retrospective Analysis for Research and Applications (MERRA) Dataset . . . . .	15
3.1.2 Turbine Production Dataset . . . . .	17
3.1.3 Anemometer Dataset . . . . .	17
3.1.4 Extrapolation of Anemometer Dataset . . . . .	19
3.2 Methods of Determining Atmospheric Variables at the Tur- bine Height . . . . .	22
3.2.1 Methods 1a and 1b: Boundary-Layer Similarity The- ory . . . . .	23
3.2.2 Methods 2a and 2b: Extrapolation of Variables . . . . .	29
3.2.3 Methods 3a and 3b: Interpolation of Variables . . . . .	30
3.3 Methods of Determining Power Losses Due to Icing . . . . .	32
3.3.1 Wind Industry Method . . . . .	32

3.3.2	Method to Determine Observed and Predicted Power Losses Due to Icing . . . . .	32
4	RESULTS . . . . .	<b>39</b>
4.1	Accuracy of MERRA-Derived Wind Speeds and Energy Production . . . . .	39
4.2	Temporal Variability in Icing Prediction . . . . .	46
4.3	Prediction of Annual Power Losses Due to Icing . . . . .	53
4.4	Applicability to a Different Location . . . . .	58
5	DISCUSSION . . . . .	<b>62</b>
5.1	Suitability of the MERRA-Derived Wind Speeds . . . . .	62
5.2	Suitability of the MERRA-Derived Temperature and Relative Humidity . . . . .	67
5.3	Suitability of MCP/WAsP-derived Wind Speeds . . . . .	74
5.4	Prediction of Annual Losses Due to Icing . . . . .	78
5.4.1	Assumptions and Potential Errors in Observed Icing Losses . . . . .	79
5.4.2	Assumptions and Potential Errors in Predicted Icing Losses . . . . .	81
5.5	Losses Due to Other Factors . . . . .	81
5.6	Financial Implications of Icing Losses . . . . .	82
5.7	Extrapolating Results Regionally . . . . .	84
5.7.1	Retraining the Dataset at Valley City . . . . .	86
5.8	Impact of Residual Error on the MCP/WAsP Analysis . . . . .	89
5.9	Future Work . . . . .	93
6	CONCLUSIONS . . . . .	<b>95</b>
	REFERENCES . . . . .	<b>98</b>

## LIST OF FIGURES

Figure	Page	
1	U.S. annual and cumulative wind power capacity growth including new installations for each quarter of each year. Figure from American Wind Energy Association (2013). . . . .	4
2	Schematic of a typical wind turbine with major components labelled (Encyclopædia Britannica). . . . .	5
3	Type of accreted ice as a function of wind speed and air temperature. Figure from International Standards Organization (2001). . . . .	9
4	The location of the turbines used in this study within North Dakota. The four MERRA gridpoints used at each turbine are the vertices of the purple squares. . . . .	16
5	Relative humidity calculation using World Meteorological Organization (WMO) standards, showing that below 0 °C (273.15 K), saturation is never achieved (Cattin et al., 2008). . . . .	29
6	Equation 3.24 fitted to the 2 m, 10 m, and 50 m MERRA wind speed data for a single time step with $a=0.03416$ , $b=0.9201$ , $R^2=0.9999$ , and $RMSE=0.2603$ . . . . .	30
7	Manufacturer's power curve for a NEG Micon NM52/900 turbine with air density of $1.27 \text{ kg m}^{-3}$ . . . . .	33



8	Observed power production at the Petersburg location (blue) compared with expected power production (green) calculated using the boundary-layer similarity method for the first week of November 2009. Icing is assumed to occur when observed power production is less than 80% of the expected power production for time periods that meet the temperature and wind speed criteria (red). . . . .	34
9	Temperature profile at the Petersburg location as calculated using boundary-layer similarity theory for the first week of November 2009 (blue) compared with the temperature threshold for icing prediction (red). . . . .	35
10	Relative humidity profile at the Petersburg location as calculated using boundary-layer similarity theory for the first week of November 2009 (blue) compared with the 95% relative humidity threshold for icing prediction (red). . . . .	36
11	Expected power generated at the Petersburg location calculated from boundary-layer similarity theory for the first week of November 2009 (blue). Periods of time where both temperature and relative humidity thresholds are met for icing are shown in red. . . . .	37
12	A comparison of energy production at the Petersburg location calculated from wind speed derived from boundary layer similarity theory (blue) and boundary layer similarity theory with Measure-Relate-Predict (MRP) derived wind speed (green). The observed production is shown in red. . . . .	40
13	A comparison of energy production at the Petersburg location calculated from wind speed derived from the interpolation method (blue) and the interpolation method with Measure-Relate-Predict (MRP) derived wind speed (green). The observed production is shown in red. . . . .	41
14	A comparison of energy production at the Petersburg location calculated from wind speed derived from the extrapolation method (blue) and the extrapolation method with Measure-Relate-Predict (MRP) derived wind speed (green). The observed production is shown in red. . . . .	41
15	Average hourly energy production for each season (October to March) at the Petersburg location as calculated from wind speed derived from boundary layer similarity theory (solid blue), the extrapolation method (solid magenta), and the interpolation method (solid green). The same methods using MRP/WAsP-derived wind speeds are shown as dashed lines. Observed is shown with the dashed black line. . . . .	43

16	A comparison of wind speed as a function of height for the interpolation method (red), the extrapolation method (blue), and the boundary layer similarity method (green) for December 23, 2011 at 0600Z. The cyan dots are the MERRA-provided wind speeds, and the magenta dot is the MCP/WAsP-derived wind speed. . . . .	44
17	Seasonal average wind speed calculated from boundary layer similarity theory (blue), the extrapolation method (magenta), the interpolation method (green), and the MCP/WAsP method at the Petersburg location. . . . .	45
18	Predicted and observed icing losses (MWh) at the Petersburg location using the boundary-layer similarity method with MCP/WAsP-derived winds and a relative humidity of 97.7 % for each three month period making up the 2007/2008 winter season. . . . .	47
19	Predicted and observed icing losses (MWh) at the Petersburg location using the boundary-layer similarity method with MCP/WAsP-derived winds and a relative humidity of 97.7 % for each monthly period making up the 2007/2008 winter season. . . . .	48
20	Predicted and observed icing losses (kWh) at the Petersburg location using the boundary-layer similarity method with MCP/WAsP-derived winds and a relative humidity of 97.7 % for each weekly period of January 2008. . . . .	49
21	The difference between the predicted icing losses ( $L_P$ ) and observed icing losses ( $L_O$ ) at the Petersburg location for October 2009 using the boundary layer similarity method. . . . .	50
22	The difference between the predicted icing losses ( $L_P$ ) and observed icing losses ( $L_O$ ) at the Petersburg location for January 2010 using the boundary layer similarity method. . . . .	50
23	The difference between the predicted icing losses ( $L_P$ ) and observed icing losses ( $L_O$ ) at the Petersburg location for the period October 2009 to December 2009 using the boundary layer similarity method. . . . .	51
24	The difference between the predicted icing losses ( $L_P$ ) and observed icing losses ( $L_O$ ) at the Petersburg location for the period January 2010 to March 2010 using the boundary layer similarity method. . . . .	52

25	The difference between the predicted icing losses ( $L_P$ ) and observed icing losses ( $L_O$ ) at the Petersburg location for the period October 2009 to March 2010 (blue dots) using the boundary layer similarity method. . . .	53
26	A comparison of the eleven-year, eight-year, and three-year mean annual predicted energy production in MWh at the Petersburg location for each method. . . . .	56
27	A comparison of the three MCP/WAsP methods and the industry method in predicting the annual losses due to icing at the Petersburg location. .	57
28	A comparison of the eleven-year, eight-year, and three-year mean annual predicted energy lost due to icing in MWh at the Petersburg location for the MCP/WAsP methods ( $I_{pred}$ ) and industry method ( $I_{ind}$ ). . . . .	58
29	A comparison of the three MCP/WAsP methods and the industry method in predicting the annual losses due to icing at the Valley City location. .	60
30	A comparison of the eleven-year, eight-year, and three-year mean annual predicted energy lost due to icing in MWh for the MCP/WAsP methods and industry method at the Valley City location. . . . .	61
31	A comparison of the 50 m wind speeds determined using the MCP/WAsP method (green) and the MERRA-derived wind speeds (blue) at a MERRA grid point located at N 48.00°, W 98.00°. . . . .	64
32	A comparison of the 50 m wind speeds determined using the MCP/WAsP method (green) and the MERRA-derived wind speeds (blue) at a MERRA grid point located at N 48.00°, W 98.00°. . . . .	65
33	A comparison of hourly 10 m MERRA temperature (green) and observed surface temperature (blue) recorded at the Devil's Lake ASOS station for January 2007. . . . .	68
34	A comparison of hourly 10 m MERRA temperature (green) and observed surface temperature (blue) recorded at the Devil's Lake ASOS station for January 2010. . . . .	68
35	A comparison of hourly 10 m MERRA calculated relative humidity (green) and observed surface relative humidity (blue) recorded at the Devil's Lake ASOS station for January 2007. . . . .	69

36	A comparison of hourly 10 m MERRA calculated relative humidity (green) and observed surface relative humidity (blue) recorded at the Devil's Lake ASOS station for January 2010. . . . .	70
37	Comparison of the relative humidity calculated using the boundary-layer similarity method at 72.3 m (blue), the interpolation method at 72.3 m (red), and the surface value at 10 m (green). . . . .	71
38	Comparison of the temperature calculated using the boundary-layer similarity method at 72.3 m (blue), the interpolation method at 72.3 m (red), and the surface value at 10 m (green). . . . .	72
39	Comparison of wind speeds derived solely from MCP (blue) at the meteorological tower and derived from both MCP and WAsP (green) at the turbine location for October 2005. . . . .	75
40	Comparison of wind speeds derived using only MCP and both MCP and WAsP for October 2005 at the Petersburg location with the line of best fit shown in red (slope=1.032, y-intercept=0.1392). . . . .	76
41	Comparison of wind speeds derived using only MCP and both MCP and WAsP for January 2006 at the Petersburg location with the line of best fit shown in red (slope=1.045, y-intercept=0.1088). . . . .	77
42	A comparison of the determination of the optimal relative humidity using the boundary layer similarity method with MCP/WAsP winds at Petersburg (green) and Valley City (red). . . . .	86
43	A comparison of the boundary-layer similarity method with MCP/WAsP-derived winds at Valley City using the Petersburg result (dark blue) and by retraining the data (light blue) to predict annual losses due to icing. Observed losses are the red dashed line while the industry method losses are the black line. . . . .	87
44	A comparison of the eleven-year, eight-year, and three-year mean annual predicted energy lost due to icing in MWh at the Valley City location for the industry method and both untrained and trained boundary-layer similarity methods with MCP/WAsP-derived winds. . . . .	89
45	The boundary layer similarity method with MCP derived winds (with and without residual error) to predict percentage annual losses due to icing at the Petersburg location as compared to the industry method. . . . .	90

46	The boundary layer similarity method with MCP derived winds (with and without residual error) to predict annual losses due to icing at the Petersburg location as compared to the industry method. . . . .	92
47	MCP/WAsP-derived wind speeds with and without residual error included in the analysis at the Petersburg location for January 2006. . . . .	93

## LIST OF TABLES

Table	Page
1 Typical properties of accreted atmospheric ice. Table from International Standards Organization (2001). . . . .	8
2 Meteorological parameters controlling atmospheric icing. Table from International Standards Organization (2001). . . . .	8
3 Number of days during which the average temperature was below $-20\text{ }^{\circ}\text{C}$ ( $253.15\text{ K}$ ) at the Devil's Lake (DVL) ASOS station from 1990-2005 . . .	10
4 Overview of the six methods used to determine temperature, relative humidity and wind speed at the turbine hub height (72.3 m). . . . .	22
5 Eleven-season mean of wind speed ( $\text{m s}^{-1}$ ) and hourly energy production (kWh) and their standard deviations for each of the six methods used in this study. No observed wind speed data exists for this location . . . . .	46
6 The optimal relative humidity values at the Petersburg location determined for each method based on eight years of data. . . . .	54
7 A comparison of the mean absolute difference between the observed annual losses and both the predicted annual losses and the industry method at the Petersburg location for the three test seasons and the entire dataset.	55
8 A comparison of the mean absolute difference between the observed annual losses and both the predicted annual losses and the industry method at the Valley City location for the three test seasons and the entire dataset.	59
9 A comparison of the mean monthly temperatures of the 10 m MERRA data and at the Devil's Lake (DVL) ASOS station. . . . .	69

10	A comparison of the mean monthly relative humidity of the 10 m MERRA data and at the Devil's Lake (DVL) ASOS station. . . . .	70
11	Comparison of the percentage of time for the month of December 2007 when calculated temperatures are lower than the surface value and calculated relative humidities are higher than the surface value. . . . .	74
12	Estimates of annual financial losses for a single turbine at the Petersburg location for each of the three MCP/WAsP prediction methods, the industry method, and the observed icing losses, assuming a cost of energy production of \$30/MWh. . . . .	83
13	Predicted average annual losses due to icing compared with observed icing losses for Valley City and Petersburg locations over all eleven years, over the eight training years, and over the three testing years. . . . .	85
14	A comparison of the mean absolute difference between the observed annual losses and both the predicted (untrained and trained) annual losses and the industry method for the three test seasons and the entire dataset. Data is for the Valley City location . . . . .	88
15	A comparison of the mean absolute difference between the observed annual losses and both the predicted annual losses (with and without residuals) and the industry method at the Petersburg location for the three test seasons and the entire dataset. Predicted losses are determined with MCP/WAsP-derived wind speeds. . . . .	91

## ACKNOWLEDGMENTS

First, my advisor, Dr. Gretchen Mullendore, for always being available to discuss new ideas and solutions to problems that popped up along the way. Her patience and support throughout this whole process is deeply cherished. I would like to thank Dr. Brandon Storm for guiding the committee and I through the many facets of the wind energy industry, and for allowing me to learn along side him the intricacies of wind resource assessment. I would like to thank Dr. David Delene for his constructive and insightful comments at the various stages of this research. I thank him for reading and commenting on the many revisions of this manuscript and appreciate the high standards he sets for me. I would like to thank both Wanda Seyler and MaryAnn Gregoire, for all their assistance in the administrative details they've helped me with over the past two and half years and for always having a smile on their faces. As a newcomer to the field of atmospheric science I sincerely appreciate all of the knowledge that has been passed on to me by both faculty and students within the department. I would like to thank EAPC Wind Energy for providing me with employment and the necessary funding to complete this research. I would also like to thank Mr. Ed Rekkedal of Minnkota Power Co-Op for providing us with the turbine production data. Last but not least, I would like to thank all of my friends and family for supporting me in my crazy endeavour to move to a new country to pursue a Masters degree.



I dedicate this thesis to my parents, Gail and John, and to my two wonderful sisters, Aimee and Kerri, for their continued love and support.

## ABSTRACT

The Northern Plains region of the United States is home to a significant amount of potential wind energy. However, in winter months capturing this potential power is severely impacted by the meteorological conditions, in the form of icing. Predicting the expected loss in power production due to icing is a valuable parameter that can be used in wind turbine operations, determination of wind turbine site locations and long-term energy estimates which are used for financing purposes. Currently, losses due to icing must be estimated when developing predictions for turbine feasibility and financing studies, while icing maps, a tool commonly used in Europe, are lacking in the United States. This study uses the Modern-Era Retrospective Analysis for Research and Applications (MERRA) dataset in conjunction with turbine production data and in-situ wind measurements to investigate six methods of predicting seasonal losses (October-March) due to icing at two sites located in Petersburg, ND and Valley City, ND. The prediction of icing losses is based on temperature and relative humidity thresholds and is accomplished using six methods. Three methods use a Measure-Correlate-Predict (MCP) and flow model (WAsP) analysis for the determination of wind speeds and MERRA for temperature and relative humidity, while three methods use MERRA for all three variables. For each season from 2002 to 2010, the predicted losses due to icing are determined for a range of relative humidity thresholds and compared with observed icing losses. An optimal relative humidity is then determined and tested on all seasons from 2002 to 2013. The prediction methods are then compared to a common practice used in the wind energy industry of assuming a constant

percentage loss for icing over the same time period.

The three methods using MERRA data alone show severe deficiencies in the accurate determination of wind speeds which leads to a large underprediction in accurate power output. Of the three MCP/WAsP methods, the method using boundary-layer similarity theory to determine temperature and relative humidity shows the most accuracy in predicting icing losses closest to observed losses at the Petersburg location with an average absolute difference of  $2.13 \% \pm 1.29 \%$ . This is a significant improvement over using a constant value which produces an average absolute difference of  $5.87 \% \pm 4.64 \%$ . Analysis at the Valley City location shows similar results when the datasets are retrained to that location.

## CHAPTER 1

### INTRODUCTION

Wind turbines operating in cold regions of the world are prone to higher production losses and increased loads due to ice accumulation compared to those operating in temperate locales. In many cases, standard turbines are operating outside their design limits when exposed to either extremely low temperatures or meteorological conditions conducive to icing. As a result, these extreme conditions can lead to premature mechanical failures and thus financial losses. In addition to the mechanical issues, icing can also impact the health and safety of those in the vicinity. Heavy loads of ice can increase the noise levels of a wind turbine and ice can be thrown from the blades, potentially onto nearby roadways. In addition, energy yield calculations for sites where icing conditions prevail have a higher uncertainty compared with standard conditions (Baring-Gould et al., 2012).

The selection of potential wind turbine locations involves a rigorous process that comprises long-term feasibility studies, siting studies, and a financial analysis. As part of these feasibility studies, power losses due to icing must be estimated. These losses are typically estimated as a constant percentage of total annual production. Power losses due to icing can be highly variable between icing events, between seasons, and across different locations within a wind farm or regionally, so by utilizing a constant and unchanging percentage for prediction of these losses, that variability is not represented. For instance, if the predicted power losses for a location are under-

predicted, the turbine owner or operator will be losing anticipated revenue since the turbine experiences more icing than was estimated. On the other hand, suppose at a potential location, predicted icing losses are so high that it would make a wind turbine inviable financially and so a decision is made to not build. If that location, however, actually experiences less icing than predicted and thus, less power losses thereby making the location financially viable, then that represents a complete loss of financial revenue since the decision was made to not build at that location.

It is clear that the accurate prediction of power losses due to icing can have significant financial implications, so the goal of this thesis is to develop methods that are more accurate than the commonly used methods to determine these losses. The presented methods are based on climatological data from a reanalysis dataset and verified using wind turbine power production data. Chapter 2 provides an overview of wind power and the meteorological aspects important for icing. Chapter 3 introduces the datasets used and the methods and procedures that are developed to determine an improved method of predicting power losses due to icing. Chapter 4 provides the results of the analysis, including the accuracy of the datasets used in the analysis. Chapter 5 discusses the results, highlights the best performing method, and includes an analysis of a second turbine based on the best performing method. Finally, Chapter 6 summarizes the main conclusions of the research.

## CHAPTER 2

### BACKGROUND

The harnessing of wind resources has long been utilized for providing mechanical means for pumping water or grinding grain, but by the early 20th century the emergence of fossil fuel-generated power provided a much more consistent power source. The 1970s saw the re-emergence of wind energy as a means to provide power due to the increasing cost of fossil fuels. Since the 1970s, the technology has steadily improved and during the late 20th century worldwide capacity had been doubling every year (Ackerman and Söder, 2000). Since 1999, the cumulative capacity in the United States has increased by 2500 % (American Wind Energy Association, 2013, Figure 1) to become one of the top two countries in total capacity (Fried, 2013) and the leading producer of wind energy in 2010 (U.S. Energy Information Administration, 2013). Wind energy technology utilizes a number of scientific disciplines such as aerodynamics, structural dynamics, various branches of engineering, and meteorology. This chapter aims to provide a general overview of the science behind the extraction of power from wind and emphasizes some of the meteorological aspects important for icing that must be taken into account.

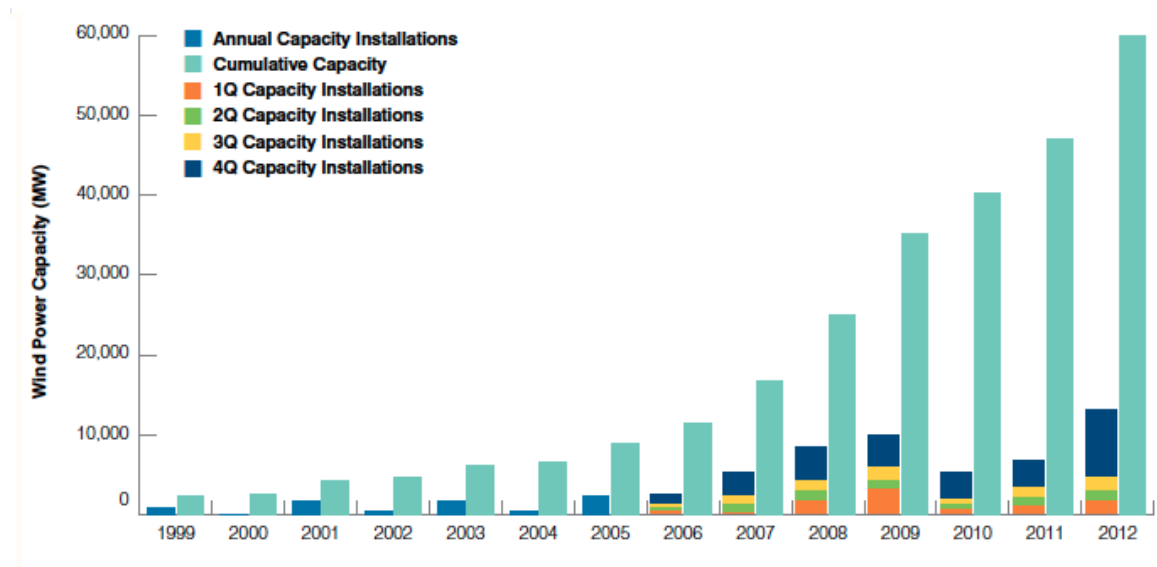


Figure 1: U.S. annual and cumulative wind power capacity growth including new installations for each quarter of each year. Figure from American Wind Energy Association (2013).

## 2.1 Physics of Wind Energy Extraction

The total amount of energy ( $E$ ) flowing through some area ( $A$ ), over some time ( $t$ ) is

$$E = \frac{1}{2}At\rho V^3 \quad (2.1)$$

where  $\rho$  is the air density in  $\text{kg m}^{-3}$  and  $V$  is the wind speed in  $\text{m s}^{-1}$ . The amount of power ( $P$ ) is simply the rate at which energy is generated over time and is therefore

$$P = \frac{1}{2}\rho AV^3 \quad (2.2)$$

The energy in the wind is converted into the rotational energy of the wind turbine, which reduces the speed of the air as it passes through the turbine area. In an isolated system, extracting all of the energy from the airstream would result in the wind speed dropping to zero as all of the wind's kinetic energy would be converted to rotational

energy. If the wind on the downstream side of the turbine blades is zero, then no further air is physically able to flow through the same area from the upstream side. If this ideal situation were the case, then the flow of air through the turbine blade area would stop and no further power could be generated. In reality, there is a limit to how much energy can be extracted from an airstream by the turbine blades, known as the Betz Law which states that no turbine can extract more than 59.3 % of the available kinetic energy of the wind (Betz, 1926). More recently, however, CFD models have shown this limit to be even lower at 30.1 % (Gorban et al., 2001).

## 2.2 Wind Turbine Overview

Wind turbines can be categorized on both their orientation (horizontal or vertical) and by the aerodynamic principle by which they generate power (lift or drag). Turbines in use today are predominantly horizontal-axis and operate using aerodynamic lift (Ackerman and Söder, 2000).

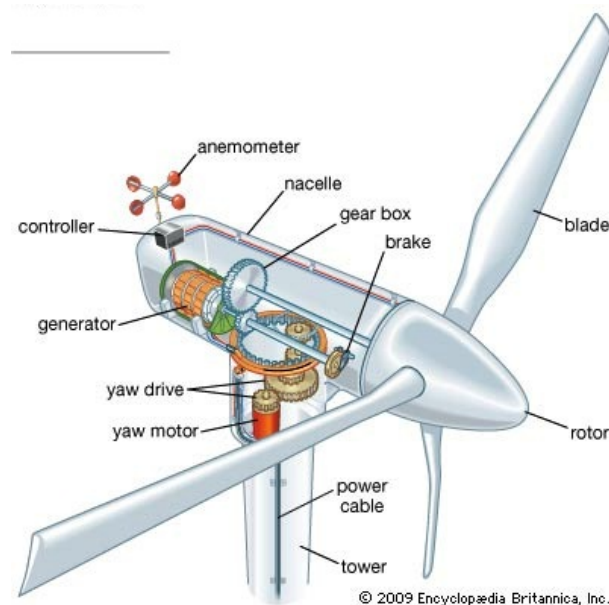


Figure 2: Schematic of a typical wind turbine with major components labelled (Encyclopædia Britannica).



As wind interacts with the blades of a typical turbine (Figure 2), both lift and drag forces are generated. Lift acts perpendicular to the airflow and drag acts parallel to the airflow. The lift force causes the blades to spin and generate torque. As the wind speed increases, the lift and drag forces also increase and thus the power generated increases as well. At high wind speeds, safety must be considered, and so turbines will cease operation at what is termed the cut-out wind speed, typically  $20 - 25 \text{ m s}^{-1}$  at hub height, to prevent excessive loads on the structure. Conversely, the turbine will not operate at speeds below what is called the cut-in speed, typically  $3 - 5 \text{ m s}^{-1}$  at hub height. Below this speed, sufficient lift is not generated and so the turbine will not spin (Ackerman and Söder, 2000).

Modern-day utility-scale turbines reach the highest efficiency with wind speeds typically between  $12$  and  $16 \text{ m s}^{-1}$ . Above this speed but below the cut-out speed, the power output must be limited to keep the power output close to its rated capacity, thereby preventing the electrical system from being overloaded. In addition, the driving forces on the blades cause excessive loads on the entire structure that must be limited. To accomplish this, turbine blades are regulated via stall regulation, pitch regulation, or a combination of both. Stall regulation involves promoting the stall effect by means of altering the turbine blade profile through the use of spoilers or stall strips. These have the effect of lowering the power output at higher wind speeds. Pitch regulation involves changing the angle at which the blades encounter the oncoming air stream, thus the aerodynamic forces are altered in order to maintain a constant power output (Ackerman and Söder, 2000).

### 2.3 Power Losses Due to Icing

The moving parts of a turbine lead to frictional losses, contamination of the blade surfaces (insects, dust, and dirt) lead to changes in the aerodynamics of the blades, turbulence of the air stream changes the aerodynamic performance of the turbine, and finally, meteorological factors causing icing can also impact the blade surfaces. During icing events, ice accumulates on the turbine blades, reducing the aerodynamic efficiency and torque, which leads to power losses. Light icing events, can produce a large enough change in surface roughness of the blade to cause a drop in production, while severe icing events can introduce complete loss of production if the turbine blades stop turning (Hochart et al., 2008). Jasinski et al. (1998) mention that the slightest amount of surface roughness caused by icing has the potential to reduce energy production by 20 %.

The three main forms of icing which impact wind turbine power production, are rime ice, glaze ice, and wet snow accretion. Each has different properties and is formed under different atmospheric conditions (Tables 1 and 2). Typically forming between 0 °C (273.15 K) and -20 °C (253.15 K), rime ice occurs when super-cooled liquid water droplets from clouds or fog are transported by the wind or by gravity and impact a hard surface, such as a turbine blade, whose temperature is near or below freezing. Small droplets form soft rime, which is fragile and snow-like, while large droplets form hard rime which has a higher density and can adhere firmly on surfaces, making it difficult to remove. Glaze ice, typically forming between 0 °C (273.15 K) and -6 °C (267.15 K), is caused by freezing precipitation or wet in-cloud icing and forms a smooth, transparent, and homogeneous layer of ice that adheres strongly to the structure. Glaze ice is typically of higher density than rime ice. Wet

snow, typically forming between 0 °C (273.15 K) and 3 °C (276.15 K), occurs when wet snow accumulates and adheres to the surface. If a temperature decrease occurs after accretion, the wet snow will freeze and form a layer of ice on a surface (Baring-Gould et al., 2012).

Table 1: Typical properties of accreted atmospheric ice. Table from International Standards Organization (2001).

Type of Ice	Ice Density (kg m <sup>-3</sup> )	Adhesion and Cohesion	Color	Shape
Glaze	900	Strong	Transparent	Evenly Distributed/Icicles
Wet Snow	300 to 600	Weak(forming) Strong (frozen)	White	Evenly Distributed/Eccentric
Hard Rime	600 to 900	Strong	Opaque	Eccentric, Pointing Windward
Soft Rime	200 to 600	Low to Medium	White	Eccentric, Pointing Windward

Table 2: Meteorological parameters controlling atmospheric icing. Table from International Standards Organization (2001).

Type of Ice	Air Temperature (°C)	Wind Speed (m s <sup>-1</sup> )	Droplet Size	Water Content of Air	Typical Duration
Glaze (precip)	-10 to 0	Any	Large	Medium	Hours
Wet Snow	0 to 3	Any	Flakes	Very High	Hours
Glaze (in-cloud)	see Figure 3	see Figure 3	Medium	High	Hours
Hard Rime	see Figure 3	see Figure 3	Medium	Medium	Days
Soft Rime	see Figure 3	see Figure 3	Small	Low	Days

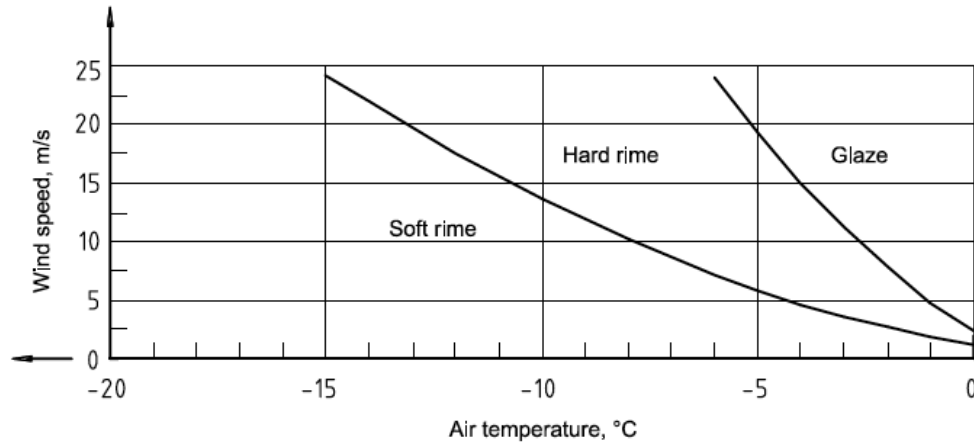


Figure 3: Type of accreted ice as a function of wind speed and air temperature. Figure from International Standards Organization (2001).

Low temperature climate areas are those regions where periods with temperatures below the operational limits of standard wind turbines without cold weather modifications occur. More specifically the temperature must average  $-20\text{ }^{\circ}\text{C}$  ( $253.15\text{ K}$ ) more than nine days per year or the average annual temperature must be below  $0\text{ }^{\circ}\text{C}$  ( $273.15\text{ K}$ ). Icing climate areas are those where icing events occur. A cold climate region exists when both types of climate occur (Baring-Gould et al., 2012).

To classify the current study area, a nearby Automated Surface Observing System (ASOS), located in Devils Lake, ND, is used. This ASOS is located approximately 73 km to the west of one of the study sites in Petersburg, ND. Table 3 shows that from 1990 to 2005, the average number of days per year during which the temperature dropped below  $-20\text{ }^{\circ}\text{C}$  ( $253.15\text{ K}$ ) was 30.1.

Table 3: Number of days during which the average temperature was below  $-20\text{ }^{\circ}\text{C}$  ( $253.15\text{ K}$ ) at the Devil's Lake (DVL) ASOS station from 1990-2005

Year	# of Days Below $-20\text{ }^{\circ}\text{C}$
1990	22
1991	20
1992	23
1993	43
1994	44
1995	39
1996	55
1997	31
1998	21
1999	22
2000	28
2001	17
2002	21
2003	41
2004	31
2005	23
Average	30.1

Due to the close proximity and similar topography, it is safe to assume that a similar temperature statistic exists at the study location and since icing is known to occur it can be classified as a cold climate region.

When power loss occurs due to icing, the incident is termed an icing event. Each icing event is made up of four separate phases: meteorological icing, instrumental icing, incubation time, and recovery time (Baring-Gould et al., 2012). Meteorological icing is the period during which meteorological conditions are favorable for ice accretion. Instrumental icing is the period during which ice remains on a structure, or when the turbine is disturbed by ice. Incubation time is the delay between the onset of

meteorological icing and instrumental icing. Lastly, recovery time is the delay between the end of meteorological icing and the end of instrumental icing. It is important to note that the incubation time and recovery time are not equal since they depend on different factors. The recovery time is a function of how quickly ice will melt or fall off and, if conditions are right, ice may remain on a turbine for many hours, or even days, after meteorological icing has ended.

### **2.3.1 Methods of Determining Icing Conditions**

Determining whether icing conditions are present can be accomplished directly, by measuring the ice accretion, or indirectly, by measuring variables that cause icing or that correlate with the occurrence of icing (Fikke et al., 2007). Total ice accretion can be measured directly using various types of instruments that measure changes in vibrating frequency, changes in electrical properties, or optical properties (Fikke et al., 2007). To indirectly determine icing conditions, one has to consider the meteorological conditions that impact icing, including wind speed, air temperature, liquid water content (LWC), and droplet size distribution. LWC and droplet size distribution are difficult to measure operationally since there are many unwanted variables, such as turbine shadowing, that exist when placing an instrument at the turbine hub height, so other variables must be measured. A simplified approach has been to define icing events as periods of time where the temperature is below 0 °C (273.15 K) and the relative humidity is above 95% (Fikke et al., 2007). However, recommended practices (Baring-Gould et al., 2012) suggest that the combination of air temperature below 0 °C (273.15 K) and a high relative humidity strongly overestimates the frequency of icing on structures. If water droplets are small enough, they may be transported around a turbine blade rather than hitting it and accreting on the surface. In addition, measurements of relative humidity are generally performed using WMO standards

where the saturation water vapor pressure is calculated with respect to water. Below 0 °C (273.15 K), saturation cannot be reached using that procedure. Cattin et al. (2008) showed that calculating relative humidity with respect to the saturation vapor pressure over ice for temperatures below 0 °C (273.15 K), improved the detection of icing conditions by 10 % in their studies. In addition, they found that by including a third parameter, sky temperature, which uses the incoming long-wave radiation, icing detection seemed to improve.

### **2.3.2 Modeling of Icing**

The modeling of icing on turbine blades focuses on short-term icing events and is used to understand ice accretion mechanisms and how this accreted ice affects the aerodynamic characteristics of the blades. Although the goal of this study is the prediction of seasonal icing losses (i.e. not single icing events), this section is included to provide information on ice modeling research and to contrast it with the icing prediction algorithm used in this study. In order for the modeling of icing to be successful, it must describe the frequency, duration, and severity of icing events, in addition to estimating the amount of ice accreted. As computing power improves, the precision and accuracy of these models increases as well. In general, the two main categories of ice models are empirical models, relying on statistical analysis of historical data and physical models, relying on the specific definition of the required parameters.

Empirical models rely on historical or climatological data at a particular location. Most are used to determine only the frequency of icing events, but some more sophisticated models can describe both the frequency and the rate of icing accretion that occurs. For example, the frequency of in-cloud icing events could be determined given historical temperature, site elevation, and cloud information. The empirical model is

modified to include statistical values of other parameters such as wind speed, wind direction, and droplet size distribution in order to estimate the ice accretion at a particular site (Rindeskär, 2010). Nevertheless, the physical models can still describe icing events more accurately.

Physical models rely on the specific definition of both the meteorological parameters and the turbine shape and size. These models can be used to determine ice accretion or to predict icing events in the short-term by combining mesoscale models such as the Weather Research and Forecasting (WRF) model or the Coupled Ocean/Atmosphere Mesoscale Prediction System (COAMPS) (Chen et al., 2003) with ice accretion models. Ice accretion prediction can be accomplished using the Turbine Blade Icing Model (TURBICE) (Makkonen et al., 2001) or the Lewis Ice Accretion Program (LEWICE) (Wright, 2008), which model ice growth on two-dimensional airfoil sections. TURBICE, developed by the Technical Research Centre of Finland, models ice growth in an airflow perpendicular to the airfoil axis. It calculates the impact point on the turbine blade and can determine the ice density and surface roughness. In addition, it determines the heating demand for melting of accumulated ice. Wind tunnel tests show the TURBICE models ice accretion in good agreement for dry-growth but not for wet-growth, which is common where temperatures are near 0 °C (273.15 K). LEWICE, developed by NASA, is primarily used to model accretion on airplane wings but has been modified for other applications. It uses an iterative process to model both dry growth and wet growth icing in addition to calculating heating power, similar to TURBICE (Rindeskär, 2010).

Case studies performed in Switzerland using a physical model developed by Makkonen (2000) combined with two mesoscale models showed good potential for describing the



frequency of icing but simulating ice loads were less precise (Dierer et al., 2009). In addition, Rindeskär (2010) used both a statistical method, dependent on temperature, wind speed, and liquid water content, and physical models to determine ice loads. That study found that the statistical approach was unsatisfactory in reproducing ice loads that compared well with observations, but similar to Dierer et al. (2009), the physical models did show some promise in the timing of icing events. That study also was unable to determine any significant correlation between ice load and power losses.

The model used in this study is an empirical model that uses downscaled global historical meteorological data in order to predict total seasonal power losses due to icing at a particular location. By predicting seasonal losses rather than losses associated with individual events, the temporal error, especially in terms of length and severity, is not as critical as in the case studies previously mentioned.

## CHAPTER 3

### DATA AND METHODOLOGY

This chapter aims to describe the methods and procedures that are developed in order to determine the best method for predicting annual power losses due to icing at specific wind turbines located in North Dakota. The first section describes each of the three datasets used in the analysis. These data include the Modern-Era Retrospective Analysis for Research and Applications (MERRA) provided by the National Aeronautics and Space Administration (NASA), the wind turbine production data, and in-situ anemometer data. In addition, the procedure to extrapolate the anemometer dataset to the turbine locations is included. The second section outlines the six methods of determining the required atmospheric variables (wind speed, temperature, and relative humidity) at the turbine height. The final section describes the method used to determine icing-induced power losses.

#### 3.1 Experimental Data

##### 3.1.1 Modern-Era Retrospective Analysis for Research and Applications (MERRA) Dataset

NASA's MERRA dataset (Rienecker et al., 2011) is one of several reanalysis datasets that are used to create a completely gridded meteorological dataset with worldwide coverage from 1979 to the present, which corresponds to the satellite era. The location of the two wind turbines and the area of MERRA coverage used to analyze each one are shown in Figure 4.

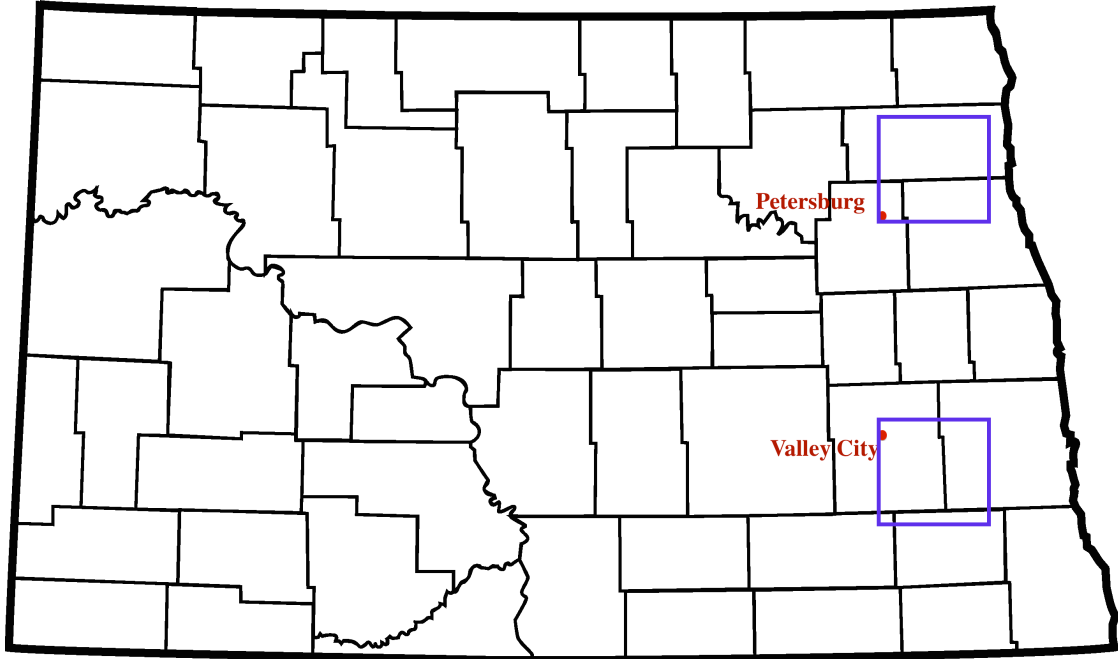


Figure 4: The location of the turbines used in this study within North Dakota. The four MERRA gridpoints used at each turbine are the vertices of the purple squares.

Three subsets of the MERRA dataset are used: a two-dimensional, surface-level, hourly-averaged dataset containing standard meteorological parameters, herein referred to as the surface-level dataset; a three-dimensional, 72-level, 6-hourly instantaneous dataset containing standard meteorological parameters, herein referred to as the model-level dataset; and a two-dimensional, surface-level, hourly-averaged dataset containing surface turbulent flux parameters, herein referred to as the surface flux dataset. The surface-level dataset contains temperature and specific humidity at 2 m and 10 m, wind speed at 2 m, 10 m, and 50 m, and surface pressure. The model-level dataset contains temperature, specific humidity, and wind speed at 72 levels throughout the atmosphere. For each time step, the vertical distance between each of the 72 levels varies, so the depth of each level (in Pa) is provided as well. However, only the first level above the surface is needed. The surface flux dataset contains parameters that can be used in surface layer and boundary layer analyses. These include sensible

and latent heat fluxes, roughness lengths, displacement height, and surface scaling parameters. Each variable is determined at the location of the turbine using a linear, horizontal interpolation between the four grid points that surround the turbine location. These grid points are spaced  $2/3^\circ$  ( $\approx 52$  km) in the east-west direction and  $1/2^\circ$  (55.6 km) in the north-south direction.

### 3.1.2 Turbine Production Dataset

Minnkota Power Co-Op (herein referred to as Minnkota), based in Grand Forks, North Dakota, owns and operates the two wind turbine sites shown in Figure 4. The turbines are NEG Micon NM52/900 with a 72.3 m hub height, rotor diameter of 52 m, and rated power of 900 kW. The turbine production dataset contains hourly power production data of both turbines since they began operation in 2002 until the present. These data are calculated by taking the average of the four 15-minute instantaneous values over each one hour period. In addition to production data, a record of periods when the turbines underwent maintenance is included for 2008 until 2012. Some of these records indicate periods when the turbines were not running due to icing, however, since a full record does not exist for the time period of this study, these data are not used.

### 3.1.3 Anemometer Dataset

A meteorological tower located in close proximity to one of the turbines (location withheld due to confidentiality), is outfitted with several instruments, including cup anemometers (Vector A100LK and NRG #40C), direction vanes (NRG #200P), a temperature sensor (NRG #110S), and a barometric pressure sensor (NRG #BP20). One of each type of anemometers are placed in pairs opposite each other at three heights above the ground (20.12 m, 41.53 m and 59.46 m) while a direction vane is

located two meters below each of the pairs of anemometers. The temperature and pressure sensors are located two meters and one meter above the ground, respectively. These instruments were in use and collecting data beginning in June 2010 and continue to collect data at the time of this writing. The subset of data from June 2010 to December 2012 is used in this study. As with any in-situ measurement, the data from each anemometer must undergo a quality control procedure to eliminate any invalid data. The quality control procedure is accomplished using Windographer, wind industry software developed by Mistaya Engineering Inc (2013). The two major issues impacting the data are tower shading and instrument icing. Tower shading occurs when the airflow is disrupted by the tower structure itself, leading to inaccurate measurements for certain wind directions. Since the anemometers at each height are located on opposite sides of the tower, only one of each pair will ever experience tower shading at a given time and only for specific wind directions. For these data, wind directions within 25 degrees of the orientation of any anemometer were eliminated. For example, if an anemometer is oriented at 90 degrees, data whose wind directions are from 65 degrees through 115 degrees are eliminated for that anemometer only.

Unfortunately, eliminating data due to instrument icing is not as straightforward as the tower shading elimination process. In cases where there is no instrument that directly measures icing, the data elimination process becomes subjective. For example, when a direction vane shows a minimal change in its measurement (less than 0.01 degrees per 10 minute time step), and the temperature is less than 2 °C (275.15 K), icing is assumed for that time period. If during that same time period an anemometer at the same height shows a wind speed of less than 0.5 m s<sup>-1</sup>, icing is assumed to be affecting that device as well. Data can also be removed if it appears that ice may be impacting the measurements outside of the above criteria, which can occur if ice

remains on one of the instruments for a significant period of time before it finally melts or falls off.

The quality controlled anemometer data for each pair is combined together to produce a single set of measurements for each height, also known as a patched dataset. The Vector anemometer is used as the primary source, except in cases where data had been removed in the quality control process, and then the measurements from the NRG anemometer are used for that time period. If, for the same time period, measurements from the NRG anemometer were also removed in the quality control process, then that time period will have no data. The resultant dataset then consists of one set of wind speed and direction measurements at three heights. The quality control procedure was done by EAPC Wind Energy who have provided the data for this study.

#### **3.1.4 Extrapolation of Anemometer Dataset**

The quality controlled dataset covers only a short period of time and a single location that is not co-located with the turbine and so it must be lengthened, or long-term corrected to cover the same time period of both the Minnkota and MERRA datasets. The dataset also must be extrapolated spatially to the turbine location and vertically to the turbine hub height. The long-term correction is accomplished by using Measure-Correlate-Predict (MCP) analysis. MCP analyses are used to predict the wind resources for wind power development. This prediction is accomplished by modeling the relationship between in-situ wind data and concurrent data from a nearby reference site with the desired long-term time record. The regression model is then used to predict the long-term wind speed and direction distributions at the target site based on long-term data. Although several MCP algorithms exist (Rogers et al., 2005), the method used for this study is a 1st order linear regression model as outlined

in Thørgersen et al. (2013). The MCP analysis is performed using WindPRO, wind industry software developed by EMD International A/S (2013b).

For this algorithm, the anemometer dataset is the in-situ measurement, while the long-term reference data is the 50-m wind speed data from the closest MERRA grid point, located 18 km from the meteorological tower. Using the closest grid point is more beneficial than interpolating to the measurement site using the four nearest MERRA grid points, as was done section 3.1.1. The regression model used in WindPRO has the form

$$Y = \beta_1 x + \beta_0 + e \quad (3.1)$$

where  $Y$  is the MERRA wind speed,  $x$  is the measured wind speed,  $e$  is the residual error and the  $\beta$  terms are the regression parameters. The regression model is binned in one-degree increments according to the wind direction of the reference data and so each wind direction will have its own set of regression parameters and residual error. The regression parameters are estimated by minimizing the squared sum,  $SS_R$ , of the following equation:

$$\sum_{i=1}^n [Y_i - (\beta_1 x_i + \beta_0)]^2 \quad (3.2)$$

The residual errors are calculated using what is referred to as first order Gaussian resampling. The reference wind speed range is divided into a number of intervals. Within each interval, the observed scatter, or residual, is found as a standard deviation of the scatter together with the bias of the observations. Both are applied when transferring the reference data to the site data (EMD International A/S, 2013a). WindPRO allows the user to turn on or turn off the residual error in its calculations,

with the documentation recommending they be left on. In consultation with Dr. Brandon Storm, however, leaving the residual error on can introduce an unrealistic wind speed time series, that could impact analyses on time scales shorter than a day (2014, personal communication). The residual error is left on for the initial analysis, however, the impact of removing the residual is presented as a comparison in Chapter 5.

The result of the MCP analysis is that the wind speeds are estimated at the meteorological tower for the required time period (August, 2002 through July, 2013). The use of measured or long-term corrected data for wind resource calculations results in estimates that are only representative of the location of the measurements. In order to apply these measured wind speed statistics to a region, some method is required to transform the wind speed statistics. This is accomplished using Wind Atlas Analysis and Application Program (WAsP) (Troen and Petersen, 1989). WAsP consists of a comprehensive set of models for the horizontal and vertical extrapolation of meteorological data in order to estimate wind resources. The models are based on the physical principles of flows within the boundary layer and take into account the effects of surface conditions, sheltering due to obstacles, and the variations in height of the meteorological station in which the measurements are taken. WindPRO allows the user to apply WAsP to the data using the PARK module in order to produce a long-term corrected dataset at the turbine location and height (72.3 m AGL). This module also includes an air density correction at the turbine height based on climatological data.



### 3.2 Methods of Determining Atmospheric Variables at the Turbine Height

In order to properly relate the MERRA and anemometer datasets to the Minnkota dataset, the atmospheric variables that will be used in the icing prediction algorithms need to be calculated at the height of the turbine. A single height is used rather than a range because since the turbine blades are 26 m long, they will experience different meteorological conditions as they rotate. The center of this axis of rotation is the hub height of the turbine (72.3 m AGL) and so this point represents the average conditions experienced by the blades. Three methods have been developed to determine temperature, relative humidity, and wind speed using the MERRA dataset. In the preceding section, wind speeds were determined from the anemometer dataset and so for each method, both sets of wind speeds are used, for a total of six methods for testing, shown in Table 4.

Table 4: Overview of the six methods used to determine temperature, relative humidity and wind speed at the turbine hub height (72.3 m).

	Temperature	Relative Humidity	Wind Speed
Method 1a	Boundary-Layer Similarity Theory	Boundary-Layer Similarity Theory	Boundary-Layer Similarity Theory
Method 1b	Boundary-Layer Similarity Theory	Boundary-Layer Similarity Theory	MCP/WAsP-Analysis
Method 2a	10 m Values	10 m Values	Extrapolation of Surface Values
Method 2b	10 m Values	10 m Values	MCP/WAsP-Analysis
Method 3a	Interpolation of Surface and Upper Level	Interpolation of Surface and Upper Level	Interpolation of Surface and Upper Level
Method 3b	Interpolation of Surface and Upper Level	Interpolation of Surface and Upper Level	MCP/WAsP-Analysis

### 3.2.1 Methods 1a and 1b: Boundary-Layer Similarity Theory

In many situations within the boundary layer, deriving laws based on first principles is limited to our knowledge of the governing physics involved (Stull, 1988). Turbulence within the boundary layer is one such example. The equations of motion describe turbulent fluctuations but generating solutions to these equations is very difficult. Similarity theory aims to organize and group experimental data in order to create empirical relationships for these types of situations (Beljaars, 1992). Atmospheric stability plays an important role in the behavior of the atmosphere and the profile of atmospheric variables. From Beljaars (1992) the stability of the boundary layer can be represented by the Obukhov length,  $L$  (m), defined as:

$$L = -\frac{U_{*o}^3 \bar{\theta}_v}{\kappa g \overline{w'\theta'_v}} \quad (3.3)$$

where  $U_{*o}$  is the shear velocity ( $\text{m s}^{-1}$ ),  $\kappa$  is the von Karmen constant, typically equal to 0.41,  $\bar{\theta}_v$  is the surface virtual potential temperature (K),  $\overline{w'\theta'_v}$  is the kinematic virtual potential temperature flux ( $\text{K m s}^{-1}$ ), and  $g$  is the gravitational constant ( $9.81 \text{ m s}^{-2}$ ). Obukhov lengths with positive values less than 500 m are considered stable, negative values greater than -500 m are unstable, and values above 500 m or below -500 m are neutral (Pena et al., 2009). The wind, temperature, and moisture profiles behave differently throughout the boundary layer and so each is represented by its own set of equations based on the stability of the atmosphere. However, these relationships change depending on the position within the boundary layer. The surface layer extends to approximately 10% of the height of entire planetary boundary layer while above that is the mixed layer.

Within the surface layer, many properties are assumed to be constant, including surface fluxes and friction velocities, while in the mixed layer they are decreasing until the top of the boundary layer (Stull, 1988; Gryning et al., 2007).

The MERRA surface flux dataset and the surface level dataset contain all the variables needed to perform boundary layer similarity calculations. The kinematic virtual potential temperature flux used to calculate the Obukhov length is determined from:

$$\overline{w'\theta'_v} = \frac{h}{\rho C_p} + 0.61\theta \frac{e}{\rho\lambda} \quad (3.4)$$

where  $h$  is the sensible heat flux ( $\text{W m}^{-2}$ ),  $\rho$  is the air density ( $\text{kg m}^{-3}$ ),  $C_p$  is specific heat capacity of air at constant pressure ( $\text{J kg}^{-1}$ ),  $e$  is the latent heat flux ( $\text{W m}^{-2}$ ),  $\lambda$  is the latent heat of vaporization of water ( $\text{J kg}^{-1}$ ), and  $\theta$  is the potential temperature (K).

Pena et al. (2009) show that the following equations for the wind profile can be used above the surface layer as they showed good agreement with observations up to 100 m for a very stable atmosphere, and up to 300 m for all other stability classes. The stability parameter  $\Psi_m$  is taken from Beljaars and Holtslag (1991).

For a stable atmosphere:

$$U = \frac{U_{*o}}{\kappa} \left[ \ln\left(\frac{z}{z_o}\right) + b \frac{z}{L} \left(1 - \frac{z}{2z_i}\right) \right] + \frac{U_{*o}}{\kappa} \left[ \frac{\kappa z}{\lambda} \left(1 - \frac{z}{2z_i}\right) - \frac{z}{z_i} \right] \quad (3.5)$$

For a neutral atmosphere:

$$U = \frac{U_{*o}}{\kappa} \left[ \ln\left(\frac{z}{z_o}\right) + \frac{\kappa z}{\lambda} \left(1 - \frac{z}{2z_i}\right) - \frac{z}{z_i} \right] \quad (3.6)$$

For an unstable atmosphere:

$$U = \frac{U_{*o}}{\kappa} \left[ \ln\left(\frac{z}{z_o}\right) - \Psi_m + \frac{\kappa z}{\lambda} \left(1 - \frac{z}{2z_i}\right) - \frac{z}{z_i} \right] \quad (3.7)$$

where:

$$\Psi_m = 2 \ln\left(\frac{1+x}{2}\right) + \ln\left(\frac{1+x^2}{2}\right) - 2 \tan^{-1} x + \frac{\pi}{2} \quad (3.8)$$

$$x = \left(1 - 16 \frac{z}{L}\right)^{\frac{1}{4}} \quad (3.9)$$

$$\lambda = 0.00027 \frac{G}{f_c} \quad (3.10)$$

and

$$G = \frac{U_{*o}}{\kappa} \sqrt{\left(\ln\left(\frac{U_{*o}}{z_o f_c}\right) - 1.9\right)^2 - 4.9^2} \quad (3.11)$$

$z$  is the height above the displacement height (m),  $z_o$  is the roughness length (m),  $z_i$  is the height of the planetary boundary layer (m), and  $f_c$  is the Coriolis parameter ( $s^{-1}$ ). The coefficient,  $b$ , is an experimentally determined constant and found to be either 6.0 or 4.7 depending on the experimental data (Pena et al., 2009). For time periods where the turbine is determined to be above the boundary layer, the geostrophic wind speed,  $G$ , will be assumed.

Within the surface layer, Paulson (1970) showed that the potential temperature profile is given by:

$$\theta = \theta_s + \theta_* [\ln(\frac{z}{z_o}) - \Psi_H] \quad (3.12)$$

where for stable conditions:

$$\Psi_H = (1 + \frac{2z}{3L})^{\frac{3}{2}} + \frac{2}{3} (\frac{z}{L} - \frac{5}{0.35}) \exp(-\frac{0.35z}{L}) + \frac{7}{3} \quad (3.13)$$

and for unstable conditions:

$$\Psi_H = 2 \ln(\frac{1 + x^2}{2}) \quad (3.14)$$

$\theta$  is the potential temperature (K) at some height,  $z$  (m), above the displacement height.  $\theta_s$  is the potential temperature at the surface (K), and  $\theta_*$  is the surface temperature scale (K).

For neutral conditions, the stability parameter,  $\Psi_H$ , is zero. Above the surface layer, the potential temperature profile is assumed to be constant from the top of the surface layer to the entrainment zone which is consistent with Stull (1988).

Similar to the potential temperature profile, the moisture profile within the surface layer is:

$$q = q_s + q_* [\ln(\frac{z}{z_o}) - \Psi_Q] \quad (3.15)$$

where for stable conditions:

$$\Psi_Q = \frac{-5z}{L} \quad (3.16)$$

and for unstable conditions:

$$\Psi_Q = 2 \ln\left(\frac{1+x^2}{2}\right) \quad (3.17)$$

$q$  is the specific humidity at some height,  $z$  (m), above the displacement height,  $q_s$  is the surface specific humidity, and  $q_*$  is the surface humidity scale. For neutral conditions, the stability parameter,  $\Psi_Q$ , is zero. Similar to the temperature profile, the moisture profile is assumed to be constant from the top of the surface layer to the entrainment zone.

The potential temperature is converted to temperature using:

$$T = \frac{\theta}{\left(\frac{100000}{P}\right)^{0.286}} \quad (3.18)$$

and the specific humidity is converted to relative humidity,  $\phi$ , using:

$$\phi = 100 \times \frac{w}{w_s} \quad (3.19)$$

and

$$w = -\frac{q}{q-1} \quad (3.20)$$

where  $w$  is the water vapor mixing ratio and  $w_s$  is the saturation water vapor mixing ratio.

The saturation water vapor mixing ratio is temperature dependent and calculated according to Murray (1967):

$$w_s = \frac{380}{p} \exp\left(\frac{17.269(T - 273.16)}{T - 35.86}\right) \quad (3.21)$$

for  $T \geq 273.16$  K and:

$$w_s = \frac{380}{p} \exp\left(\frac{21.875(T - 273.16)}{T - 7.66}\right) \quad (3.22)$$

for  $T < 273.16$  K.

The pressure,  $p$  (Pa), is adjusted for the height,  $h$ , above ground using:

$$p = p_o - \rho gh \quad (3.23)$$

where  $p_o$  is the surface pressure (Pa). For temperatures below freezing, the saturation water vapor mixing ratio is calculated with respect to ice because using the World Meteorological Organization (WMO) standard of calculating with respect to water results in saturation never being reached as shown in Figure 5.

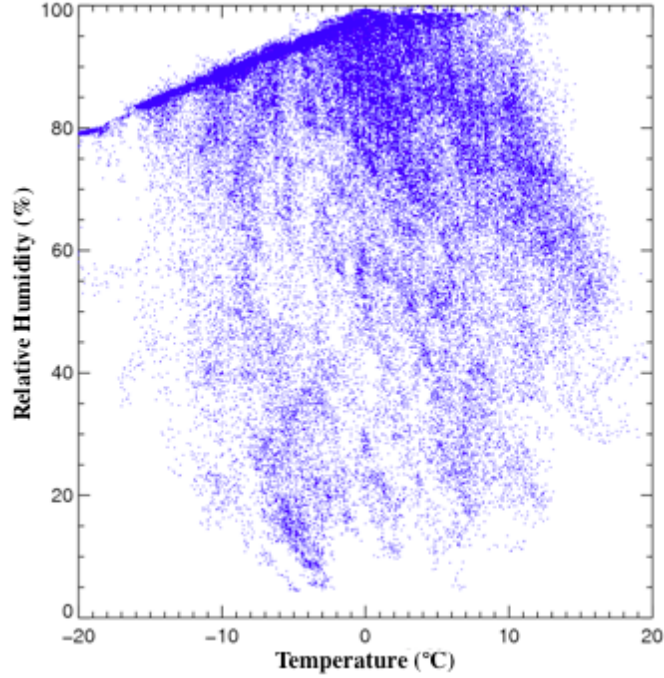


Figure 5: Relative humidity calculation using World Meteorological Organization (WMO) standards, showing that below 0 °C (273.15 K), saturation is never achieved (Cattin et al., 2008).

### 3.2.2 Methods 2a and 2b: Extrapolation of Variables

The surface level MERRA dataset contains derived wind speeds at 2 m, 10 m, and 50 m, and temperature and moisture variables at 2 m and 10 m. To determine the wind speed at the height of the turbine, the provided wind speeds are fitted to a curve of the form:

$$z = au^b \quad (3.24)$$

where  $z$  is the height above the ground (m), and  $u$  is the wind speed ( $\text{m s}^{-1}$ ), as shown in Figure 6.



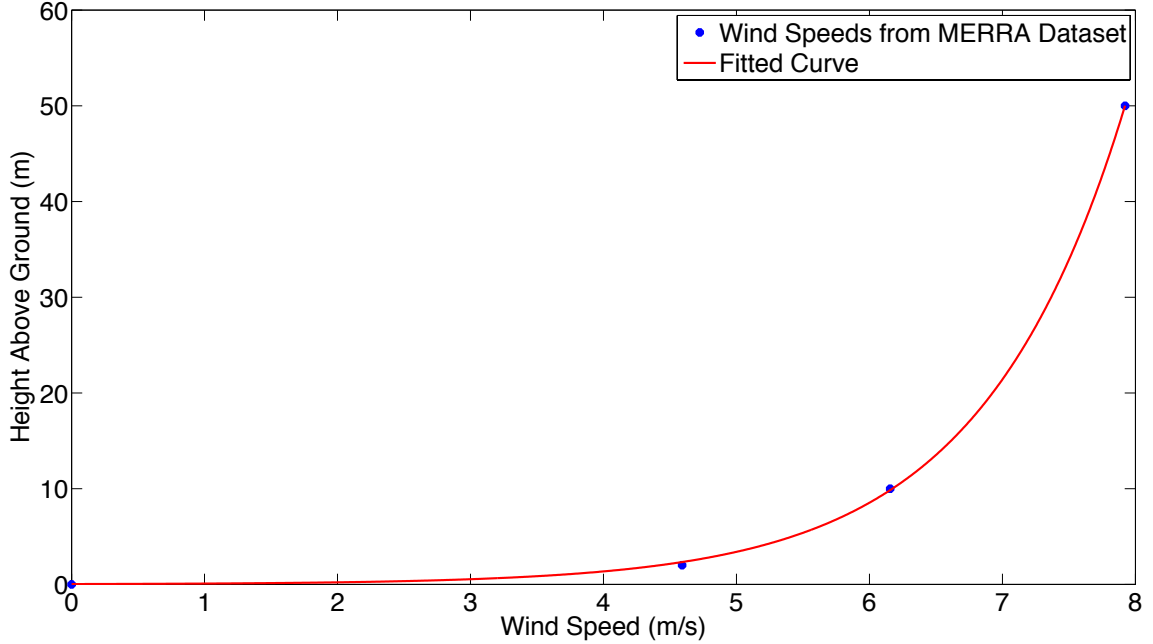


Figure 6: Equation 3.24 fitted to the 2 m, 10 m, and 50 m MERRA wind speed data for a single time step with  $a=0.03416$ ,  $b=0.9201$ ,  $R^2=0.9999$ , and  $RMSE=0.2603$ .

The coefficients of fit are given by  $a$  and  $b$ , with each time step having different coefficients. Equation 3.24 is rearranged and solved for the wind speed at the turbine height ( $z=72.3$  m):

$$u = \frac{\ln\left(\frac{z}{a}\right)}{b} \quad (3.25)$$

Unlike the wind speed, the temperature and moisture variables cannot be extrapolated from the 2 m and 10 m values as their atmospheric profiles cannot be accurately defined by an exponential function. For this method, the temperature and relative humidity values at 10 m will be used as the turbine height value.

### 3.2.3 Methods 3a and 3b: Interpolation of Variables

This method combines the surface level dataset and the model level dataset in order to interpolate the atmospheric variables at the turbine height. The model level dataset,

with a six hour temporal resolution, is resampled to a one hour resolution, using linear interpolation of each variable. At each hour, the two layers that bracket the turbine height are chosen. In all cases, one layer will be the surface level, and the second layer will be the first layer in the model level dataset. In order to interpolate between these two levels, the height of the first model layer is computed using the hypsometric equation:

$$h = \frac{RT}{g} \ln\left(\frac{P_1}{P_2}\right) \quad (3.26)$$

where  $R$  is the gas constant for dry air ( $287 \text{ J kg}^{-1} \text{ K}^{-1}$ ),  $T$  is the mean temperature of the layer (K),  $P_1$  and  $P_2$  are the atmospheric pressure (Pa) at the top and bottom of the layer, respectively, and  $g$  is the acceleration due to gravity ( $9.81 \text{ m s}^{-2}$ ). The temperature and relative humidity are easily calculated using a linear interpolation between these two levels. The wind speed,  $V_{turb}$ , at the turbine height,  $z_{turb}$ , is interpolated between the levels according to Holt and Wang (2012):

$$V_{turb} = V_b \left(\frac{Z_{turb}}{Z_b}\right)^\alpha \quad (3.27)$$

and

$$\alpha = \frac{\ln \frac{V_b}{V_a}}{\ln \frac{Z_b}{Z_a}} \quad (3.28)$$

where  $V_a$  and  $V_b$  are the wind speed at the levels above and below the turbine, respectively.  $Z_a$  and  $Z_b$  are the heights of the levels above and below the turbine, respectively. In this case, the values below the turbine height are always the surface level values at a height of 10 m, while the values above the turbine height are always those at the first model level, which has a different height at each time step.

### 3.3 Methods of Determining Power Losses Due to Icing

#### 3.3.1 Wind Industry Method

In the siting process of proposed wind turbines, the industry standard is to estimate the amount of power that will be lost annually due to various factors. This can be done by assuming a general loss for all factors such as maintenance, turbulence effects, and environmental factors or specific losses for each factor. In some cases, where data are available, icing losses can be more readily determined through the use of icing maps, while in other cases, a simple estimate is used. Although there is no universal industry method, most consulting agencies and developers do not use complex icing prediction algorithms that may be in use by wind turbine manufacturers. As such, for this study a constant value is used that represents the best estimate for icing losses prior to construction of a turbine or wind farm. For the turbines investigated in this study, no previous icing loss data is available and so in consultation with Dr. Brandon Storm of EAPC Wind Energy, the estimated annual loss in power due to icing ( $L_{ind}$ ) would amount to approximately 4.7% (2013, personal communication).

#### 3.3.2 Method to Determine Observed and Predicted Power Losses Due to Icing

Reanalysis data does not include complex variables such as liquid water content or droplet size distribution, so the icing prediction algorithm will be based on the simplified approach outlined in Fikke (2007). The relative humidity will be calculated with respect to ice when temperatures are below freezing, as suggested by Cattin et al. (2008). Icing is assumed to occur when the temperature is less than 273.16 K and the relative humidity is above a certain threshold, with Fikke (2007) suggesting the threshold be 95%. The goal of this study is to determine the optimal relative

humidity threshold that should be used when predicting power losses due to icing.

Observed icing losses are determined from the Minnkota dataset in conjunction with wind speeds from the other datasets. The Minnkota dataset does not include nacelle-based anemometry or indicators for icing and so periods of icing need to be estimated. The observed power output is compared to the expected power output (Figure 8), which is converted from wind speed to power using the turbine power curve. A typical power curve (Figure 7) allows wind speed to be converted directly to turbine power output and is based on the manufacturer's own analysis of the turbine under various atmospheric conditions. Since power curves are dependent on air density, the 10 m air density from the MERRA dataset is used. This could have an effect on both the observed and predicted icing losses in that the expected power output would be slightly higher than it should be which could cause an increase in both the observed and predicted losses.

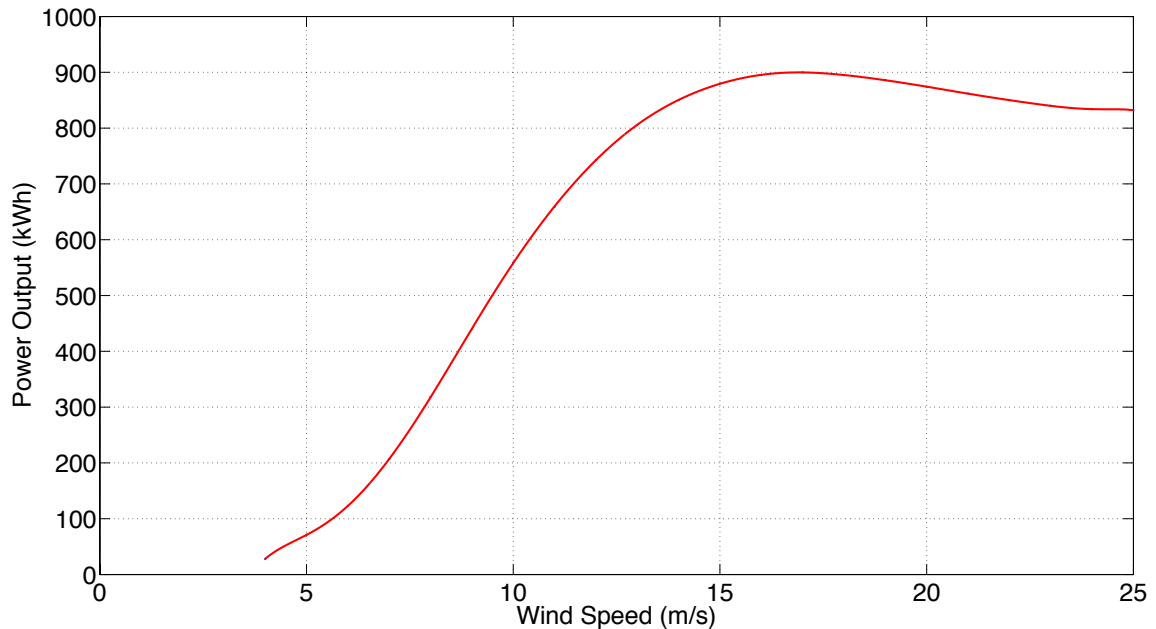


Figure 7: Manufacturer's power curve for a NEG Micon NM52/900 turbine with air density of  $1.27 \text{ kg m}^{-3}$ .

Icing is assumed when the following conditions are met:

- Temperature is below 273.16 K.
- Predicted wind speed is greater than  $4 \text{ m s}^{-1}$ .
- Observed power output is 80% or less than that of the expected power output.

The 80% threshold is chosen in order to maximize the capture of light icing events as Jasinski et al. (1998) found that even minor icing can cause a 20% drop in power production. When the above conditions are met, icing loss is calculated as the difference between the observed power output and the expected power output.

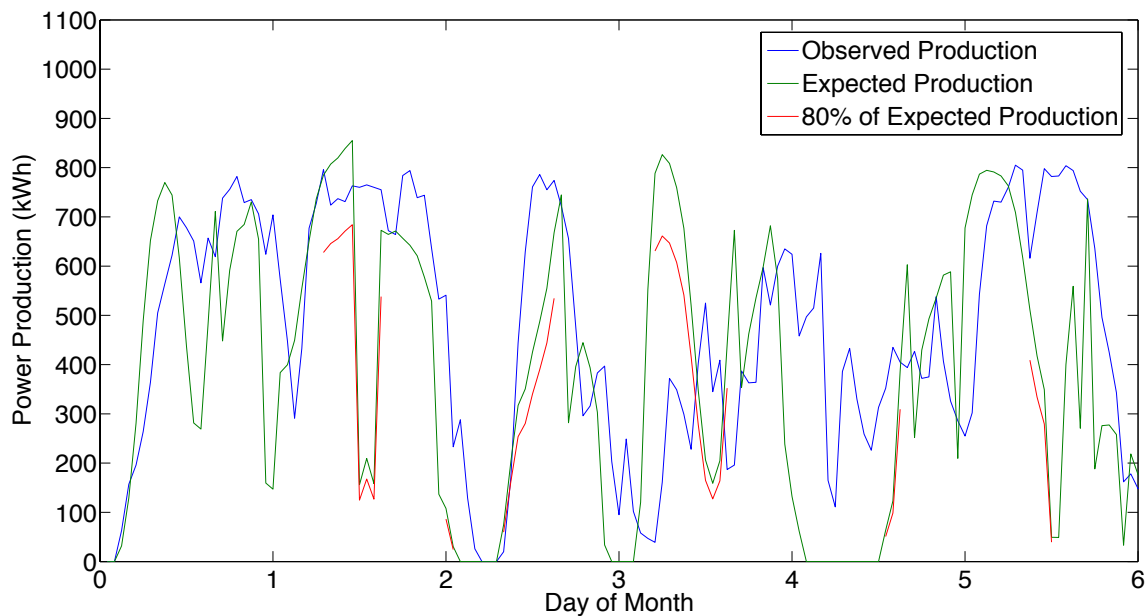


Figure 8: Observed power production at the Petersburg location (blue) compared with expected power production (green) calculated using the boundary-layer similarity method for the first week of November 2009. Icing is assumed to occur when observed power production is less than 80% of the expected power production for time periods that meet the temperature and wind speed criteria (red).

For the entire six-month period of each season, the observed total amount of power lost due to icing,  $I_{obs}$ , is determined, while the total amount of power generated,

$P_{obs}$ , for the twelve month period from August 1 to July 31, is given in the Minnkota dataset. Due to the fact that  $P_{obs}$  is the total power generated after all losses are taken into account, the observed annual loss,  $L_O$ , as a percent includes the total loss due to icing in the denominator and is:

$$L_O = 100 \times \frac{I_{obs}}{I_{obs} + P_{obs}} \quad (3.29)$$

Predicted icing losses are determined for each method outlined in Section 3.2. For each one-hour time step, the calculated temperature and relative humidity are checked against the chosen thresholds (e.g. 273.16 K and 95%) as shown in Figures 9 and 10.

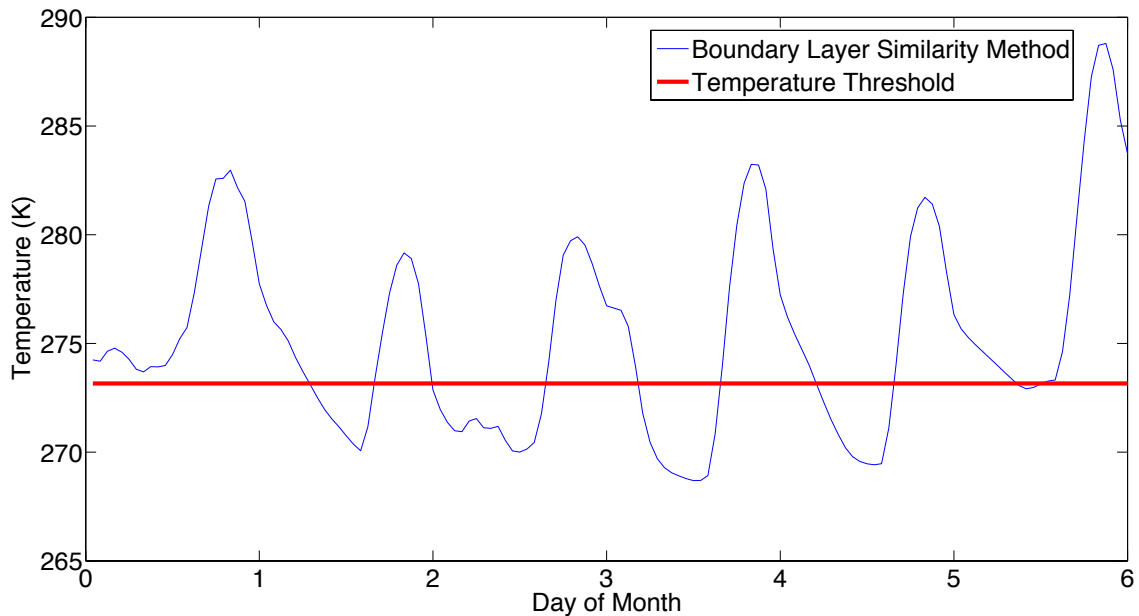


Figure 9: Temperature profile at the Petersburg location as calculated using boundary-layer similarity theory for the first week of November 2009 (blue) compared with the temperature threshold for icing prediction (red).

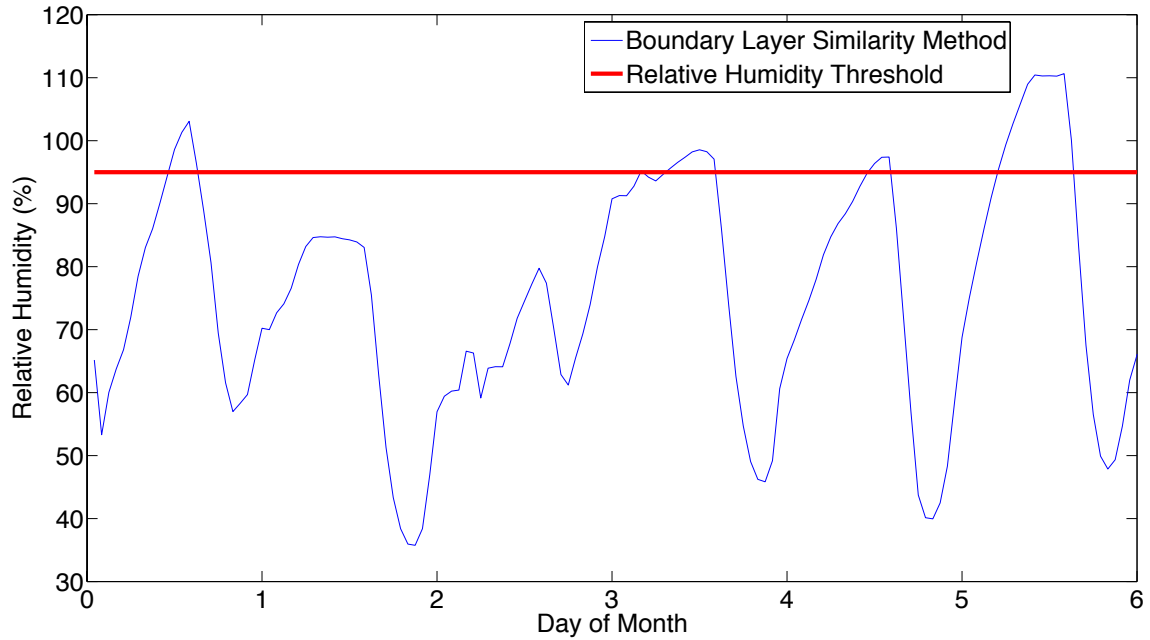


Figure 10: Relative humidity profile at the Petersburg location as calculated using boundary-layer similarity theory for the first week of November 2009 (blue) compared with the 95% relative humidity threshold for icing prediction (red).

For those periods of time where both thresholds are met, it is assumed that all power that would be generated for those times is lost due to icing. Figure 11 shows the expected power generated for the first week of November 2009 and the three periods of time where the thresholds are met.

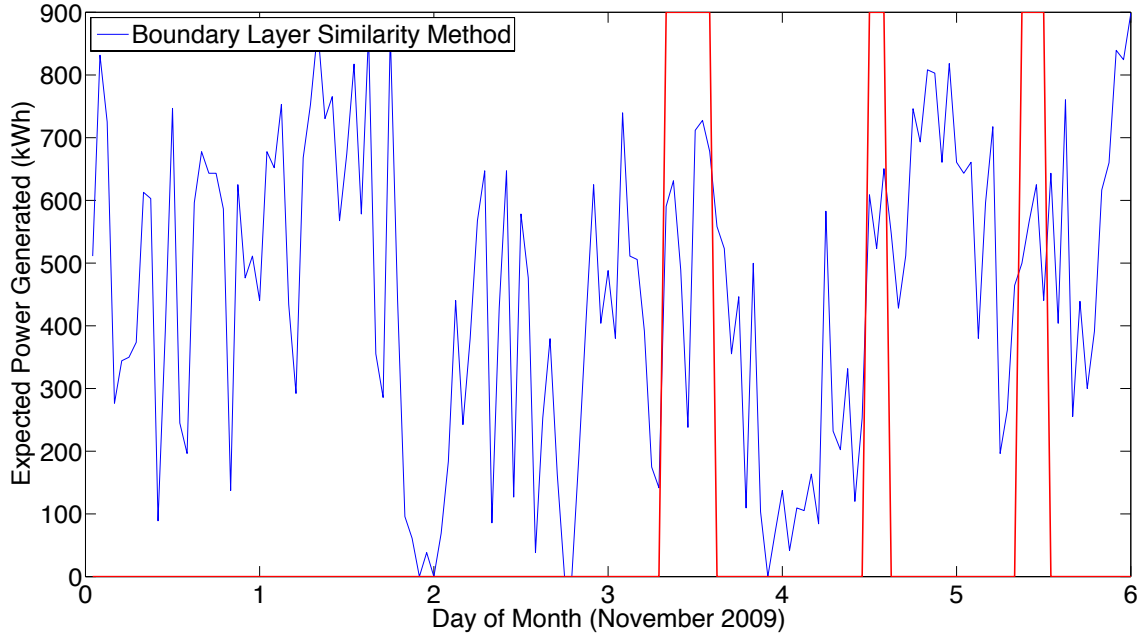


Figure 11: Expected power generated at the Petersburg location calculated from boundary-layer similarity theory for the first week of November 2009 (blue). Periods of time where both temperature and relative humidity thresholds are met for icing are shown in red.

For the six-month period of each season, the total predicted power lost due to icing,  $I_{pred}$ , is determined from all periods when the thresholds are met. The total amount of power,  $P_{pred}$ , expected to be generated for the twelve-month period from August 1 to July 31, assuming no losses, is also determined. The predicted annual loss,  $L_P$ , due to icing is simply:

$$L_P = 100 \times \frac{I_{pred}}{P_{pred}} \quad (3.30)$$

For the full analysis, the predicted annual loss due to icing is determined for relative humidities ranging from 90% to 105% in 0.2% increments, for each of the six methods outlined in the preceding sections, and for each of the eight training years beginning August 1, 2002 and ending July 31, 2010. To determine the optimal relative humidity threshold for each method, the difference,  $L_D$ , between the observed losses,  $L_O$ , and



the predicted losses,  $L_P$ , is calculated for each relative humidity threshold for each season.  $L_D$  is then averaged for each relative humidity value over the eight seasons. The optimal relative humidity threshold exists when this averaged  $L_D$  is minimized. This minimum point is the interpolated value between the two relative humidities that bracket the point at which  $L_D$  is zero. The three years from August 1, 2010 to July 31, 2013 are used to test the optimal relative humidity threshold using the same procedure outlined in this section, where the optimal value is used instead of the full range that is used in the training years.

## CHAPTER 4

### RESULTS

This chapter aims to provide a summary of the performance of each of the methods described in section 3.2 in predicting power losses due to icing as outlined in section 3.3. The first section looks at the accuracy of the MERRA-derived wind speeds and quantifies the differences between those and the MCP/WAsP-derived wind speeds to determine the best method of calculating wind speeds. The next section provides an analysis of and quantifies the temporal variability of icing prediction in order to determine the best time period over which to sum icing losses in the analysis. The final two sections provide the results of the methods used to predict power losses due to icing and how the best method applies to a second location.

#### 4.1 Accuracy of MERRA-Derived Wind Speeds and Energy Production

In order to determine if MERRA makes a suitable dataset for icing prediction, the accuracy of each method outlined in section 3.2. for calculating wind speeds, and by extension, energy production, must first be determined. Unfortunately, no wind speed data is available at the Minnkota turbine site used for this research. However, the turbine dataset represents a proxy for the wind speeds, in the form of energy production since the turbine power curve can be applied to the wind speeds. To eliminate any possibility of turbine icing affecting the data, the month of October 2011 is chosen as the best month for comparison of derived winds to observations. In general, October is early enough in the season that any periods of icing, if they occur,

are limited in duration due to the fact that temperatures drop below freezing much less than during the other 5 months tested. Based solely on this month, the MCP/WAsP-derived winds (green lines on Figs. 12, 13, and 14) seem to be more accurate than simply using MERRA-derived winds (blue lines on Figs. 12, 13, and 14) to calculate power production.

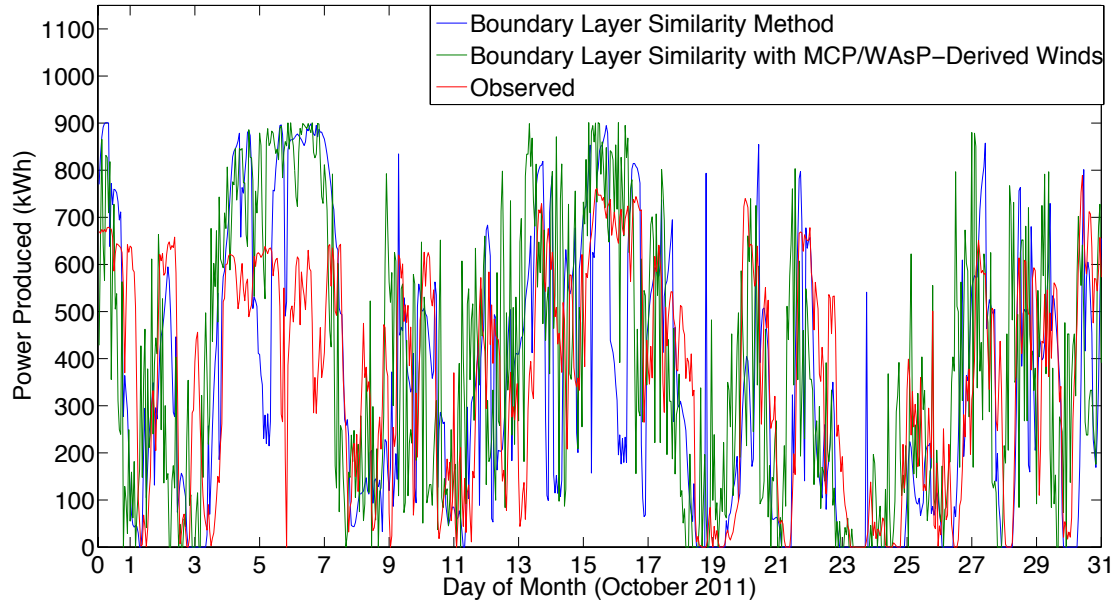


Figure 12: A comparison of energy production at the Petersburg location calculated from wind speed derived from boundary layer similarity theory (blue) and boundary layer similarity theory with Measure-Correlate-Predict (MCP) derived wind speed (green). The observed production is shown in red.

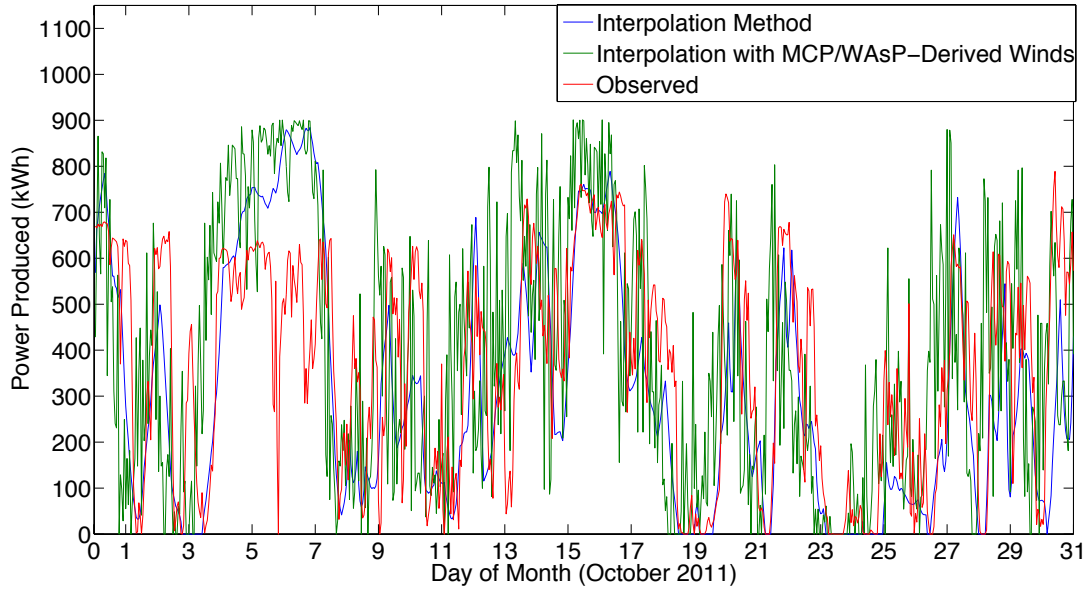


Figure 13: A comparison of energy production at the Petersburg location calculated from wind speed derived from the interpolation method (blue) and the interpolation method with Measure-Correlate-Predict (MCP) derived wind speed (green). The observed production is shown in red.

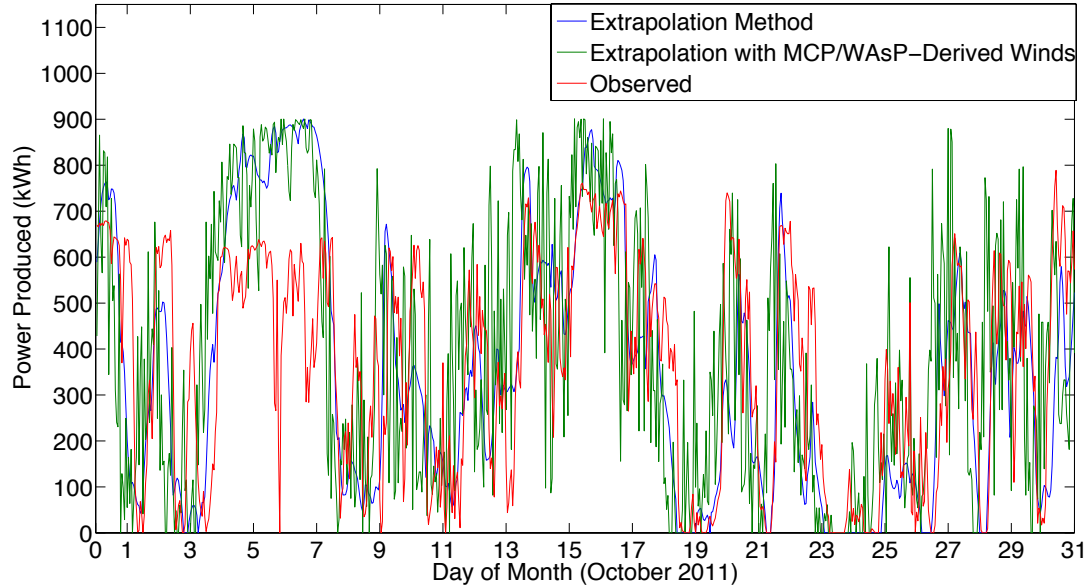


Figure 14: A comparison of energy production at the Petersburg location calculated from wind speed derived from the extrapolation method (blue) and the extrapolation method with Measure-Correlate-Predict (MCP) derived wind speed (green). The observed production is shown in red.

One pattern that stands out is that the interpolation method and extrapolation method produce curves that are much more smoothed out than the boundary layer similarity method curve (blue lines on Figs. 13, 14, and 12, respectively). In addition, with the exception of the area between 100 hours and 175 hours, each method does seem to match with the pattern of the observed energy production curve (red line in Figs. 12, 13, and 14). Although the curves seem to match with the observed energy production curves, the average expected hourly energy production for the interpolation, extrapolation, and boundary layer similarity methods are 290.5 kWh, 357.2 kWh, and 361.8 kWh, respectively. For the three MCP/WAsP-derived methods, these values average 403.6 kWh, while the observed average hourly energy production is 417.55 kWh. To investigate further, the average hourly energy production calculated using each method is compared for each season. Each of the three methods using MCP/WAsP-derived winds (dashed colored lines on Figure 15) show a better correlation to the observed values (dashed black line on Figure 15) than the methods using MERRA-derived winds (solid colored lines on Figure 15).

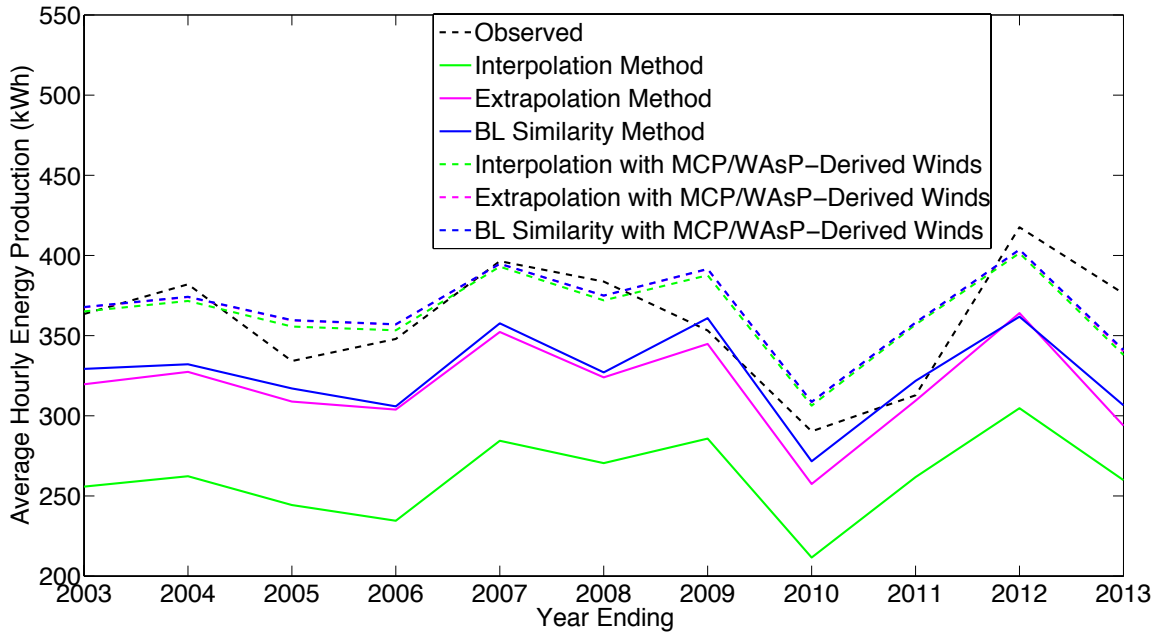


Figure 15: Average hourly energy production for each season (October to March) at the Petersburg location as calculated from wind speed derived from boundary layer similarity theory (solid blue), the extrapolation method (solid magenta), and the interpolation method (solid green). The same methods using MCP/WAsP-derived wind speeds are shown as dashed lines. Observed is shown with the dashed black line.

Each of the three methods using MERRA-derived wind speeds produces a different wind speed profile from the surface to the turbine height, as shown in Figure 16. As expected based on the power production correlation, the wind profiles generated using only MERRA data (red, blue, and green lines on Figure 16) show wind speeds at the turbine height that are lower than the MCP-method (magenta dot).

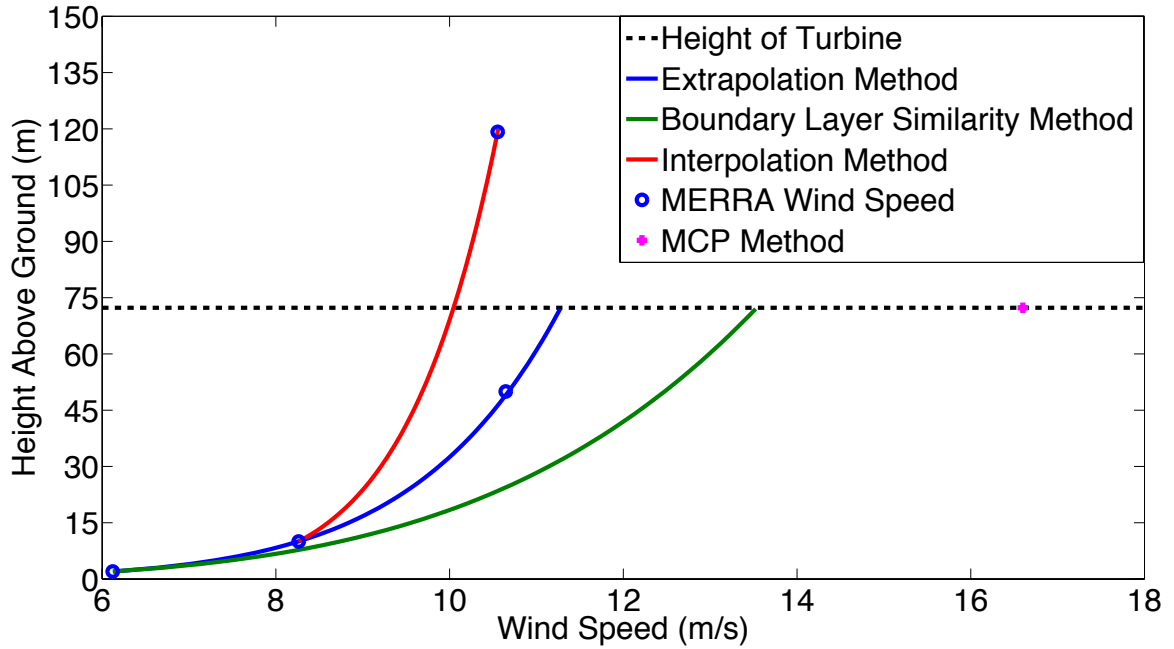


Figure 16: A comparison of wind speed as a function of height for the interpolation method (red), the extrapolation method (blue), and the boundary layer similarity method (green) for December 23, 2011 at 0600Z. The cyan dots are the MERRA-provided wind speeds, and the magenta dot is the MCP/WAsP-derived wind speed.

On a seasonal basis, the same wind speed correlation exists, with the mean seasonal MCP/WAsP-derived winds (red line on Figure 17) being the highest and the wind speeds determined from the interpolation method (green line on Figure 17) being significant lower. This enforces the result that the methods using only MERRA data are under predicting the wind speeds at the turbine height, and thus under predicting the power production.

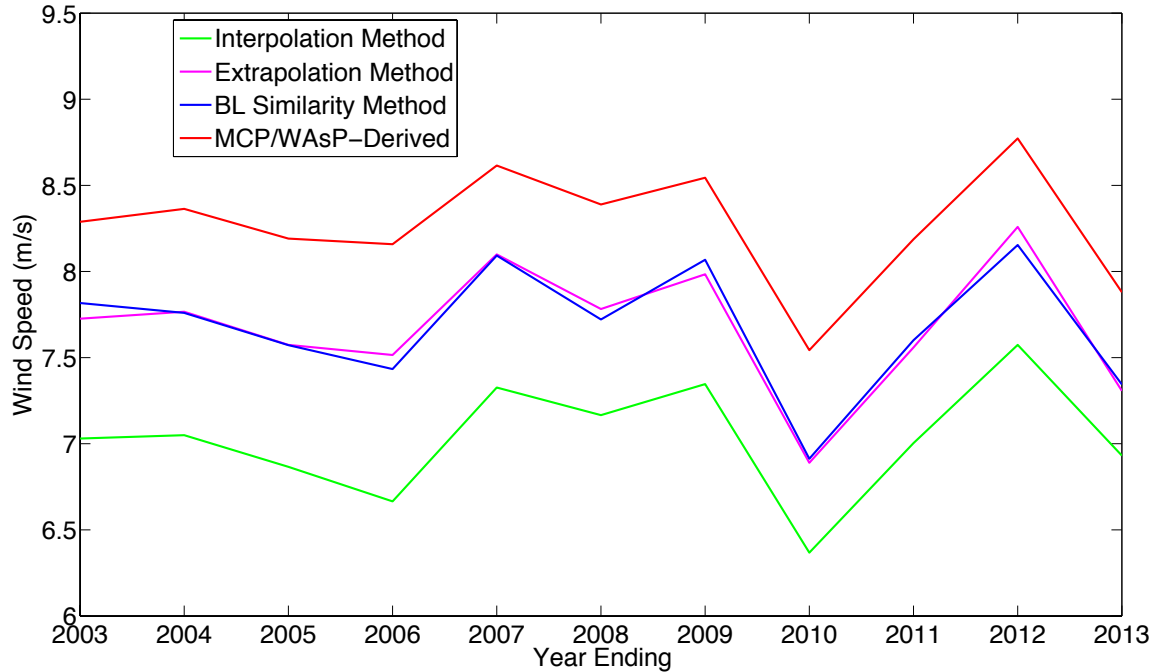


Figure 17: Seasonal average wind speed calculated from boundary layer similarity theory (blue), the extrapolation method (magenta), the interpolation method (green), and the MCP/WAsP method at the Petersburg location.

The 11-season means (Table 5) for both wind speed and hourly energy production agree with each of the relationships seen in the seasonal means (Figs. 15 and 17). The energy production from the MCP/WAsP methods is between 1.1 % and 1.9 % higher than observed, while the three methods not using MCP/WAsP-derived wind speeds are between 9.2 % and 27.3 % lower than observed. In addition, the mean wind speed of the three non-MCP/WAsP methods is between 7.1 % and 15 % lower than the mean MCP/WAsP-derived wind speeds. Again, this shows that the wind speeds derived solely from MERRA data are being under predicted, leading to an under prediction of energy production. Although the MERRA-derived winds are being under predicted, they are still used in three of the methods to better understand how the under prediction will impact the icing prediction algorithms and allow a better comparison of all methods.



Table 5: Eleven-season mean of wind speed ( $\text{m s}^{-1}$ ) and hourly energy production (kWh) and their standard deviations for each of the six methods used in this study. No observed wind speed data exists for this location

	11-Season Mean Wind Speed ( $\text{m s}^{-1}$ )	11-Season Mean Hourly Energy Production (kWh)
Extrapolation Method	$7.678 \pm 0.380$	$283.10 \pm 31.41$
Interpolation Method	$7.030 \pm 0.333$	$230.38 \pm 26.61$
Boundary Layer Similarity Method	$7.680 \pm 0.368$	$285.97 \pm 30.04$
Extrapolation with MCP/WAsP Winds	$8.267 \pm 0.343$	$306.82 \pm 33.49$
Interpolation with MCP/WAsP Winds		$306.02 \pm 35.67$
Boundary Layer Similarity with MCP/WAsP Winds		$305.88 \pm 34.28$
Observed	-	$359.79 \pm 37.30$

## 4.2 Temporal Variability in Icing Prediction

In order to determine the significance of time periods over which the predicted icing losses are determined, a test is performed on one season to analyze time scales shorter than six months (i.e. shorter than one season). For this test season, the predicted and observed icing loss (MWh) is determined for the three-month periods of October through December and January through March using the boundary-layer similarity theory method with MCP/WAsP-derived winds. Figure 18 shows that for both three-month periods, the predicted losses due to icing ( $L_P$ ) match closely with the observed losses due to icing ( $L_O$ ).

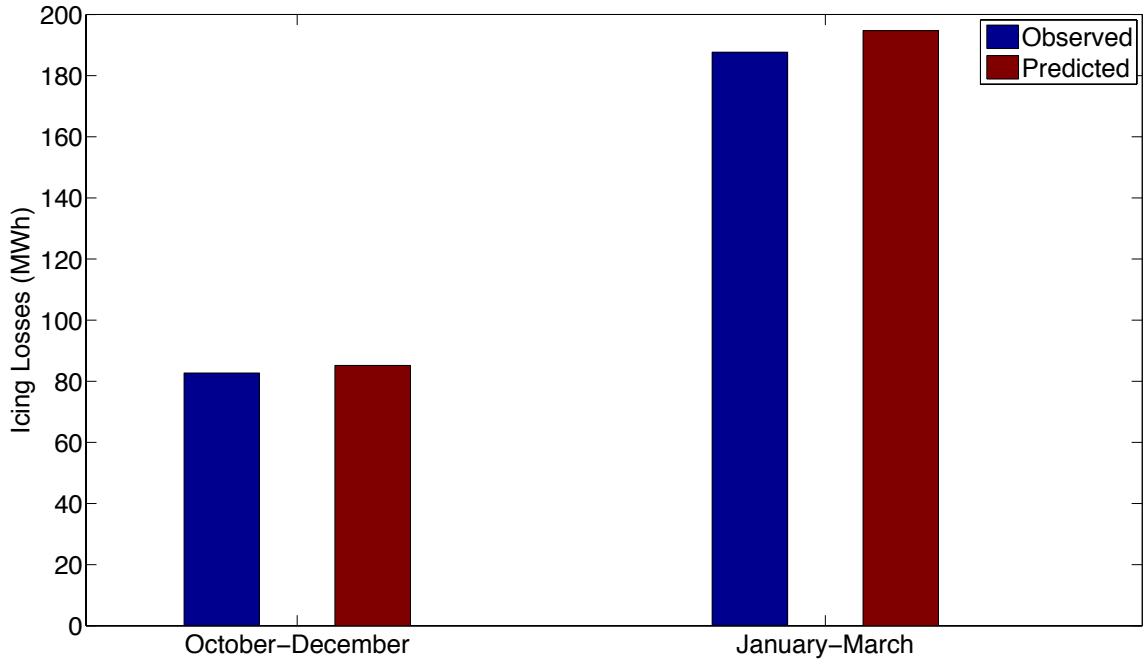


Figure 18: Predicted and observed icing losses (MWh) at the Petersburg location using the boundary-layer similarity method with MCP/WAsP-derived winds and a relative humidity of 97.7 % for each three month period making up the 2007/2008 winter season.

Looking at monthly time scales (Figure 19) there is some variability. For the months of October, November, January, and March, the icing losses are under-predicted, while in the remaining months, the icing losses are over-predicted.

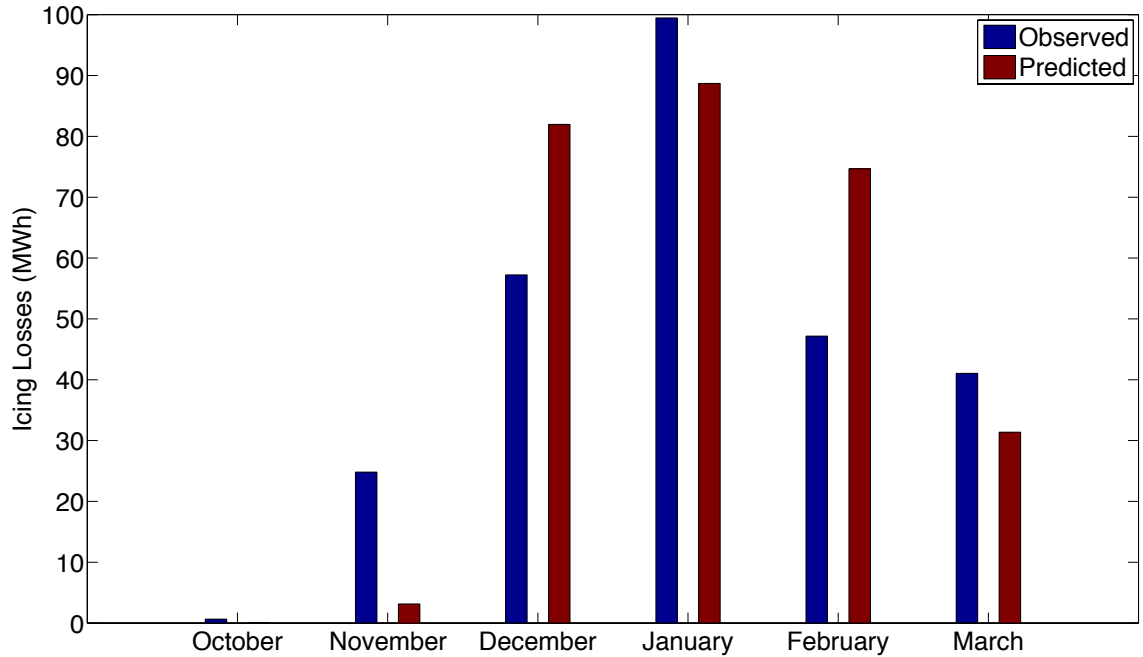


Figure 19: Predicted and observed icing losses (MWh) at the Petersburg location using the boundary-layer similarity method with MCP/WAsP-derived winds and a relative humidity of 97.7 % for each monthly period making up the 2007/2008 winter season.

As the month of January has the highest amount of observed losses due to icing while also having predicted losses that closely match the observed losses, a weekly analysis is performed on this month (Figure 20). Similar to the monthly analysis, the weekly analysis also shows both under-prediction and over-prediction of icing losses.

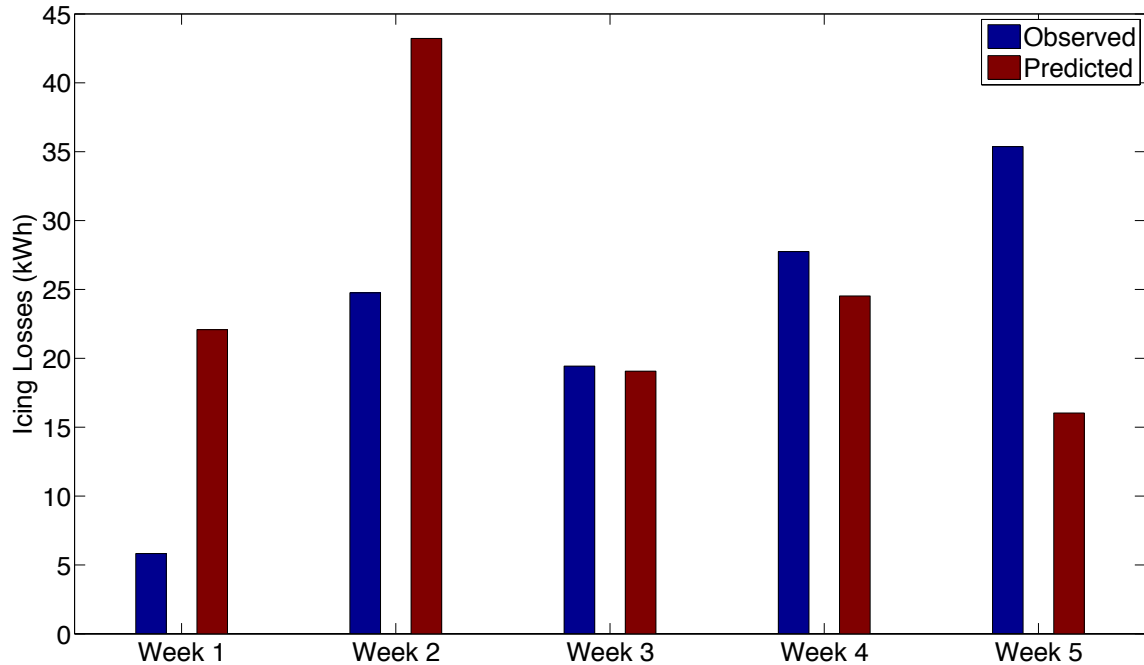


Figure 20: Predicted and observed icing losses (kWh) at the Petersburg location using the boundary-layer similarity method with MCP/WAsP-derived winds and a relative humidity of 97.7 % for each weekly period of January 2008.

In addition to the raw energy losses due to icing, the icing prediction methods are highly dependent on accurately determining the optimum relative humidity. As such, the variability of the temporal resolution used for the seasonal analyses is investigated to determine its effect on relative humidity. Each method is analyzed every hour and the resultant observed and predicted icing losses are summed and analyzed monthly, three-monthly, and six-monthly (seasonally). The difference between the observed icing losses and predicted icing losses ( $L_D$ ) is calculated for each relative humidity threshold between 90 % and 105 %. The monthly analysis is performed on October 2009 (Figure 21) and January 2010 (Figure 22).

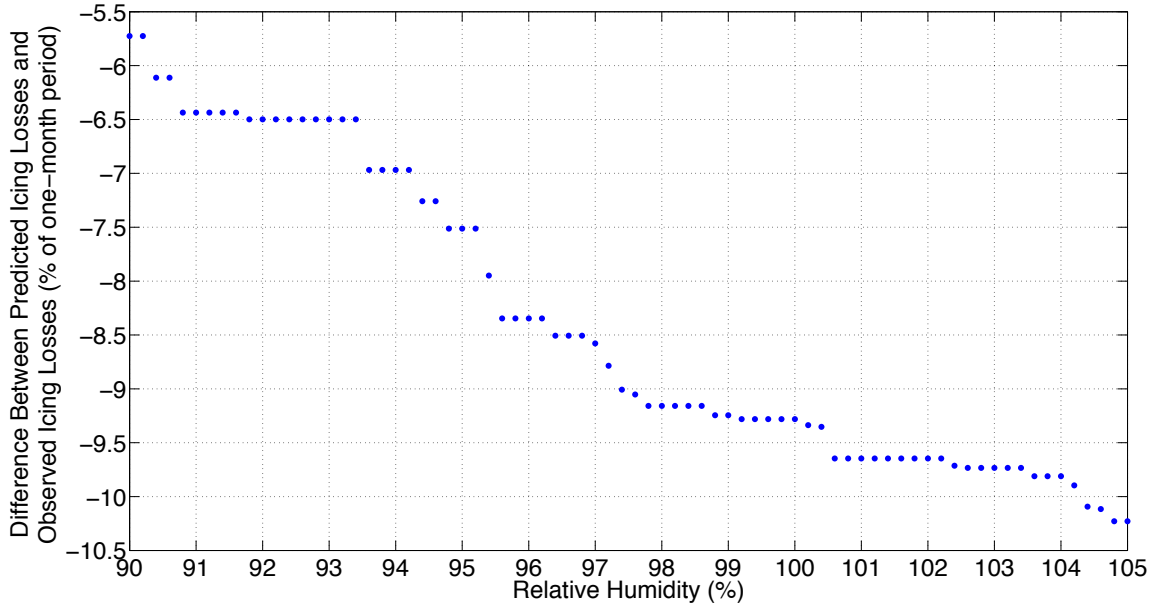


Figure 21: The difference between the predicted icing losses ( $L_P$ ) and observed icing losses ( $L_O$ ) at the Petersburg location for October 2009 using the boundary layer similarity method.

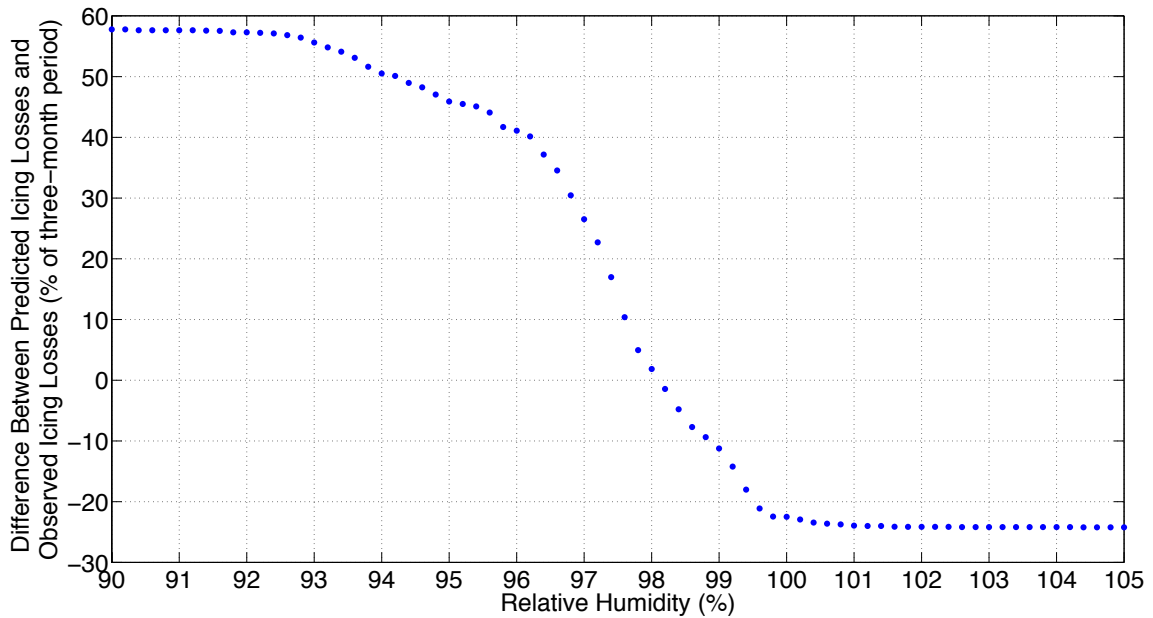


Figure 22: The difference between the predicted icing losses ( $L_P$ ) and observed icing losses ( $L_O$ ) at the Petersburg location for January 2010 using the boundary layer similarity method.

In the case of October, the optimum relative humidity is not located within the range of the data, as the difference between the observed and predicted icing losses never reaches 0 for any of the relative humidity thresholds. For January, however, an optimal relative humidity does exist at just over 98 %. Of note, however, is that a small change in the relative humidity produces a large change in the difference between the predicted and observed losses. For example, a change from 97 % to 98 % in the relative humidity produces a change of over 20 % in the difference between observed and predicted icing losses. These types of patterns emerge in all six methods when analyzing the data on monthly time scales and show that a monthly time scale is too variable for the required analysis. There is some improvement when looking at three-monthly time scales (Figures 23 and 24) in that an optimum humidity exists for both periods, however there is a significant difference.

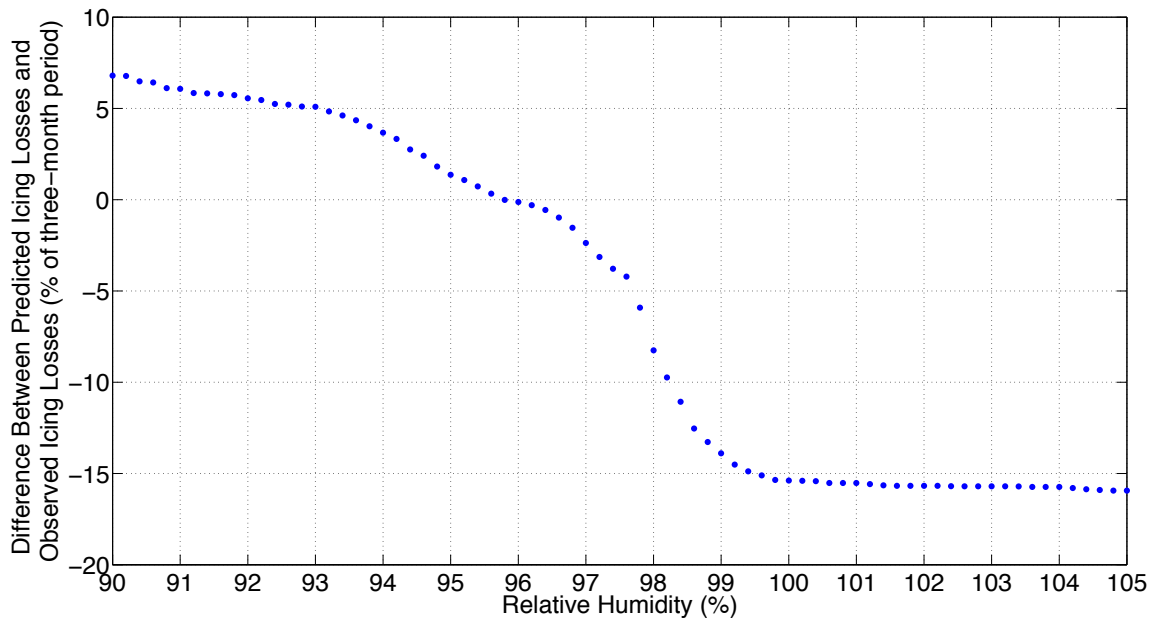


Figure 23: The difference between the predicted icing losses ( $L_P$ ) and observed icing losses ( $L_O$ ) at the Petersburg location for the period October 2009 to December 2009 using the boundary layer similarity method.

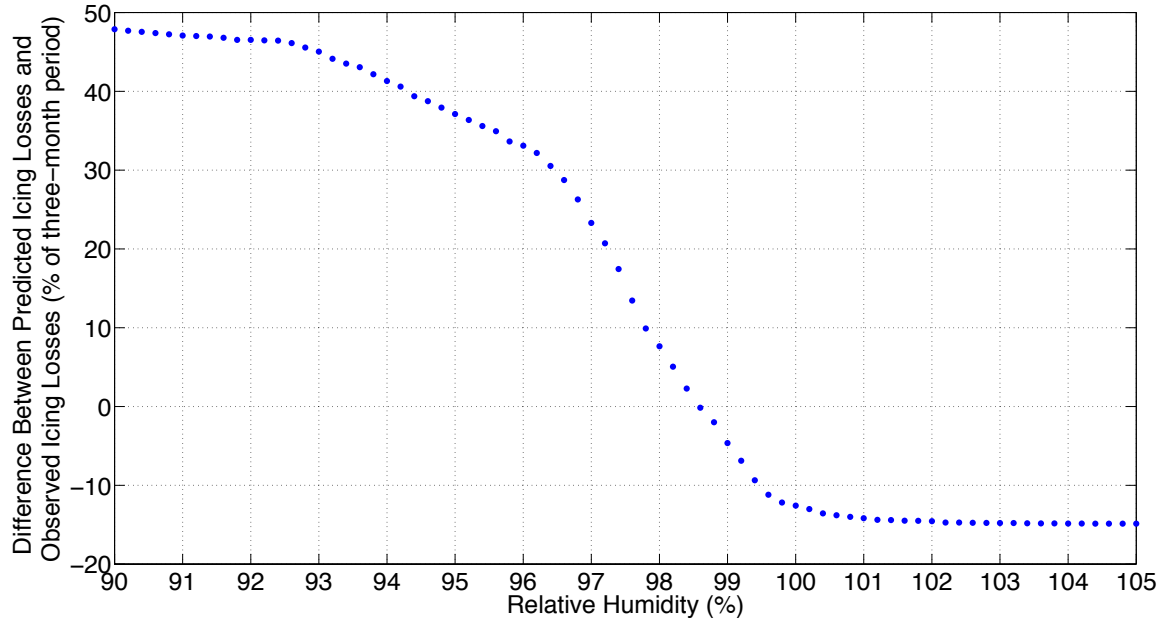


Figure 24: The difference between the predicted icing losses ( $L_P$ ) and observed icing losses ( $L_O$ ) at the Petersburg location for the period January 2010 to March 2010 using the boundary layer similarity method.

The optimum relative humidity threshold is 96.1 % for the October to December period and 98.6 % for the January to March period, showing that some variability is still evident at three-month time scales. In addition, for the the January to March time period the rate of the change of the difference between the predicted and observed losses is quite significant for small changes in relative humidity, similar to the monthly analysis in January. At the seasonal scale (Figure 25), the rate of change of the difference is smaller than both three-month periods and the optimum relative humidity lies between their respective values, at 97.9 %.

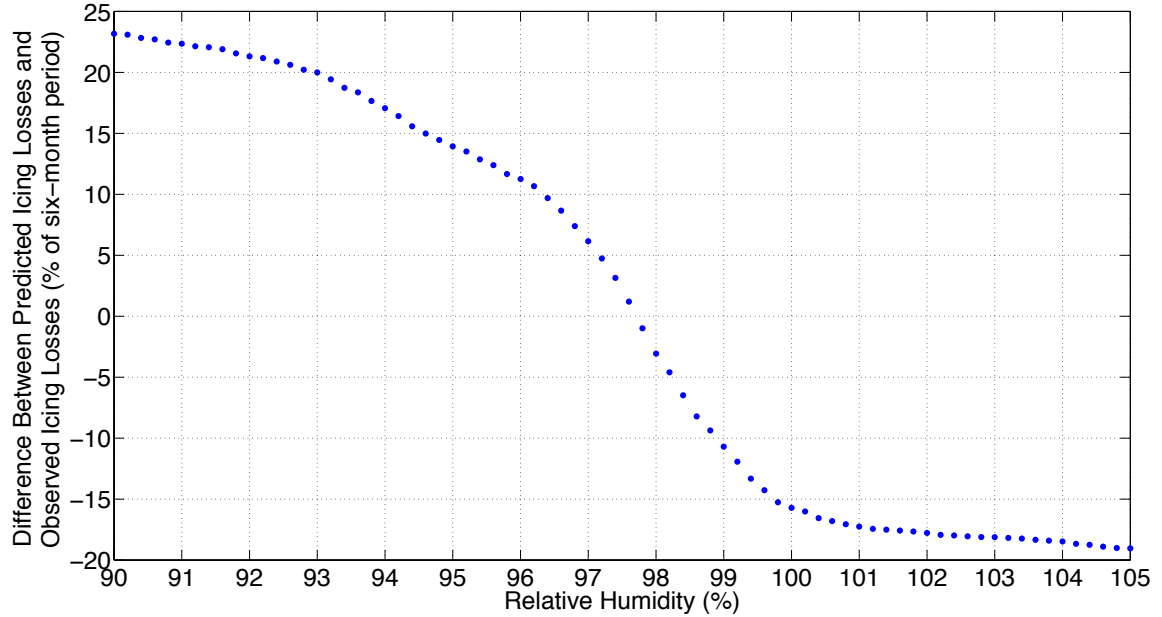


Figure 25: The difference between the predicted icing losses ( $L_P$ ) and observed icing losses ( $L_O$ ) at the Petersburg location for the period October 2009 to March 2010 (blue dots) using the boundary layer similarity method.

The temporal resolution analysis shows that variability does exist over the three different time periods, however, the six-month time scale shows the lowest variability. In addition, the wind industry reports on annual time scales and with icing generally not occurring in the Northern Plains for more than six months of a year, moving forward, the icing prediction methods are all analyzed over this six-month seasonal time scale.

### 4.3 Prediction of Annual Power Losses Due to Icing

Each of the six methods is analyzed for each of the eight winter seasons from 2002 to 2010 and the optimal relative humidity is calculated for each method, shown in Table 6. The methods using MCP/WAsP-derived wind speeds each produce a relative humidity threshold lower than their non-MCP/WAsP method counterpart, however, in the case of the boundary layer similarity methods, the difference is not as significant.



Table 6: The optimal relative humidity values at the Petersburg location determined for each method based on eight years of data.

Method	Optimal Relative Humidity
Extrapolation	95.9 %
Extrapolation with MCP/WAsP-derived winds	94.9 %
Interpolation	95.9 %
Interpolation with MCP/WAsP-derived winds	94.1 %
Boundary Layer Similarity	97.9 %
Boundary Layer Similarity with MCP/WAsP-derived winds	97.7 %

The optimal relative humidity threshold is tested on all eleven winter seasons, eight of which were used in its development, and three that were not, in order to determine which method performs the best against current industry methods. Table 7 shows that for the three test seasons alone, and for the full eleven seasons, all of the tested methods more closely predict the annual icing losses than the industry method, and the methods using MCP/WAsP-derived wind speeds perform the best. One important note to make is that although the MCP/WAsP-derived methods use the identical wind speeds, the difference between the observed losses and the industry method does change between those methods. Since temperature is required to determine the observed losses and it is calculated differently for each of the methods, it leads to small differences in the observed icing losses.

Table 7: A comparison of the mean absolute difference between the observed annual losses and both the predicted annual losses and the industry method at the Petersburg location for the three test seasons and the entire dataset.

Method	3 Year		11 Year	
	Absolute Difference Between Observed and Predicted Losses	Absolute Difference Between Observed and Industry Method	Absolute Difference Between Observed and Predicted Losses	Absolute Difference Between Observed and Industry Method
Extrapolation	2.21 ± 1.93 %	3.24 ± 1.67 %	1.80 ± 1.54 %	1.99 ± 1.83 %
Interpolation	1.78 ± 2.15 %	2.47 ± 1.56 %	1.69 ± 1.59 %	1.89 ± 1.24 %
Boundary layer similarity	2.08 ± 1.31 %	4.16 ± 2.91 %	1.96 ± 1.35 %	3.11 ± 2.34 %
Extrapolation with MCP/WAsP-derived winds	2.50 ± 1.62 %	5.86 ± 4.61 %	2.04 ± 1.27 %	5.36 ± 2.60 %
Interpolation with MCP-derived winds	2.60 ± 2.35 %	5.83 ± 4.58 %	2.24 ± 1.54 %	5.33 ± 2.59 %
Boundary layer similarity with MCP/WAsP-derived winds	2.13 ± 1.29 %	5.87 ± 4.64 %	1.94 ± 1.13 %	5.40 ± 2.63 %

On closer inspection of the raw energy production data, it is found that for the methods that do not use MCP/WAsP-derived winds, the amount of predicted energy production ( $P_{pred}$ ) is significantly less than would be expected from the observed values ( $P_{obs}$ ), as shown in Figure 26. This also backs up the results of section 4.1, in that the non-MCP/WAsP methods under predict the wind speeds at the turbine height.

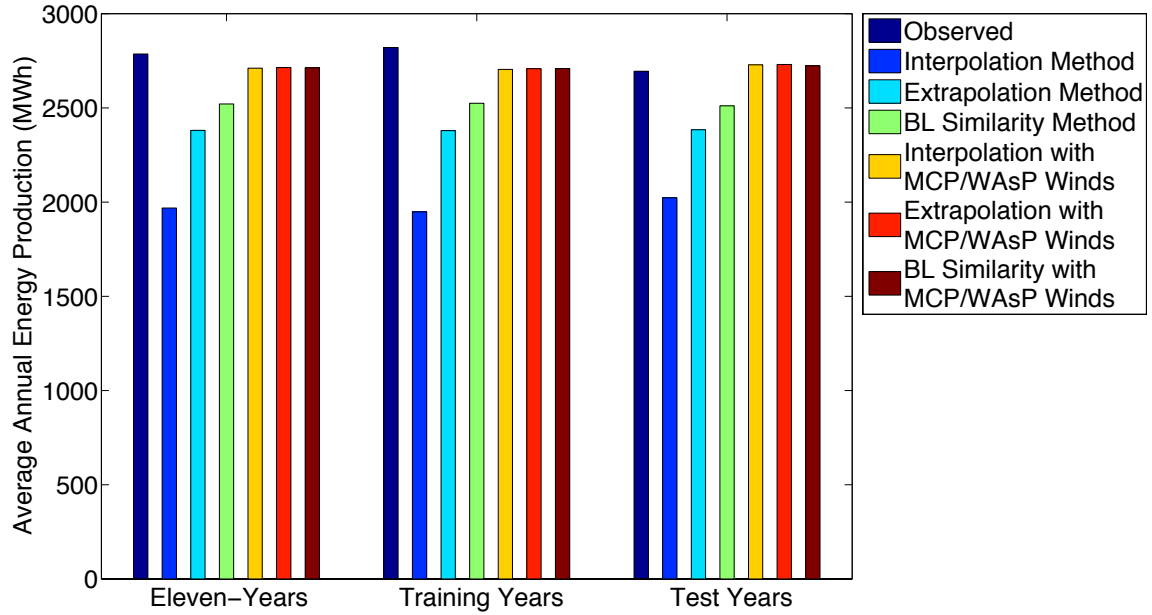


Figure 26: A comparison of the eleven-year, eight-year, and three-year mean annual predicted energy production in MWh at the Petersburg location for each method.

Knowing that the non-MCP/WAsP methods cannot accurately predict the proper wind speed at the turbine height, any comparison of them to the industry method cannot prove or disprove that they are more accurate. However, the three methods that utilize MCP/WAsP-derived wind speeds can be compared to the industry method and their accuracy can be determined. In all but one season, the three MCP/WAsP methods more accurately predicted the annual losses due to icing ( $L_{pred}$ ) than the industry method ( $L_{ind}$ ), as shown in Figure 27.

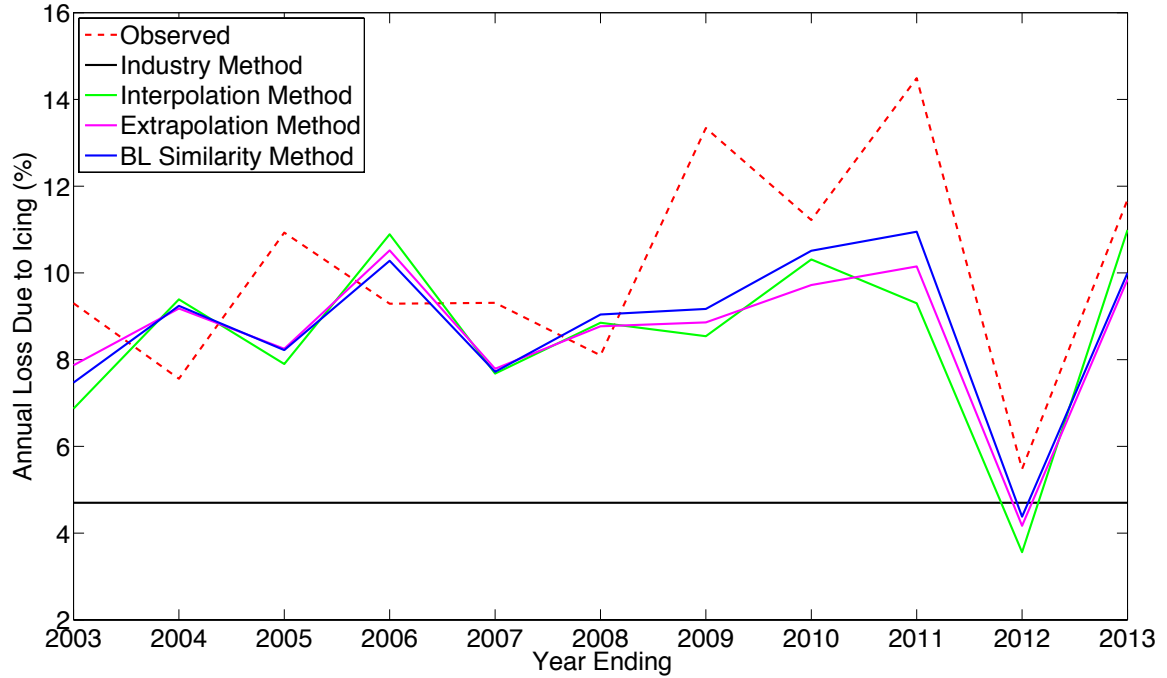


Figure 27: A comparison of the three MCP/WAsP methods and the industry method in predicting the annual losses due to icing at the Petersburg location.

When looking at the three, eight, and eleven-year mean annual icing losses shown in Figure 28, it is clear that the MCP/WAsP methods ( $I_{pred}$ ) are also much more accurate than the industry method ( $I_{ind}$ ) in predicting annual energy lost due to icing ( $I_{obs}$ ), with the boundary layer similarity method slightly outperforming the other two methods.

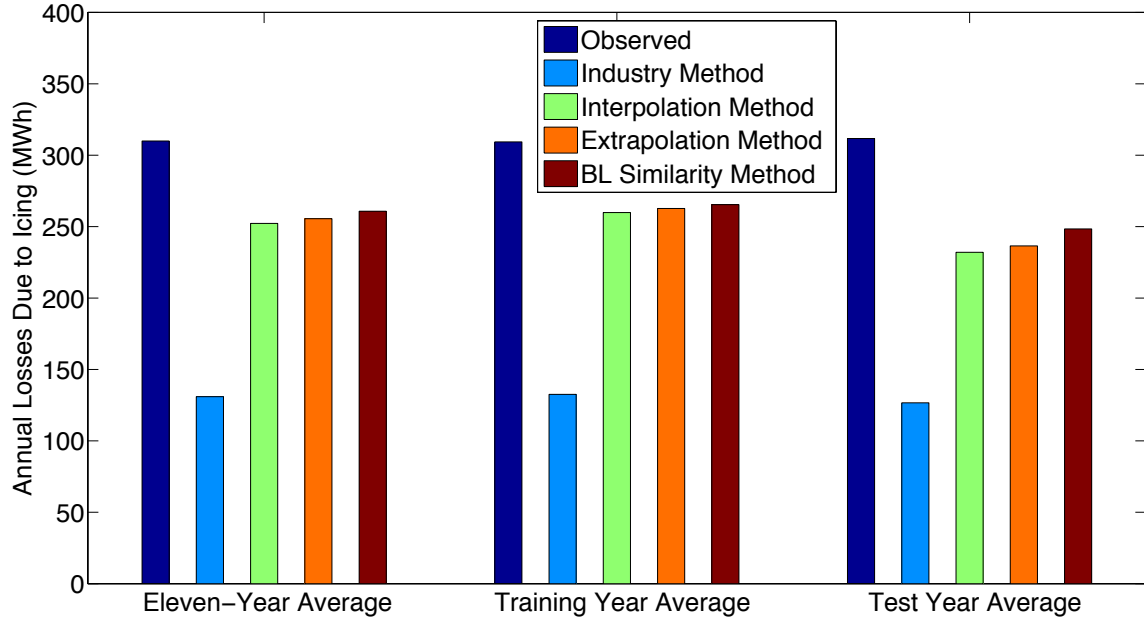


Figure 28: A comparison of the eleven-year, eight-year, and three-year mean annual predicted energy lost due to icing in MWh at the Petersburg location for the MCP/WAsP methods ( $I_{pred}$ ) and industry method ( $I_{ind}$ ).

#### 4.4 Applicability to a Different Location

Minnkota owns and operates an identical turbine in Valley City, ND, located approximately 121 km to the south of the Petersburg turbine. The same anemometer data used in the MCP/WaSP analysis at the Petersburg location is used for the Valley City location. In addition, the data is not retrained for the Valley City location, but instead the relative humidity threshold results from the Petersburg location are applied to the new location. Lastly, as the three MCP/WAsP-derived methods perform best for the Petersburg location, only those three are tested at Valley City. Table 8 shows that the three methods more closely predict the percentage observed annual losses than the industry method, with the boundary layer similarity theory method performing the best.

Table 8: A comparison of the mean absolute difference between the observed annual losses and both the predicted annual losses and the industry method at the Valley City location for the three test seasons and the entire dataset.

Method	3 Year		11 Year	
	Absolute Difference Between Observed and Predicted Losses	Absolute Difference Between Observed and Industry Method	Absolute Difference Between Observed and Predicted Losses	Absolute Difference Between Observed and Industry Method
Extrapolation with MCP/WAsP-derived winds	$4.09 \pm 1.16 \%$	$5.59 \pm 3.76 \%$	$2.79 \pm 1.11 \%$	$4.98 \pm 1.87 \%$
Interpolation with MCP/WAsP-derived winds	$4.46 \pm 1.08 \%$	$5.58 \pm 3.75 \%$	$3.33 \pm 1.26 \%$	$4.97 \pm 1.87 \%$
Boundary layer similarity with MCP/WAsP-derived winds	$3.66 \pm 1.03 \%$	$5.71 \pm 3.88 \%$	$2.94 \pm 1.11 \%$	$5.10 \pm 1.93 \%$

On a seasonal basis, Figure 29 shows that similar to the Petersburg location, in all but one season, the three MCP/WAsP methods more accurately predicted the annual losses due to icing than the industry method. As expected from Table 8, the prediction for each season is not as accurate as at the Petersburg location.

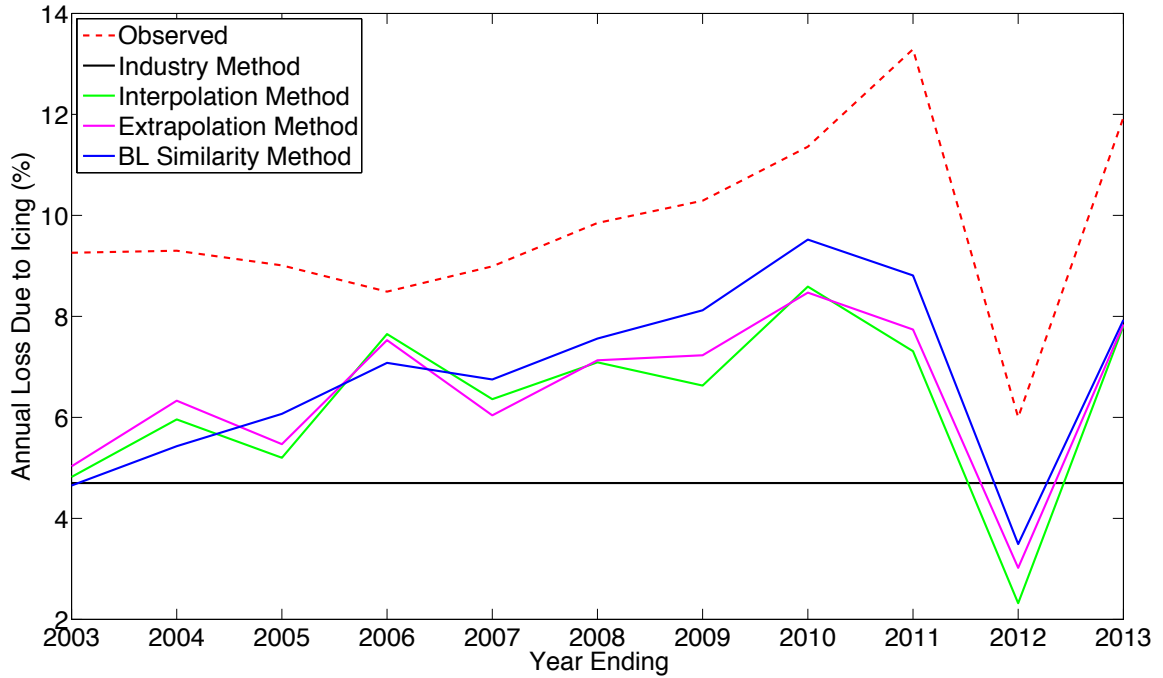


Figure 29: A comparison of the three MCP/WASP methods and the industry method in predicting the annual losses due to icing at the Valley City location.

When looking at the three, eight, and eleven-year mean annual icing losses shown in Figure 30, it is clear that even at the new location the MCP/WASP methods are still more accurate than the industry method in predicting annual energy lost due to icing. In comparison with the Petersburg location, however, the average predicted power loss due to icing is farther away from the observed values at the Valley City location for each of the respective methods.

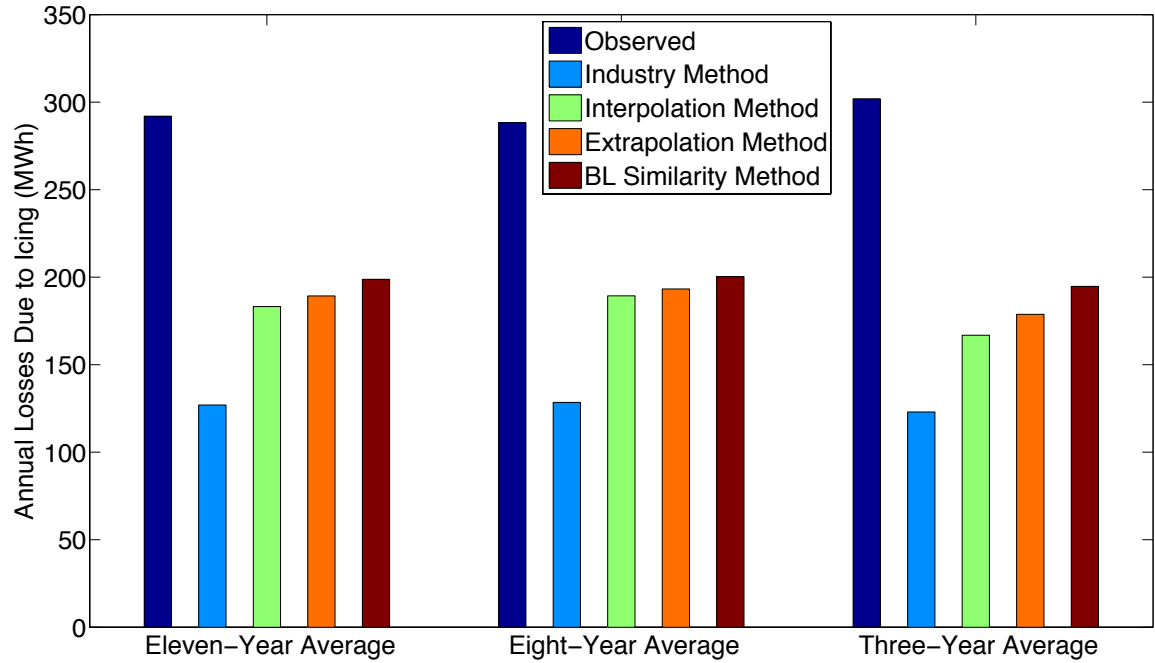


Figure 30: A comparison of the eleven-year, eight-year, and three-year mean annual predicted energy lost due to icing in MWh for the MCP/WAsP methods and industry method at the Valley City location.



## CHAPTER 5

### DISCUSSION

The previous chapter showed that the MCP/WAsP-derived methods of predicting power losses due to icing outperformed the industry method, however the question remains whether those methods are accurate considering the sources of error that are present in the analysis. The first two sections of this chapter discuss the accuracy of the wind speed, relative humidity, and temperature from the MERRA data while the next section discusses the accuracy of the MCP/WAsP-derived wind speeds. Next, the three methods using MCP/WAsP-derived wind speeds are discussed, including financial implications and an analysis of the assumptions made and how they impact the final results. The regional applicability of the final results is then tested by applying them to the Valley City location. Lastly, a short summary of potential future work is presented for this research.

#### 5.1 Suitability of the MERRA-Derived Wind Speeds

As the results in Section 4.1 show, the MERRA-derived wind speeds resulted in average hourly energy production (Figure 15, solid lines) that was, in general, lower than the observed energy production (dashed black line). Of the three methods utilizing MERRA-derived wind speeds, only the boundary-layer similarity (blue solid line) method resulted in a predicted hourly average energy production that was higher for at least one of the eleven seasons tested, and in that case it was only for two seasons. The extrapolation method (magenta solid line) produced predicted hourly

average energy production that was similar to the boundary-layer similarity method but all seasons were under-predicted. The interpolation method (green solid line) produced hourly average energy production that was significantly lower than the observed values for all seasons. The under-prediction could be explained by a variety of factors but the most likely reason is that due to the spatial and temporal resolution of the MERRA datasets, the wind speeds are already under predicted even before they are interpolated to the turbine location. In addition, the interpolation in space and time of the MERRA dataset to the turbine location also introduces some inherent error into the wind speed calculations. To investigate this potential error, wind speeds at a height of 50 m are derived at a MERRA grid point (N 48.00°, W 98.00°) using the MCP/WAsP method outlined in Section 3.1.4, and then compared to the 50 m wind speeds contained within the MERRA dataset at the same location. Figure 31 shows that for October, the MCP/WAsP-derived wind speeds show much higher variability than the MERRA wind speeds. In addition, the mean monthly wind speed for the MCP/WAsP-derived winds is  $7.63 \text{ m s}^{-1}$  while for the MERRA winds, this value is  $7.46 \text{ m s}^{-1}$ .

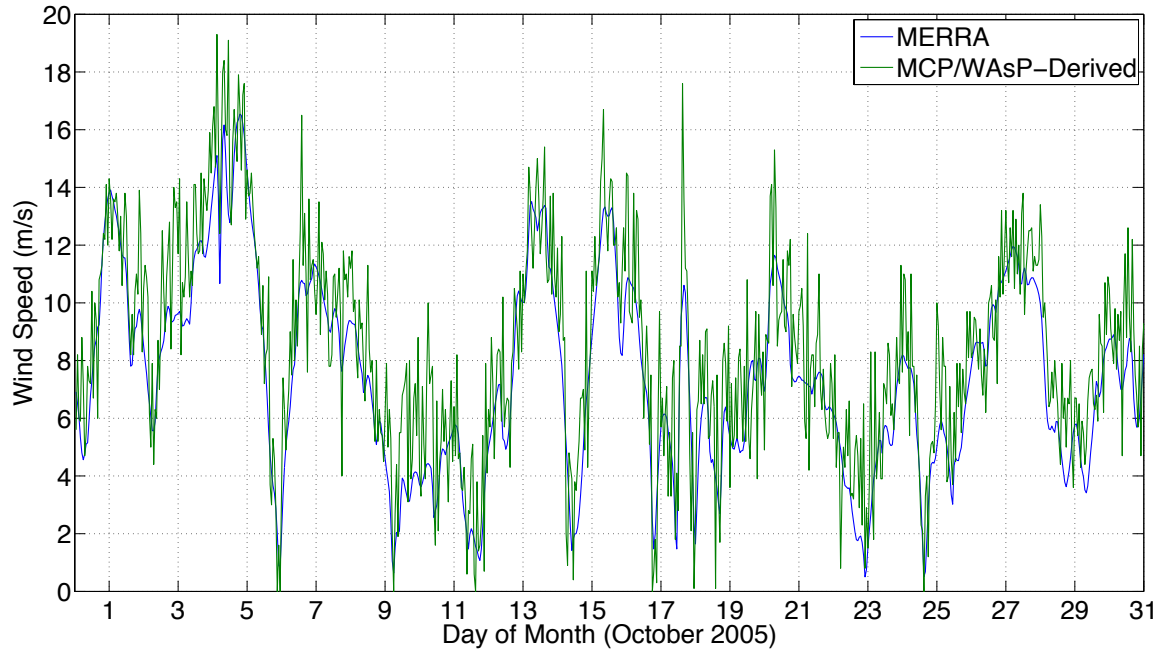


Figure 31: A comparison of the 50 m wind speeds determined using the MCP/WAsP method (green) and the MERRA-derived wind speeds (blue) at a MERRA grid point located at N 48.00°, W 98.00°.

In order to determine if the time of year has an effect, the same analysis is done for January 2006, as shown in Figure 32. Similar to the October comparison, the MCP/WAsP-derived wind speeds show much greater variability than the MERRA wind speeds. In addition, the mean monthly wind speeds are  $7.24 \text{ m s}^{-1}$  and  $6.84 \text{ m s}^{-1}$  for the MCP/WAsP-derived and MERRA-derived winds, respectively. Finally, for the six-month period from October 2005 through March 2006, the average wind speeds are  $7.36 \text{ m s}^{-1}$  for the MCP/WAsP-derived winds and  $7.11 \text{ m s}^{-1}$  for the MERRA winds.

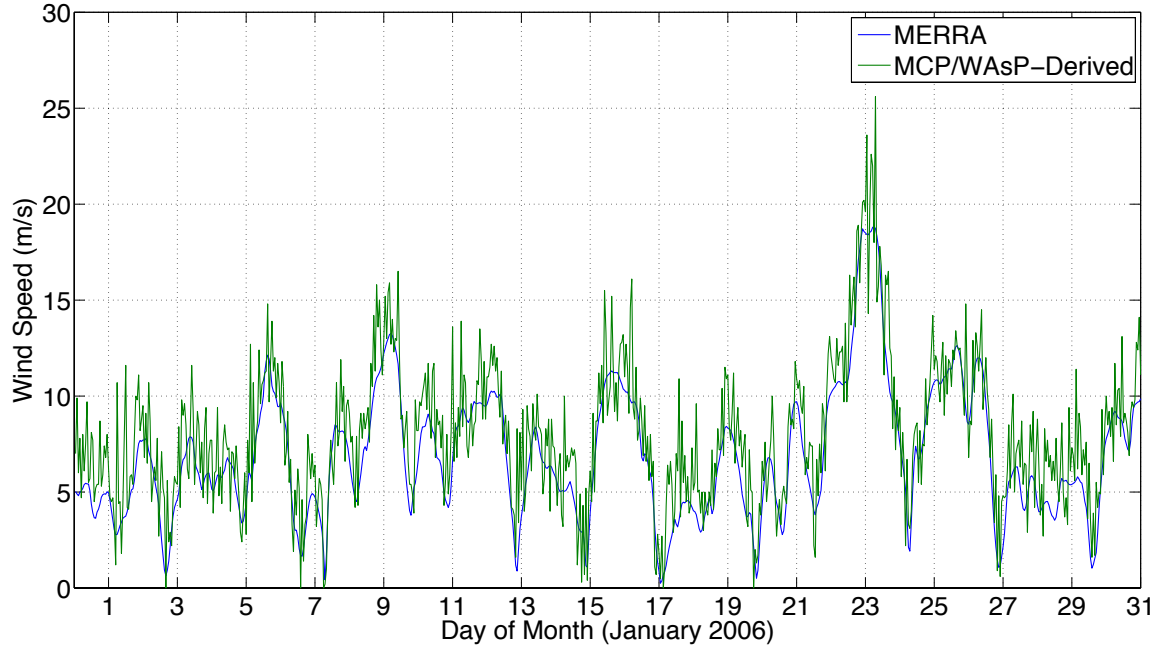


Figure 32: A comparison of the 50 m wind speeds determined using the MCP/WAsP method (green) and the MERRA-derived wind speeds (blue) at a MERRA grid point located at N 48.00°, W 98.00°.

Based on the analysis of this particular season, it is evident that the MERRA wind speeds are lower than they should be, which helps to explain why the hourly average energy production is lower than the observed production for the MERRA-derived wind speeds. The interpolation of the MERRA data to the turbine location can also help explain any error that is found in the the wind speeds. Due to the spacing of the MERRA dataset ( $1/2^\circ$  latitude by  $2/3^\circ$  longitude), the turbine location is not located at any of the grid points and so all variables were interpolated linearly to the turbine location using the four nearest MERRA grid points. This interpolation would thus assume a linear relationship for all variables, including any terrain-based variables. Since the terrain does not change linearly, any surface-based variables would be less accurate than those at the actual grid points in the MERRA datasets. For the boundary-layer similarity method, this would include all surface fluxes and surface scaling parameters. For the interpolation method, this would include the surface

pressure and the thickness of each layer of the atmosphere. For the extrapolation method, this would include all surface variables in addition to the 50 m variables. Since the extrapolation method and the boundary-layer similarity method produce average hourly production values similar to each other but much higher than the interpolation method, it is believed that the interpolation method has a further reduction in accuracy, most likely due to the temporal resolution of the datasets used with this method.

The MERRA dataset consists of two hourly-averaged datasets and one six-hourly instantaneous dataset. The boundary-layer similarity method and the surface value method each use one of the hourly-averaged datasets while the interpolation method uses a combination of the six-hourly instantaneous dataset and one of the hourly-averaged datasets. Although data with hourly and six-hourly temporal resolutions are useful for many applications, determining accurate wind speeds can be problematic because short-term variability in wind speeds cannot be resolved. As a result, the MERRA datasets are not able to capture any sudden increases or decreases in wind speed and thus the energy production based on these wind speeds may not be representative of the observed values. Secondly, since the interpolation method uses two datasets with different temporal resolution, the one with six-hourly resolution is converted to an hourly temporal resolution by interpolating linearly between time points. In doing so, any variability that may exist in reality is lost and replaced with a smooth transition. For example, if the wind speed at time 0 UTC is  $10 \text{ m s}^{-1}$  and the wind speed at 6 UTC is  $10 \text{ m s}^{-1}$ , the linear interpolation would cause the time periods in between to also be  $10 \text{ m s}^{-1}$  when in reality there could be significant changes in the wind speed that aren't inherently visible in the MERRA datasets.

This could easily explain the significant under-prediction of the average hourly wind speeds using the interpolation method.

Overall, it appears that the main source of error for the MERRA wind speeds is due to the low temporal and spatial resolution of the dataset rather than the interpolation to the turbine location. The turbine is located on a small elevated area which would also not be well represented in the MERRA data. For the six month period from October 2005 through March 2006 the mean 50 m MERRA wind speed at the grid point previously mentioned is 3.4 % lower than the MCP/WAsP-derived wind speed at the same location. Interpolating to the turbine location using the four nearest grid points produces a wind speed that is only 3.9 % lower than the MCP/WAsP-derived wind speed at the turbine location.

## **5.2 Suitability of the MERRA-Derived Temperature and Relative Humidity**

In the absence of in-situ measurements, the accuracy of both temperature and relative humidity derived from the MERRA datasets at the turbine location cannot be directly measured. However, observations from the nearest ASOS station at Devil's Lake (DVL) can be used to indirectly determine the accuracy of the MERRA temperature and relative humidity data. For two different months, the temperature trend of the MERRA data (Figs. 33 and 34) follows closely with the observed data, while the mean monthly temperatures, shown in Table 9, agree closely with each other.

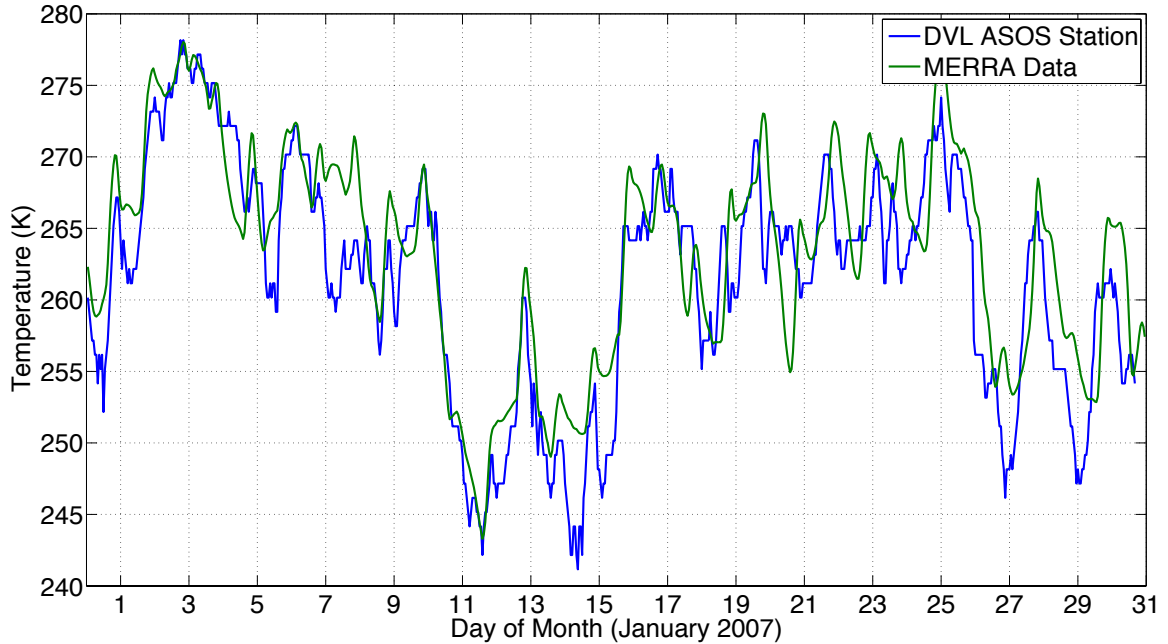


Figure 33: A comparison of hourly 10 m MERRA temperature (green) and observed surface temperature (blue) recorded at the Devil’s Lake ASOS station for January 2007.

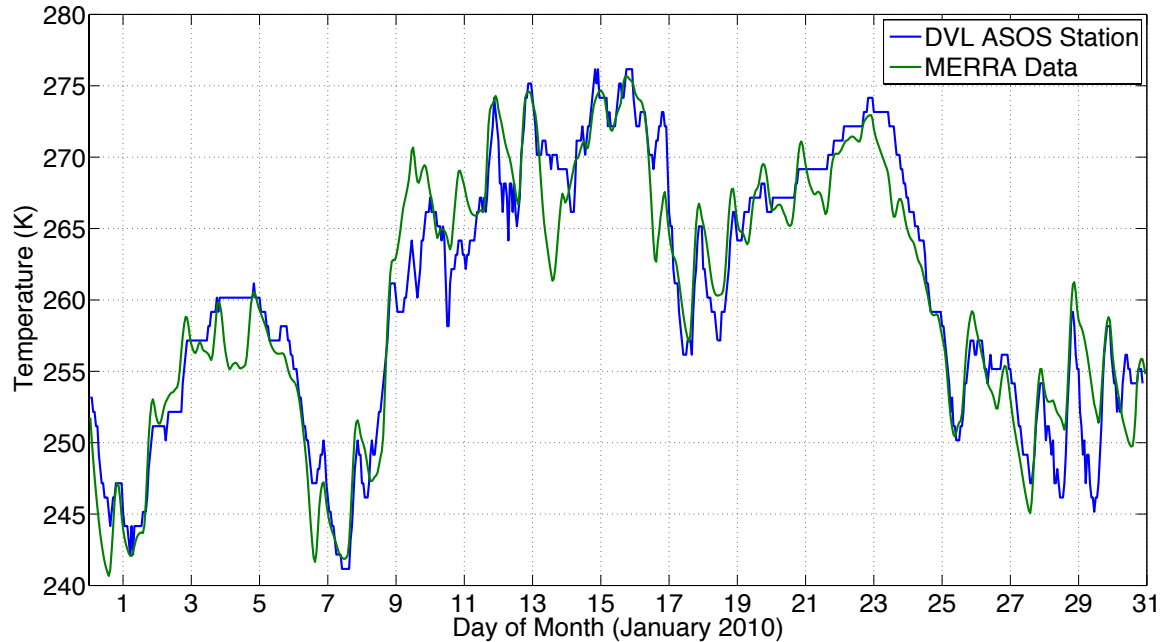


Figure 34: A comparison of hourly 10 m MERRA temperature (green) and observed surface temperature (blue) recorded at the Devil’s Lake ASOS station for January 2010.

Table 9: A comparison of the mean monthly temperatures of the 10 m MERRA data and at the Devil’s Lake (DVL) ASOS station.

Month	MERRA Temperature	DVL Temperature
January 2007	263.4 K $\pm$ 7.4 K	261.5 K $\pm$ 8.1 K
January 2010	260.2 K $\pm$ 9.0 K	260.3 K $\pm$ 9.0 K

The calculated relative humidity at the ASOS station is highly variable, however, the MERRA data does follow the same overall trend for each month, as shown in Figures 35 and 36. The relative humidity at the ASOS station is calculated automatically using the dry bulb temperature and the dew point temperature, while the relative humidity for the MERRA data is calculated using the procedure outlined in section 3.2.1.

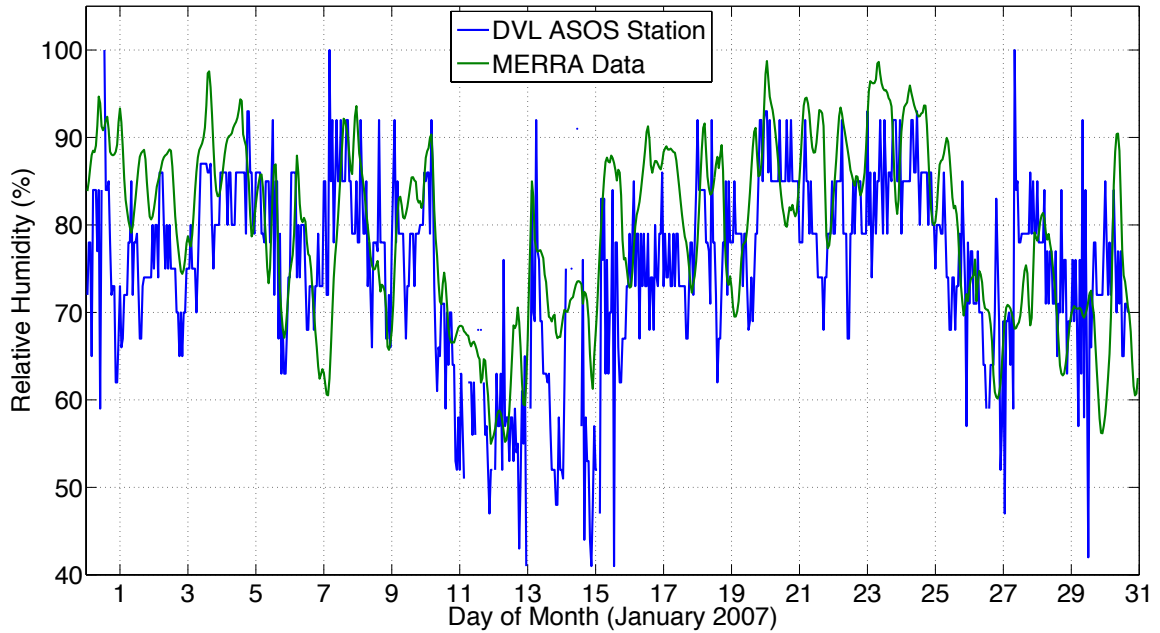


Figure 35: A comparison of hourly 10 m MERRA calculated relative humidity (green) and observed surface relative humidity (blue) recorded at the Devil’s Lake ASOS station for January 2007.



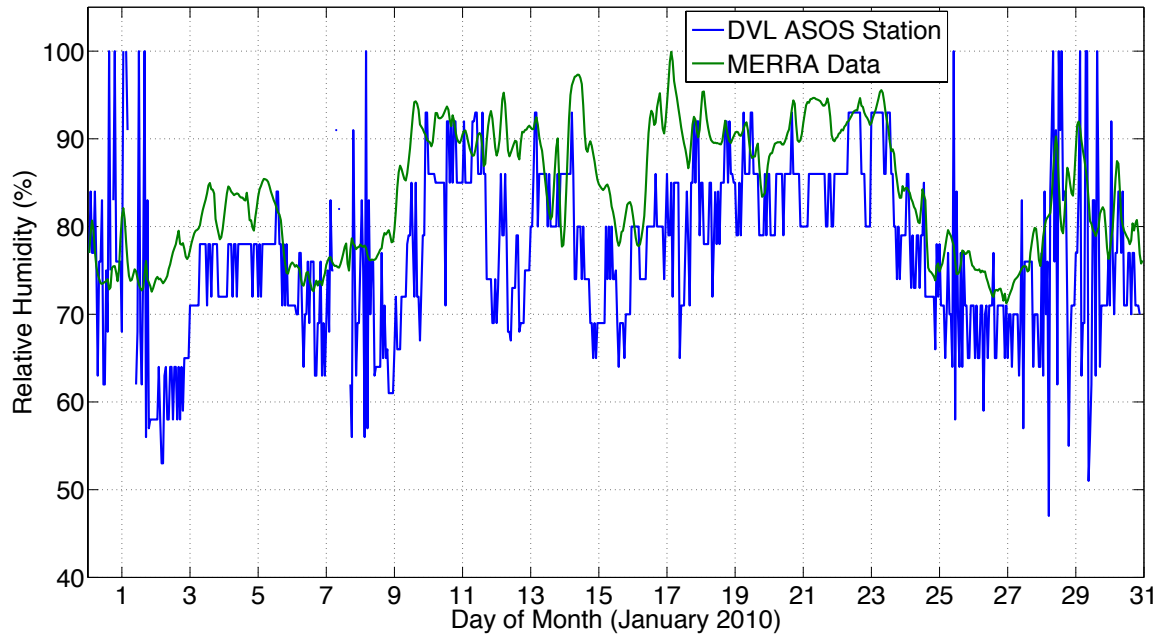


Figure 36: A comparison of hourly 10 m MERRA calculated relative humidity (green) and observed surface relative humidity (blue) recorded at the Devil's Lake ASOS station for January 2010.

Table 10 shows that the MERRA relative humidity is slightly higher than the observed data but still within range so it is safe to assume that the accuracy of the MERRA surface relative humidity is acceptable for this study.

Table 10: A comparison of the mean monthly relative humidity of the 10 m MERRA data and at the Devil's Lake (DVL) ASOS station.

Month	MERRA Relative Humidity	DVL Relative Humidity
January 2007	79.4 % $\pm$ 10.0 %	75.4 % $\pm$ 10.4 %
January 2010	83.8 % $\pm$ 7.1 %	77.2 % $\pm$ 9.4 %

With the accuracy of the MERRA surface data considered to be acceptable, the accuracy of these same variables at the turbine height is required. The temperature and relative humidity at the turbine height can be compared to the surface values and,

based on a typical atmospheric profile, their accuracy can be validated. Assuming a well-mixed boundary layer, i.e. constant specific humidity and potential temperature, the relative humidity should increase with height within the boundary layer, and so the surface value should be lower than those calculated by the interpolation and boundary-layer similarity methods. For the entire month of December 2007, the relative humidity calculated using the boundary-layer similarity method (blue line on Figure 37) is greater than or equal to the surface value (green line on Figure 37) for all time periods as expected. However, the relative humidity calculated using the interpolation method (red line on Figure 37) is, over many time periods, lower than the surface value.

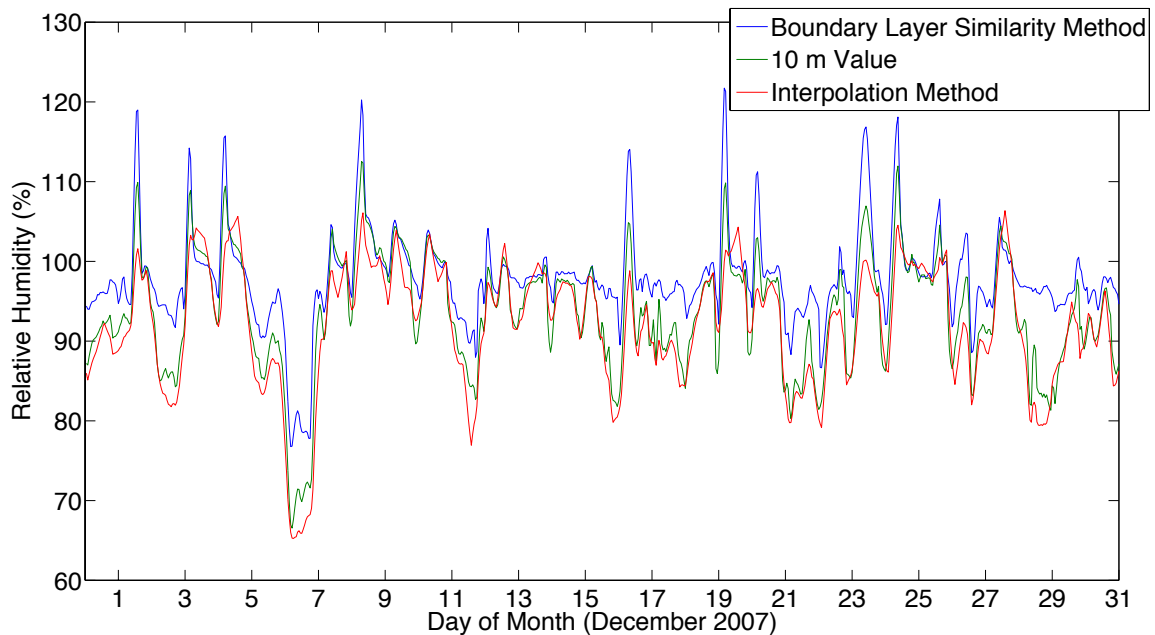


Figure 37: Comparison of the relative humidity calculated using the boundary-layer similarity method at 72.3 m (blue), the interpolation method at 72.3 m (red), and the surface value at 10 m (green).

A possible reason for this discrepancy is that the first model level may not always be within the planetary boundary layer and so a direct interpolation may not be the most accurate representation of the state of the atmosphere between the surface and

that particular height. In addition, the specific humidity is typically constant from the top of the surface layer until the top of the boundary layer and this type of profile is not taken into account with the interpolation method.

The comparison of this month between the three methods for temperature is not as straight forward as the relative humidity comparisons. Typically, the potential temperature remains constant from the top of the surface layer until the entrainment zone, and since the pressure decreases with height, the temperature decreases with height. As such, the temperature determined by the boundary-layer similarity method (blue line on Figure 38) and interpolation method (red line on Figure 38) at the turbine hub height should be lower than the surface value method (green line on Figure 38).

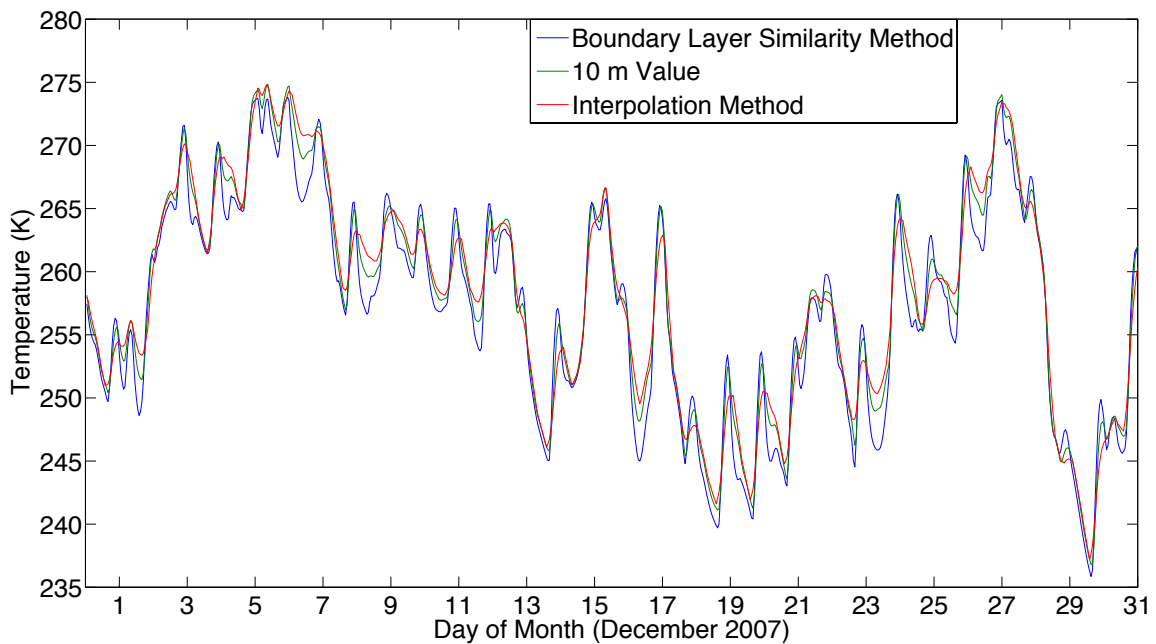


Figure 38: Comparison of the temperature calculated using the boundary-layer similarity method at 72.3 m (blue), the interpolation method at 72.3 m (red), and the surface value at 10 m (green).

In many cases, the temperature determined by the boundary-layer similarity method is lower than the surface value, most notably in the overnight hours, while other times it is higher than the surface value. However, the overall temperature trend matches well with the surface values. The temperatures determined with the interpolation method also follow a trend that matches well with the surface values, however, the variability between the maximum and minimum temperatures for each day seem to be less than both the surface values and those determined with the boundary-layer similarity method. In agreement with the typical temperature profile, there are some periods of time where the temperature calculated using the interpolation method is lower than the surface value, however there remain many periods of time where the temperature is higher than the surface value. In the cases where calculated temperatures using interpolation and boundary-layer similarity are higher than the surface values, there may be a temperature inversion layer present, however, the existence of such a layer within the boundary layer is not able to be verified.

Table 11 shows that for the month of December 2007, the boundary layer similarity method has more time periods where the temperature at the turbine height is lower than the surface and where the relative humidity is higher than the surface, as compared to the interpolation method.

Table 11: Comparison of the percentage of time for the month of December 2007 when calculated temperatures are lower than the surface value and calculated relative humidities are higher than the surface value.

	Percent of Month When Calculated Temperature is Lower than the Surface Value	Percent of Month When Calculated Relative Humidity is Higher than the Surface Value
Boundary-Layer Similarity Method	75.54 %	88.71 %
Interpolation Method	37.50 %	24.06 %

Based on the comparison between methods, it is clear that the temperature and relative humidity calculated using the boundary-layer similarity are a more realistic representation of the atmosphere at the height of the turbine hub than the interpolation method. Due to the fact that both methods have the same inherent sources of error, the boundary-layer similarity method is shown to be the best method of determining the required atmospheric variables at the hub height.

### 5.3 Suitability of MCP/WAsP-derived Wind Speeds

Section 5.1 outlined the sources of error and the drawback of using MERRA-derived wind speeds, and so this section aims to determine any increased accuracy in using MCP/WAsP-derived wind speeds. Figure 15 shows that the MERRA-derived wind speeds produced average hourly energy production values that were less than the observed values of the turbine. Figure 17 shows that MCP/WAsP-derived wind speeds are higher than the MERRA-derived wind speeds, which leads to a higher average hourly energy production and one that is closer to the observed energy production of the turbine. Using the observed energy production as a proxy for the wind speeds, it is clear that having a nearby meteorological tower with wind speed measurements

allows for a more accurate representation of the actual wind speeds at the turbine location than by using reanalysis alone.

As outlined in section 3.1.4, the method to determine MCP/WAsP-derived winds combines both the MCP analysis of the anemometer-measured winds and a translation to the turbine location by using a WAsP analysis. Together, they appear to produce the best representation of the wind speeds at the turbine location, but analyzing their individual contributions may help in determining which of the two components is most important, if at all. For the month of October 2005, the wind speeds calculated using both MCP and WAsP (green line on Figure 39) seem to correlate well with those using only MCP (blue line on Figure 39).

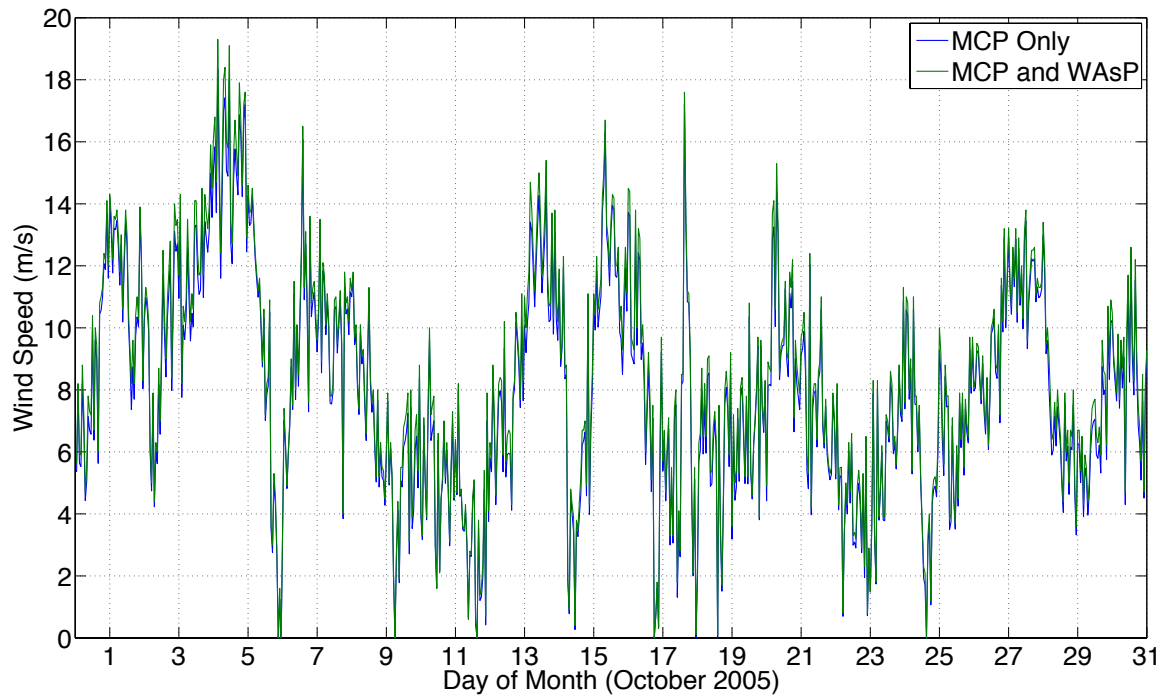


Figure 39: Comparison of wind speeds derived solely from MCP (blue) at the meteorological tower and derived from both MCP and WAsP (green) at the turbine location for October 2005.

Figure 40 verifies this conclusion, showing that the wind speeds are highly correlated over the entire time period. At higher wind speeds, the WASP translation adds a higher increase in wind speed than at lower wind speeds. Overall, the mean wind monthly wind speed for the MCP-only method is  $8.01 \text{ m s}^{-1}$  while for the full MCP/WASP method, the mean monthly wind speed is  $8.41 \text{ m s}^{-1}$ .

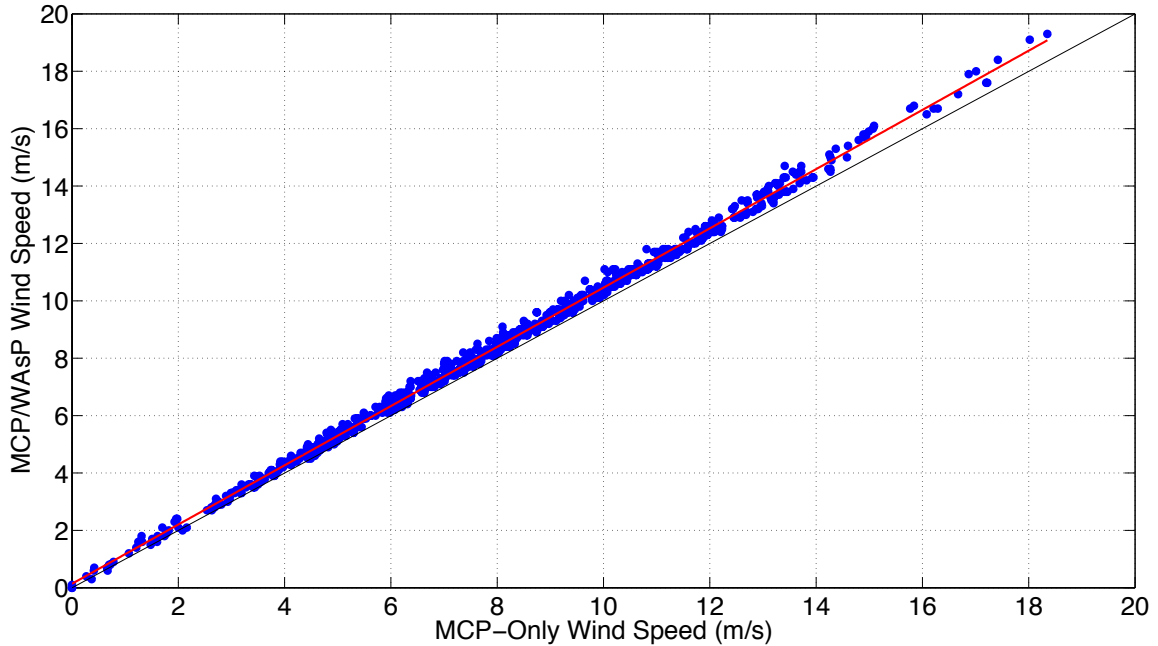


Figure 40: Comparison of wind speeds derived using only MCP and both MCP and WASP for October 2005 at the Petersburg location with the line of best fit shown in red (slope=1.032, y-intercept=0.1392).

A similar result appears when looking at January 2006, shown in Figure 41. Here, the analysis shows the same correlation between the two methods, including the small difference in mean monthly wind speed. For the MCP-only method, the mean monthly wind speed is  $7.61 \text{ m s}^{-1}$  while for the full MCP/WASP method, the mean monthly wind speed is  $8.06 \text{ m s}^{-1}$ .

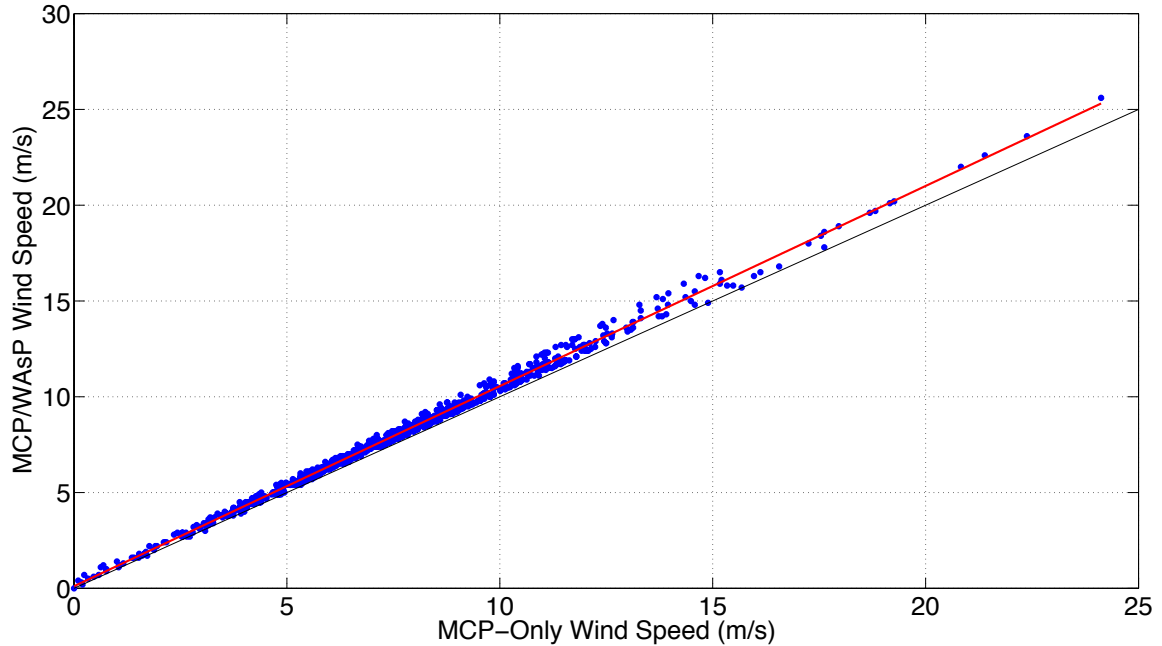


Figure 41: Comparison of wind speeds derived using only MCP and both MCP and WASP for January 2006 at the Petersburg location with the line of best fit shown in red (slope=1.045, y-intercept=0.1088).

Since the WASP translation depends only on factors that don't change over time such as surface conditions, obstacles, and the height of the measurements, the effect of doing a WASP translation is essentially identical over all time periods and is simply a shift of the MCP wind speeds upwards.

One potential drawback of using the MCP/WASP method to derive the wind speeds, however, is that it assumes the same correlation over a long period of time. For this study, the anemometer data are correlated to MERRA data for the two-year period ending June 30, 2012 and the correlation is assumed to be constant for the period from July 1, 2002 to June 30, 2013. If, for example, there was a change made to the reference data or if an error was present in the anemometer data, the correlation would be incorrect.



## 5.4 Prediction of Annual Losses Due to Icing

Section 4.3 compares the results of each of the six methods in terms of their accuracy in predicting annual icing losses compared with the industry standard. It is important to note that the industry standard used in this study is not a universal method employed by all within the wind energy industry. In sections 5.1 and 5.3 it is clear that MCP/WAsP-derived wind speeds are more accurate than MERRA-derived wind speeds, and so of the six methods used in predicting annual losses due to icing, the three methods utilizing MCP/WAsP-derived wind speeds will be the focus of this discussion. When looking at the three test years, all three methods predict, on average, annual icing losses that are closer to the observed icing losses, both in terms of actual energy lost (Figure 28) and as a percent of the total annual energy produced (Table 7), as compared to the industry method. Among the three methods, the boundary-layer similarity method is the most accurate predictor of annual icing losses, while the interpolation method is the worst performing. This verifies the conclusions of section 5.2 that showed the boundary-layer similarity method produced relative humidities and temperatures that are more realistic than the interpolation and surface value methods. Looking at the full eleven-year dataset a similar pattern emerges, with all three methods outperforming the industry method. Again, the interpolation method performs the worst of the three methods, however, in this case both the boundary-layer similarity method and surface value methods are identical in terms of predicting percentage icing losses, while the boundary-layer similarity method is still the best predictor of actual energy losses. An important advantage that the prediction methods hold over the industry method is their ability to more accurately represent the variability inherent in icing losses. The industry method is developed to account for average conditions over a long period of time and cannot

take into account the year-to-year variability. As an example, the 2012 study year showed a significant difference in observed icing losses than all previous years, but the prediction methods are able to capture this variability by predicting the smaller amount of icing losses. If an average value is used for all years, as in the industry method, that particular year would not be well represented.

Over the course of the eleven seasons, one noticeable visible pattern seen in Figure 27 is that for the majority of seasons, each of the methods under-predicts the percentage annual losses, with only three seasons being over-predicted. The eleven-, eight-, and three-year averages in Figure 28 also show that each of the methods under-predicts the actual energy losses. This can be the result of either the observed losses not being estimated accurately, or the predicted losses being lower than they should be. In determining both observed and predicted losses, assumptions were made that may impact their results.

#### **5.4.1 Assumptions and Potential Errors in Observed Icing Losses**

The method to determine observed icing losses includes the assumption that if the observed energy output is less than 80 % of the expected energy output, icing is assumed to be occurring. By stipulating this threshold of 80 %, the aim is to maximize the time periods where icing is most likely to occur. Knowing that even a small amount of icing can reduce the energy output of a turbine by 20 % (Jasinski et al., 1998), this threshold aims to capture these types of events. In reality, this threshold may need to be adjusted lower to account for local climatology, and so in this study, observed icing losses may be overestimated as a result. For example, if some other factor is influencing energy output, e.g. turbulence, the difference between the observed energy output and the expected energy output could be a result of that factor

and not icing. As a result, this difference would be misclassified as being caused by icing, and thus overestimating the observed icing losses. By adjusting the threshold to a lower value, i.e. less than 80 %, the possibility of non-icing factors impacting the results could be lessened.

Human factors also play a large role in the determination of observed icing losses for this particular turbine. In cases where there are single turbines in remote locations, when there is severe build-up of ice, it may take longer for the turbines to be reset, which happens more quickly at larger wind farms. Because of this delay, the turbine will continue to generate less than the expected amount of energy long after the atmospheric icing conditions have subsided. In the case of the Petersburg turbine, this period of time could extend to many days, especially if an icing event is followed by extreme cold weather that does not allow the ice to melt or fall off the turbine blades. Although there exists some recovery time from icing events that can be estimated for larger wind farms or turbines where ice build-up is removed in a timely manner, any recovery time for the Petersburg turbine will be highly variable and cannot be estimated. As such, periods of time where ice has built-up and yet icing conditions are no longer present, are included in the observed icing losses calculations, which causes the observed losses to be over-estimated. Lastly, all turbines require regular maintenance, however, the Petersburg turbine does not have a full set of records for when maintenance was performed. In some cases during the winter months, downtime due to maintenance could be mistaken for periods of icing, which, again, would cause the observed losses to be over-estimated.

#### 5.4.2 Assumptions and Potential Errors in Predicted Icing Losses

In determining the predicted icing losses, it is assumed that 100 % of the energy is lost during the periods of icing. This has the effect of potentially over-estimating the icing losses since it is known that not all potential energy is necessarily lost when ice begins to build up on turbine blades. However, by assuming 100 % loss during icing periods, it eliminates the guesswork needed to determine exactly what percentage of potential energy is lost when ice begins to form. Further analysis would need to be performed in order to determine a better estimate of the effects that icing has on the turbine blades and on the direct reduction in energy production. One aspect of icing that is not directly taken into account in this study is icing due to precipitation such as freezing rain or wet snow. Although the environment in which these types of precipitation fall is typically one of high relative humidity, temperatures may not necessarily be below 0 °C (273.15 K). This would introduce a slight under-prediction in icing losses since the prediction methods require temperatures be below freezing. The potential error due to this assumption may not be significant in the Northern Plains region, but for regions further south that may be impacted more by freezing rain and wet snow events, icing prediction should take precipitation into account.

#### 5.5 Losses Due to Other Factors

In using equation 3.29 to determine annual observed icing losses, the value of  $P_{obs}$  is taken directly from the Minnkota dataset and represents the net total production after all losses have been accounted for. These losses include, but are not limited to, icing, turbulence, electrical, and mechanical losses. The calculation of observed annual icing losses ( $L_O$ ) uses this net total production in addition to observed icing losses ( $I_{obs}$ ) in the denominator and so the annual losses as calculated are overpredicted

since other losses are not taken into account. For the turbine locations used in this study, these other losses typically amount to approximately 5.5 % of the gross annual production but can be variable from year-to-year much like losses due to icing. In using equation 3.30 to determine annual predicted losses, the denominator ( $P_{pred}$ ) uses the total expected production without any losses being accounted for (ie. the gross annual expected production). In order to compare both  $L_O$  and  $L_P$  and to ensure the methods are trained properly, these values must be calculated with similar denominators to avoid the inclusion of other losses with icing losses. To remain consistent with annual predicted losses, future analysis should include the calculation of annual observed losses due to icing as:

$$L_O = \frac{I_{obs}}{P_{pred}} \quad (5.1)$$

and icing losses using the industry method as:

$$I_{ind} = P_{pred} \times L_{ind} \quad (5.2)$$

where  $L_{ind}$  is the percent annual losses (4.7 %). By using equation 5.1, other losses are then excluded from the training of the prediction methods and by using equation 5.2, the seasonal losses (in MWh) based on the industry method can be directly compared to  $I_{obs}$  and  $I_{pred}$  without the impact of other losses affecting the comparison.

## 5.6 Financial Implications of Icing Losses

The potential financial losses due to icing can be estimated based solely on the results of this study. Assuming an energy price of \$30/MWh, Table 12 shows the estimates of annual financial losses due to icing for one turbine at the Petersburg location based

on Figure 28 for the three prediction methods and industry methods compared with the observed icing losses.

Table 12: Estimates of annual financial losses for a single turbine at the Petersburg location for each of the three MCP/WAsP prediction methods, the industry method, and the observed icing losses, assuming a cost of energy production of \$30/MWh.

	Average Annual Losses for the Test Years	Average Annual Losses for the Training Years	Average Annual Losses for All Years
Observed	\$9351.90 ± \$3659.46	\$9279.33 ± \$1683.69	\$9299.13 ± \$2159.61
Industry Method	\$3798.99 ± \$428.46	\$3976.68 ± \$252.18	\$3928.23 ± \$295.89
Boundary-Layer Similarity Method	\$7452.54 ± \$2996.76	\$7961.79 ± \$779.16	\$7822.92 ± \$1509.21
Extrapolation Method	\$7095.24 ± \$2811.69	\$7881.03 ± \$684.45	\$7666.74 ± \$1429.62
Interpolation Method	\$6960.75 ± \$3208.89	\$7795.71 ± \$1008.84	\$7568.01 ± \$1706.91

As the analysis in section 5.4 showed, the three methods far outperform the industry method in predicting icing losses, with the boundary-layer similarity method performing the best. Looking at the average financial losses for all eleven years, the industry method corresponds to financial losses almost 60% lower than the observed, while the interpolation method, the worst performing of the three corresponds to only a 19% under-prediction of the financial losses. If this analysis is performed for a large wind farm with up to 50 turbines, then the industry method under-predicts the observed losses by over \$268,000 while the boundary layer similarity method only under-predicts observed losses by \$73,000. Bearing in mind the assumptions outlined in sections 5.4.1 and 5.4.2, it would be fair to assume that the actual financial losses due to observed icing losses are most likely lower than this study shows, but by

how much is indeterminable without knowing the actual icing losses at the turbine location.

### 5.7 Extrapolating Results Regionally

Although the results of section 4.4 (Figure 29) show that the three methods outperform the industry method at the Valley City location for all but one year, it is worth noting that all three methods under-predict the annual losses due to icing for every year that was tested, bringing their results closer to that of the industry method. In addition, the industry method also performed relatively better at the Valley City location than at the Petersburg location, as both the three- and eleven-year average differences decreased when moving to the new location (Table 8). When analyzing the predicted average annual energy lost due to icing for the three methods and the industry method, the losses calculated from the industry method are similar to those at Petersburg, however, the losses calculated using the three methods are significantly lower than those at Petersburg, as shown in Table 13.

Table 13: Predicted average annual losses due to icing compared with observed icing losses for Valley City and Petersburg locations over all eleven years, over the eight training years, and over the three testing years.

		Predicted Average Annual Losses Due to Icing (kWh)				Observed
		Interpolation Method	Boundary-Layer Similarity Method	Extrapolation Method	Industry Method	
11 year	Petersburg	251468	260764	255558	145509	309971
	Valley City	183217	198796	189317	140690	291996
8 year	Petersburg	258974	265393	262701	147094	309971
	Valley City	189357	200312	193269	142014	288270
3 year	Petersburg	231450	248418	236508	141284	311730
	Valley City	166846	194752	178779	137160	301930

Two things become evident when comparing the energy losses at both locations. First, the observed losses at Valley City are lower than those at Petersburg. This is to be expected as Valley City is located at a more southern latitude, and one would expect temperatures to be slightly warmer at this location. This would only have impacts on icing when temperatures are near 0 °C (273.15 K) as above freezing temperatures could exist at Valley City while below freezing temperatures could exist at Petersburg. Secondly, one would expect the predicted icing losses for all methods to be similar at both locations, as they are in the same geographic area. Instead, applying the results from one location to another location in the same region does cause a noticeable deficiency in the predicted icing losses. It has yet to be determined the regional extent to which results can be applied, however, the distance between Petersburg to Valley City does show that the extent is not particularly wide. In



addition, a short-term in-situ wind speed data set is required for each method in order to perform the MCP/WAsP analysis and it is currently unknown the regional extent to which MCP/WAsP analysis can be performed from a single location.

### 5.7.1 Retraining the Dataset at Valley City

To provide a better understanding of the regional extent of the MCP/WAsP analysis, the boundary layer similarity method using MCP/WAsP-derived winds was applied at the Valley City location with the data being retrained to determine a new optimal relative humidity (Figure 42), rather than simply applying the relative humidity from the Petersburg location.

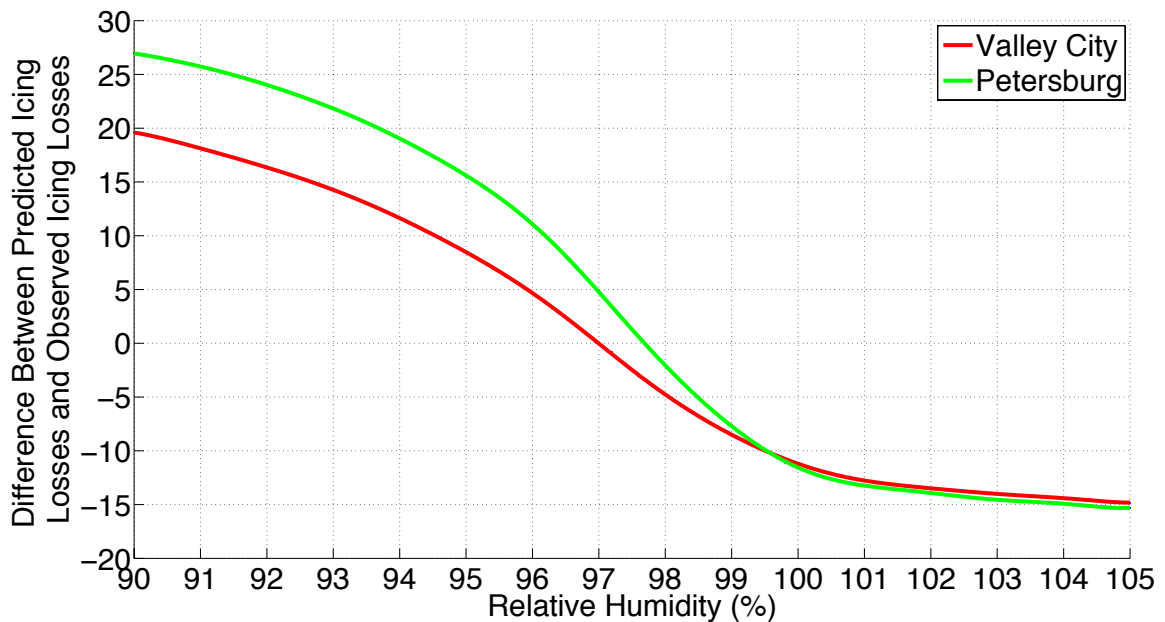


Figure 42: A comparison of the determination of the optimal relative humidity using the boundary layer similarity method with MCP/WAsP winds at Petersburg (green) and Valley City (red).

By retraining the data at the new location (Figure 43), the prediction of icing losses improves significantly, and brings the results closer in line to what was seen at the

Petersburg location, with some years being over-predicted while the majority are under-predicted.

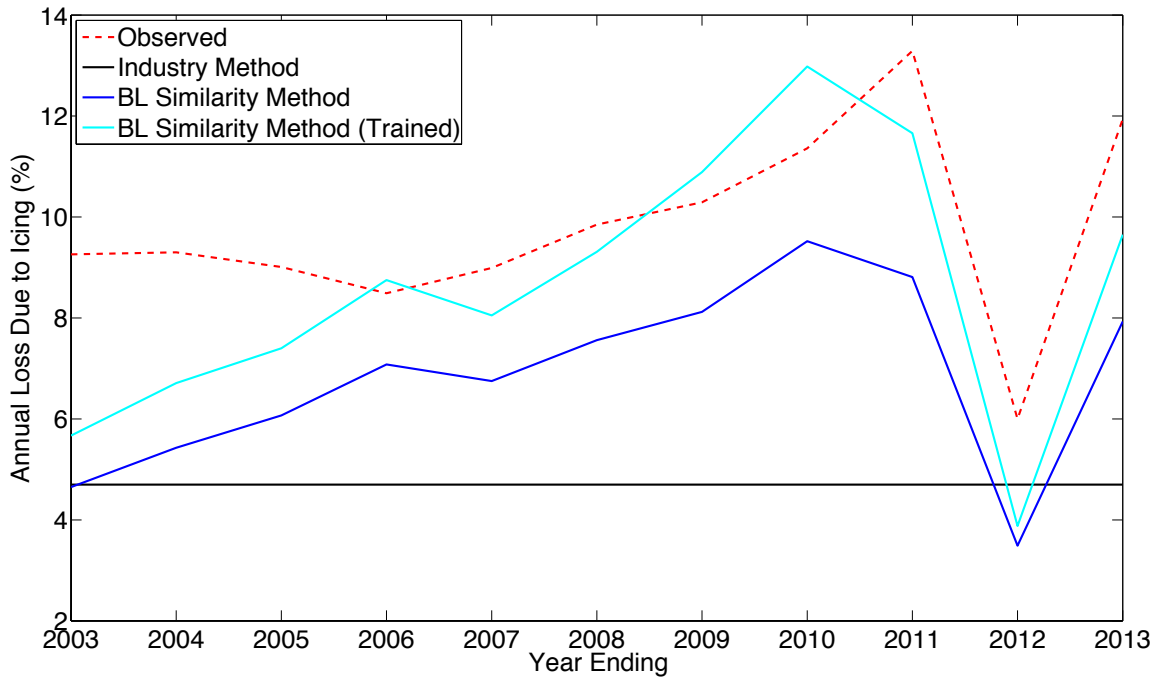


Figure 43: A comparison of the boundary-layer similarity method with MCP/WAsP-derived winds at Valley City using the Petersburg result (dark blue) and by retraining the data (light blue) to predict annual losses due to icing. Observed losses are the red dashed line while the industry method losses are the black line.

In addition, Table 14 shows that by retraining the data, the average difference between the predicted losses and the observed losses improves over the untrained data, and, in fact, shows similar results to the Petersburg location using the same method (last row of Table 7).

Table 14: A comparison of the mean absolute difference between the observed annual losses and both the predicted (untrained and trained) annual losses and the industry method for the three test seasons and the entire dataset. Data is for the Valley City location

Method	3 Year		11 Year	
	Absolute Difference Between Observed and Predicted Losses	Absolute Difference Between Observed and Industry Method	Absolute Difference Between Observed and Predicted Losses	Absolute Difference Between Observed and Industry Method
Boundary-layer similarity with MCP/WAsP-derived winds	$3.66 \pm 1.03 \%$	$5.71 \pm 3.88 \%$	$2.94 \pm 1.11 \%$	$5.10 \pm 1.93 \%$
Boundary-layer similarity with MCP/WAsP-derived winds (trained)	$2.01 \pm 0.35 \%$	$5.71 \pm 3.88 \%$	$1.62 \pm 1.00 \%$	$5.10 \pm 1.93 \%$

Lastly, in comparing the mean annual energy losses due to icing (Figure 44), the retrained dataset increases the mean annual losses due to icing to be more in line with the mean observed losses.

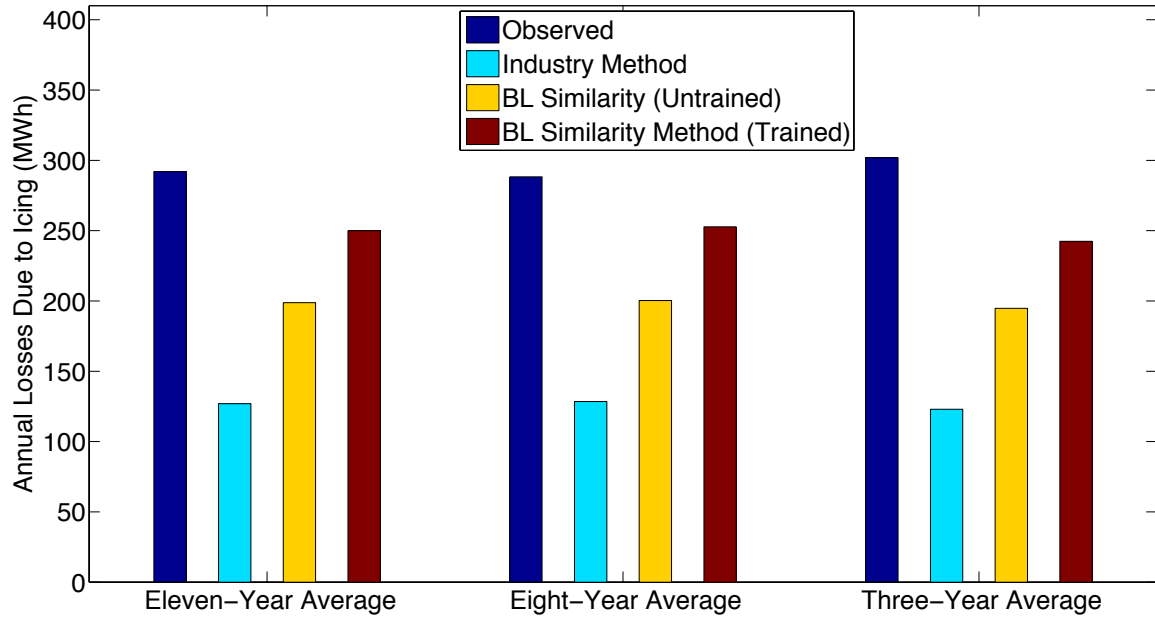


Figure 44: A comparison of the eleven-year, eight-year, and three-year mean annual predicted energy lost due to icing in MWh at the Valley City location for the industry method and both untrained and trained boundary-layer similarity methods with MCP/WAsP-derived winds.

It is clear from the analysis in this section that training the dataset at a particular location is an improvement over simply reapplying the results from a different location. It appears that the main factor influencing icing prediction is the proper determination of the optimal relative humidity for a particular site, and that MCP/WAsP-derived winds can, in fact, be applied across a large geographic area, the extent to which would need to be determined in a future analysis.

### 5.8 Impact of Residual Error on the MCP/WAsP Analysis

To better understand how the residual error within the MCP/WAsP analysis impacts the icing prediction, a case study using the boundary layer similarity method at the Petersburg location is performed with the MCP/WAsP method of determining wind speeds, neglecting the residual error of equation 3.1. The method of Section 3.3.2

is performed with the new MCP/WAsP wind speeds and a new optimal relative humidity is found. Figure 45 shows that both the observed icing losses and the predicted icing losses decrease for each season when the residual error is not included in the analysis.

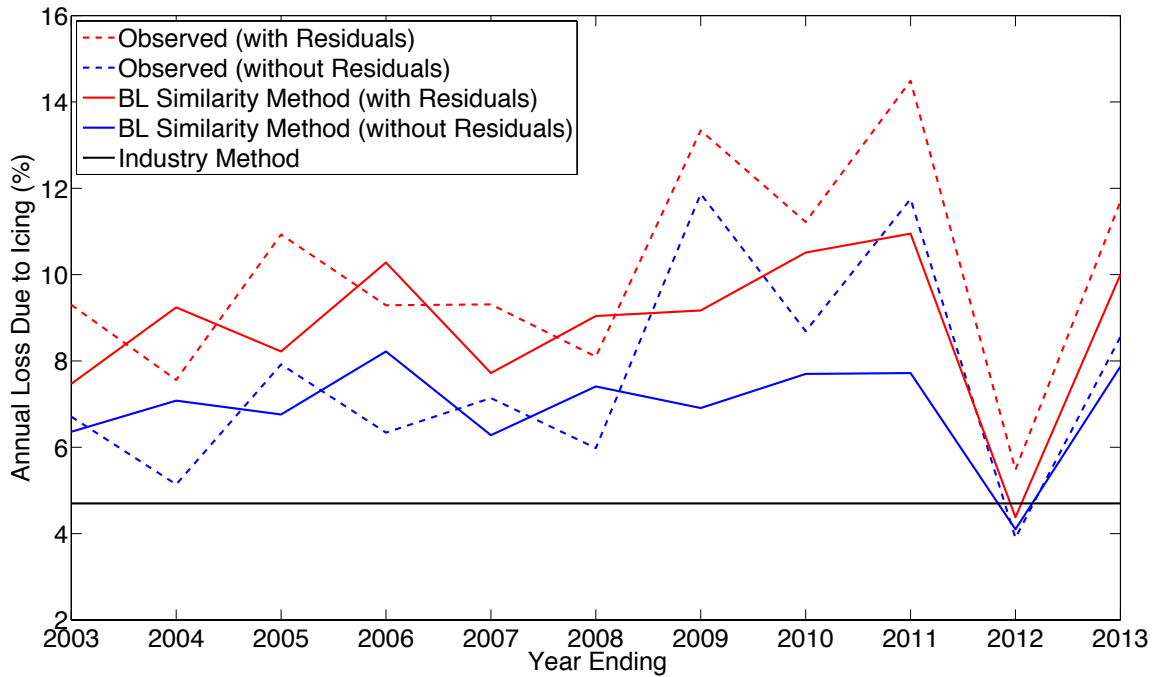


Figure 45: The boundary layer similarity method with MCP derived winds (with and without residual error) to predict percentage annual losses due to icing at the Petersburg location as compared to the industry method.

This decrease causes the industry method to perform better than the boundary layer similarity method for three of the eleven seasons (2004, 2006, and 2008), however over all three test seasons the boundary layer similarity method performs better than the industry method. Table 15 shows the same pattern when looking at the test-year and eleven-year averages. Over both time periods, the absolute difference between the observed and predicted losses does decrease when not using residual errors in the MCP/WAsP calculations. The difference between the observed losses and industry

method decreases as well, but by a larger margin, suggesting that using the residual error creates a high bias in the observed icing losses.

Table 15: A comparison of the mean absolute difference between the observed annual losses and both the predicted annual losses (with and without residuals) and the industry method at the Petersburg location for the three test seasons and the entire dataset. Predicted losses are determined with MCP/WAsP-derived wind speeds.

Method	3 Year		11 Year	
	Absolute Difference Between Observed and Predicted Losses	Absolute Difference Between Observed and Industry Method	Absolute Difference Between Observed and Predicted Losses	Absolute Difference Between Observed and Industry Method
Boundary-layer Similarity with Residuals	$2.13 \pm 1.29 \%$	$5.87 \pm 4.64 \%$	$1.94 \pm 1.13 \%$	$5.40 \pm 2.63 \%$
Boundary-layer Similarity without Residuals	$1.64 \pm 2.08 \%$	$3.90 \pm 3.12 \%$	$1.68 \pm 1.51 \%$	$3.08 \pm 2.30 \%$

Comparing the raw power production (Figure 46) the same decrease in both observed icing losses and predicted icing losses is seen for all three time periods, however the boundary layer similarity method without residuals still predicts icing losses closer to the observed losses than the industry method.

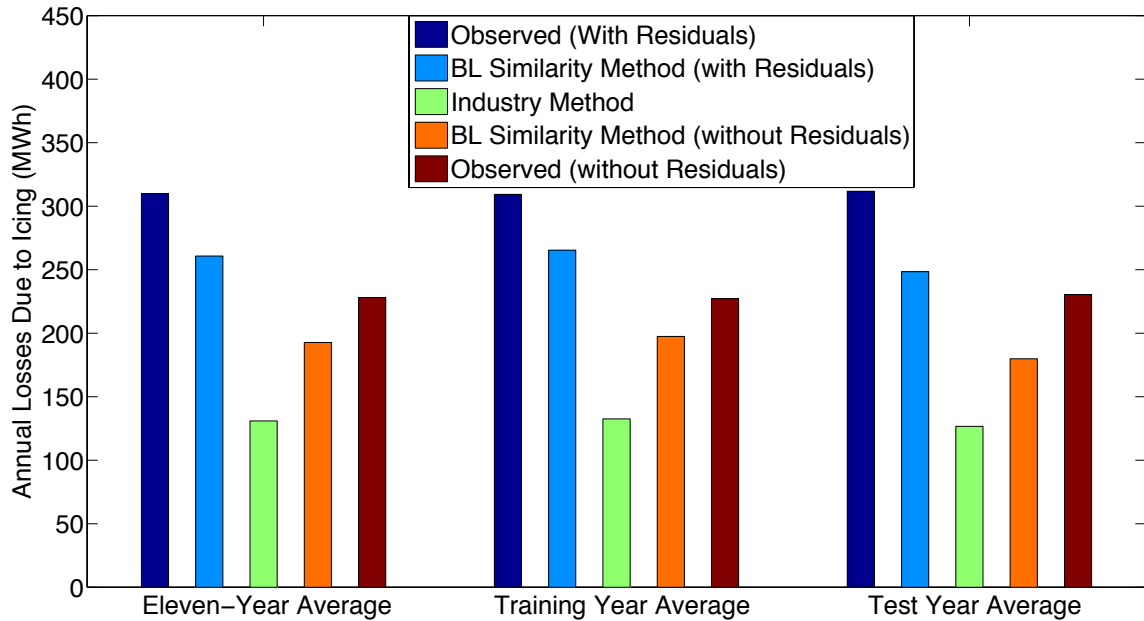


Figure 46: The boundary layer similarity method with MCP derived winds (with and without residual error) to predict annual losses due to icing at the Petersburg location as compared to the industry method.

Evidently, the use of residual errors in the MCP/WAsP analysis does create some significant differences in the icing prediction algorithm. Most notably, the observed icing losses decrease when no residual errors are used, which also decreases the predicted losses. The cause of this decrease is due to the decrease in variability in the wind speeds as shown in Figure 47.

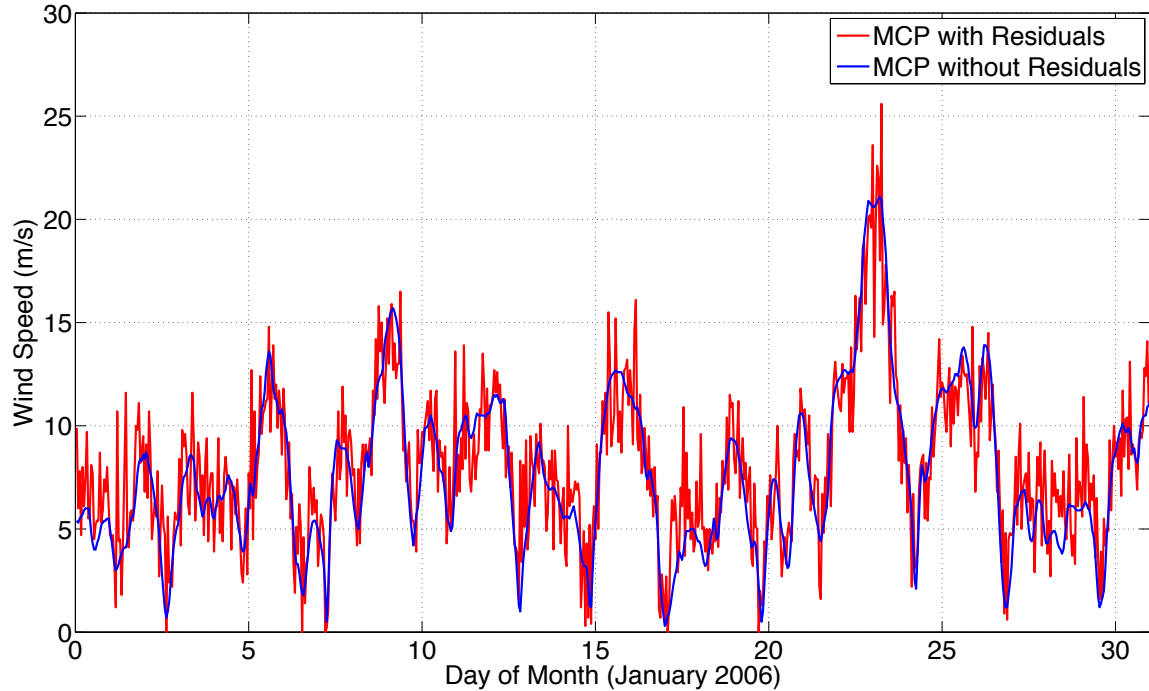


Figure 47: MCP/WAsP-derived wind speeds with and without residual error included in the analysis at the Petersburg location for January 2006.

In both analyses, the overall trend of wind speed is similar over the entire month, however using residual errors does appear to introduce a high degree of variability that may or may not be as realistic a representation of the actual wind speeds as the analysis without using residual error. A more thorough analysis of both methods is needed to determine which would be the best choice.

## 5.9 Future Work

The long term goal of this research is the eventual creation of some form of icing climatology map for the Northern Plains region of the United States. Since this research focuses mainly on one location, with a small analysis at a secondary location, it is hoped that it can be expanded to include other locations across the Northern Plains. This would require a denser set of in-situ measurements so that the MCP/WAsP



method of determining wind speeds can be performed with as little spatial error as possible. Secondly, the use of data from other wind turbines in the region is necessary in order to verify the prediction algorithm and to provide a better estimate of observed power losses due to icing, which may prove difficult if owners are unwilling to share their production data due to proprietary reasons. Some of the assumptions in determining observed losses due to icing could also be mitigated with some form of realtime observation of the turbines. Periods of icing could then be distinguished from maintenance issues or other non-icing related factors.

A major assumption in this research was using relative humidity as a proxy for other moisture variables such as liquid water content and droplet size distribution, to avoid significant amounts of complexity. For a more skillful turbine icing prediction, these additional moisture variables should be included in the prediction algorithm. However, without observations of these variables, testing of any newly developed algorithms is difficult. Note that informal discussions at recent scientific meetings (e.g. Weather-Driven Renewable Energy Section, 2013 AGU Fall Meeting) suggest that wind turbine manufacturers are already using more complex algorithms. However, as the wind manufacturers have not made these algorithms public, the details are not included here.

Finally, climate prediction models could be used to analyze the energy production outlook under changing climate conditions. Historical runs of the climate models would be first assessed, to quantify performance of the turbine icing prediction. Then, the turbine icing algorithms could be applied to future conditions for an ensemble of models with various climate change scenarios.

## CHAPTER 6

### CONCLUSIONS

The main goal of this research was to develop methods of predicting power losses due to icing that are more accurate than the current method of using a constant percentage. Six methods were developed, three of which used a combination of MCP and WAsP analysis to determine wind speeds while reanalysis data was used for specific humidity and temperature. The three remaining methods used only reanalysis data for all three meteorological variables. The three methods using reanalysis data for wind speeds showed severe deficiencies in calculating accurate power output compared with the MCP/WAsP methods. It was also determined that of the three methods employing MCP/WAsP-derived wind speeds, the boundary-layer similarity method for thermodynamic variables performed the best, as this method produced predicted losses closest to the observed losses. For this method, the average annual absolute difference between observed and predicted power losses due to icing ( $|L_o - L_p|$ ) for the three test years was  $2.13 \% \pm 1.29 \%$  compared with  $5.87 \% \pm 4.64 \%$  for the industry method of prediction ( $|L_o - L_{ind}|$ ). In terms of financial implications, observed power losses due to icing for a single turbine amount to annual losses averaging \$9351.90 for the same three years. The boundary-layer similarity method calculated average annual losses of \$7452.54 compared with only \$3798.99 for the industry method. An important caveat to take into consideration, however, is that the observed power losses due to icing may be overestimated in this study due to incomplete or non-existent records of icing events at the turbine location. Even with this potential overestima-

tion, it is felt that the impact would not hinder the conclusions of this study. However, a better estimation of observed power losses due to icing would strengthen the results considerably.

The six methods were initially trained and applied at a single location in Petersburg, North Dakota. The results of the three MCP/WAsP-derived methods were subsequently applied at a second location in Valley City, North Dakota without being retrained. Compared with Petersburg, this resulted in an increase of the average annual absolute difference between the observed and predicted losses for the three methods and a decrease while using the industry method. Although the three methods still outperformed the industry method in this case, it was felt that an improvement could be made. As such, the boundary-layer similarity method with MCP/WAsP-derived winds was applied to the Valley City location but the data was retrained. In this case, the average annual absolute difference between the observed and predicted losses was similar to the Petersburg location, which shows that training the datasets at a particular location provides a more accurate prediction, rather than assuming some regional similarity. In cases where retraining the dataset is not viable option, however, reapplying the results still provides valuable inter-annual variability and is much improved over simply using the industry method.

This research shows that there is a significant need to improve current icing prediction methods for wind energy applications. Here, it is shown that using a relative humidity threshold to define icing conditions provides a marked improvement on current industry methods. Since industry methods involve using a constant value of icing losses for each year, variability inherent in icing losses is not taken into account. By using a relative humidity threshold, the variability in icing losses is accounted for and

so even for anomalous years, the icing prediction methods can be a more accurate method of prediction. For the best performing method, both relative humidity and temperature were calculated using boundary-layer similarity theory from the MERRA reanalysis dataset, while wind speeds were determined using MCP/WAsP analysis of in-situ wind data. In addition, turbine production data was needed in order to train the dataset to a particular location. For the current industry method, it was shown that predicted losses due to icing amount to financial losses under \$4000.00 for a single turbine, which is well below the actual observed losses of nearly \$10000.00 for the turbine used in this study. The boundary-layer similarity method, however, predicted financial losses of nearly \$8000.00, showing a significant improvement. For a moderate sized wind farm, the financial implications of using this new method over the industry method would be quite significant.

## REFERENCES

- Ackerman, T. and L. Söder, 2000: Wind energy technology and current status: a review. *Renewable and Sustainable Energy Reviews*, **4**, 315–374.
- American Wind Energy Association, 2013: U.S. Wind Industry Annual Market Report 2012. Annual report, 1501 M St. NW Suite 1000, Washington, DC 20005.
- Baring-Gould, I., et al., 2012: Expert group study on recommended practices. Technical report, IEA Wind.
- Beljaars, A., 1992: The parameterization of the planetary boundary layer. *Meteorological Training Course Lecture Series*, European Centre for Medium-Range Weather Forecasts.
- Beljaars, A. and A. Holtslag, 1991: Flux parameterizations over land surface for atmospheric models. *Journal of Applied Meteorology*, **30**, 327–341.
- Betz, A., 1926: *Windenergie und ihre Ausnutzung durch Windmhlen*. Vandenhoeck and Ruprecht.
- Cattin, R., S. Kunz, A. Heimo, R. Oechslin, and M. Russi, 2008: An improved approach for the determination of in-cloud icing at wind turbine sites. Conference Proceedings at EWEC Brussels.
- Chen, S., et al., 2003: COAMPS Version 3 Model Description: General Theory and Equations. Tech. rep., Naval Research Laboratory Rep. 7500–03-448, 148 pp.

- Dierer, S., R. Cattin, S. C. Müller, B. Nygaard, P. Steiner, and B. Calpini, 2009: Modeling the risk of icing in switzerland. IWAIS XIII.
- EMD International A/S, 2013a: *WindPro 2.9 Version Manual*.
- EMD International A/S, 2013b: *WindPro Version 2.9*.
- Fikke, S., et al., 2007: COST 727: Atmospheric Icing on Structures Measurements and data collection on icing: State of the Art. Veröffentlichung meteoschweiz nr. 75, Bundesamt für Meteorologie und Klimatologie MeteoSchweiz.
- Fried, L., 2013: Global wind statistics 2012. Annual report, Global Wind Energy Council.
- Gorban, A., A. Gorlov, and V. Silantyev, 2001: Limits of the turbine efficiency for free fluid flow. *Journal of Energy Resources Technology*, **123**, 311–317.
- Gryning, S.-E., E. Batchvarova, B. Brümmer, H. Jørgensen, and S. Larsen, 2007: On the extension of the wind profile over homogenous terrain beyond the surface boundary layer. *Boundary-Layer Meteorology*, **124**, 251–268.
- Hochart, C., G. Fortin, and J. Perron, 2008: Wind turbine performance under icing conditions. *Wind Energy*, **11**, 319–333.
- Holt, E. and J. Wang, 2012: Trends in Wind Speed at Wind Turbine Height of 80 m over the Contiguous United States Using the North American Regional Reanalysis (NARR). *Journal of Applied Meteorology and Climatology*, **51**, 2188–2202.
- International Standards Organization, 2001: ISO 12494:2001 Atmospheric icing of structures.

- Jasinski, W., S. Noe, M. Selig, and M. B. Bragg, 1998: Wind turbine performance under icing conditions. *Journal of Solar Energy Engineering*, **120**, 60–65.
- Makkonen, L., 2000: Models for the growth of rime, glaze, icicles and wet snow on structures. *Philosophical Transactions: Mathematical, Physical and Engineering Sciences*, **358**, 2913–2939.
- Makkonen, L., T. Laakso, M. Marjaniemi, and K. J. Finstad, 2001: Modelling and prevention of ice accretion on wind turbines. *Wind Engineering*, **25**, 3–21.
- Mistaya Engineering, 2013: Windographer version 3.1.
- Murray, F. W., 1967: On the Computation of Saturation Vapor Pressure. *Journal of Applied Meteorology*, **6 (2)**, 203–204.
- Paulson, C., 1970: The mathematical representation of wind speed and temperature profiles in the unstable atmospheric surface layer. *Journal of Applied Meteorology*, **9**, 857–861.
- Pena, A. D., S.-E. Gryning, C. B. Hasager, and M. Courtney, 2009: Extending the wind profile much higher than the surface layer. *European Wind Energy Conference Proceedings*.
- Rienecker, M. M., et al., 2011: MERRA: NASA’s Modern-Era Retrospective Analysis for Research and Applications. *Journal of Climate*, **24**, 3624–3648.
- Rindeskär, E., 2010: Modelling of icing for wind farms in cold climate. M.S. thesis, Uppsala University.
- Rogers, A. L., J. W. Rogers, and J. F. Manwell, 2005: Comparison of the performance of four measure-correlate-predict algorithms. *Journal of Wind Engineering and Industrial Aerodynamics*, **93 (3)**, 243–264.

Stull, R. B., 1988: *An Introduction to Boundary Layer Meteorology*. Kluwer Academic Publishers.

Thørgersen, M. L., P. Nielsen, T. Sørensen, and M. V. Sørensen, 2013: An Introduction to the MCP Facilities in WindPRO. Tech. rep., EMD International.

Troen, I. and E. Petersen, 1989: *European Wind Atlas*. Risø National Laboratory, 656 pp.

U.S. Energy Information Administration, 2013: International energy statistics. URL [www.eia.gov](http://www.eia.gov).

Wright, W. B., 2008: User's manual for the improved NASA Lewis Ice Accretion Code LEWICE version 3.2. Tech. rep., NASA Contractor Rep. 2008-214255, 454 pp.